Feasibility Study for a

High-Energy, High-intensity Polarized and Tagged Real Photon Beam Facility at ELFE

Editorial Staff

G. Anton, N. d'Hose, M. Düren, K. Helbing, R. Jakob (Ed.),
J.-M. Laget, P. Levi-Sandri, D. Marchand, D. Rebreyend,
R. Van de Vyver (Ed.), L. Van Hoorebeke

Supported by the EU-TMR Network *HaPHEEP* : FMRX-CT96-0008

Contributors to the report :

G. Anton[1], S. Alekhin[2], O. Bartalini[3], M. Bassan[3], V. Bellini[4], J.P. Bocquet[5], S. Boffi[6], V. Borodulin[2], M. Capogni[3], M. Castoldi[7], A. Çelikel[8], C. Commeaux[9], A. D'Angelo[3], N. d'Hose[10], J.P. Didelez[9], M. Diehl[11], M. Düren[1], C. Gaulard[12], G. Gervino[13], F. Ghio[14], B. Girolami[14], P. Grabmayr[21], M. Guidal[9], K. Helbing[1], A. Honig[15], J. Hößl[1], E. Hourany[9], R. Jakob[6,16], M. Kantar[8], R. Kunne[9], J.-M. Laget[10], P. Levi Sandri[12], A. Lleres[5], M. Lowry[17], D. Marchand[18,9], M. Maul[19], C.A. Miller[20], D. Moricciani[3,5], A. Natter[21], L. Nicoletti[3], N.N. Nikolaev[22,23], H.J. Pirner[24], D. Rebreyend[5], G. Rouillé[9], A. Sandorfi[17], C. Schaerf[3], B. Seitz[25], S. Sultansoy[8,26], G. Tamas[10], R. Van de Vyver[18], L. Van Hoorebeke[18], S. Whisnant[27], A. Zucchiatti[12]

1. Physikalisches Institut, Universität Erlangen, 91058 Erlangen, Germany
2. IHEP, Protvino, Russia
3. INFN Sezione di Roma II and Università di Tor Vergata, Roma, Italy
4. INFN Laboratori Nazionali del Sud and Università di Catania, Italy
5. Institut des Sciences Nucléaires de Grenoble, France
6. Università di Pavia and INFN, Sezione di Pavia, I-27100 Pavia, Italy
7. INFN Sezione di Genova and Università di Genova, Italy
8. Ankara Univ., Ankara, Turkey
9. IN2P3, Institut de Physique Nucléaire, 91406 Orsay, France
10. Service de Physique Nucléaire, Centre d'Etudes de Saclay, 91191 Gif-sur-Yvette Cedex, France
11. Theory Group - SLAC, Stanford, USA
12. INFN Laboratori Nazionali di Frascati, Italy
13. INFN Sezione di Torino and Università di Torino, Torino, Italy
14. INFN Sezione Sanità and Instituto Superiore di Sanità, Roma, Italy
15. Physics Department, Syracuse University, Syracuse, NY 13244, USA
16. Fachbereich Physik, Universität Wuppertal, 42097 Wuppertal, Germany
17. LEGS Project, Brookhaven National Laboratory, Upton, NY 11973, USA
18. Dept. of Subatomic and Radiation Physics, Gent University, 9000 Gent, Belgium
19. Nordic Institute for Theoretical Physics, Blegdamsvej 17, DK-2100 Copenhagen, Denmark
20. TRIUMF, Vancouver, British Columbia, VT 2A3, Canada
21. Physikalisches Institut, Universität Tübingen, 72076 Tübingen, Germany
22. IKP(Theorie), KFA Jülich, D-52428 Jülich, Germany
23. L.D. Landau Institute for Theoretical Physics, GSP-1, 117940, Moscow 117334, Russia
24. Institut für Theoretische Physik, Universität Heidelberg, 69120 Heidelberg, Germany
25. II.Physikalisches Institut, Universität Göttingen, 37073 Göttingen, Germany
26. Inst. of Physics, Baku, Azerbaijan
27. Dept. of Physics and Astronomy, Univ. of South Carolina, Columbia, SC 29208, USA

version of: July 13, 2000

Contents

0.1 Foreword 1

0.2 General Introduction 3

1 Physics Motivation **7**

1.1 Introduction 8

1.2 Spin-dependent Diffractive Vector Meson Production 14

1.3 The Real Photoproduction Window at Skewed g_2 Spin Structure Function and... 16

1.4 J/ψ Photoproduction - I 20

1.5 J/ψ Photoproduction - II 21

1.6 ρ' Photoproduction 25

1.7 Real Compton Scattering : Soft vs. Hard Mechanisms 26

1.8 Higher-Twist Effects in Real Photon Compton Scattering 35

1.9 Color Transparency in Few Body Systems 40

1.10 Photoproduction of Charmed Hadrons and the Polarization of the Gluon 45

1.11 A Search for Nucleon Spin Content with a High Energy Real γ Beam 47

1.12 Asymmetries in Total Real Photo Absorption 50

1.13 Inverse Deeply Virtual Compton Scattering 67

2 Experiments **71**

2.1 Introduction 72

2.2 Measurement of Real Compton Scattering and Vector Meson Photoproduction at High Energies 74

2.3 Asymmetries in total real photo absorption 89
2.4 Apollon 95
2.5 Inverse Deeply Virtual Compton Scattering Experiment 96
2.6 Detector Considerations 98

3 Photon Beam Production Methods & Technical Requirements 103

3.1 Introduction 104
3.2 A Compton backscattered photon beam for ELFE at CERN . . . 110
3.3 A Photon Beam for ELFE at DESY 121
3.4 Prototype of an internal laser cavity system for polarized Compton backscattering 123
3.5 Using Coherent Bremsstrahlung for high energy photons at HERA and ELFE 130
3.6 A High-Energy, High-intensity and Highly Polarized Photon Beam for ELFE@CERN using Coherent Bremsstrahlung 141
3.7 The Photon Tagging Spectrometer 155
3.8 Polarized HD Targets 157
3.9 The Hall D Project at TJNAF 165

4 Conclusions and Outlook 167

4.1 Conclusions and Outlook 168

5 Appendix : The Apollon Project 171

0.1 Foreword

The Editors

Over the past few years, a number of people from various European research institutes, engaged in the theoretical and experimental study of nuclear physics at intermediate energies using the electromagnetic probe, has taken the initiative to form a working group with the aim to look at the possibilities for the development and construction of a high-quality real photon beam facility in Europe in the energy range up to about 20 GeV.
Such initiative was stimulated by the scientific objectives of the European TMR Network HaPHEEP (Hadronic Physics with High-Energy Electromagnetic Probes) to which several of the present authors belong.

However, this enterprise was hampered by the fact that no official collaboration was formed as the people involved were spread all over the continent (i.e. not collaborating in a specific project at a particular facility; this meant that they only occasionally met at informal workshops) and consequently, for the study of the various aspects of the anticipated facility, one could only make use of 'volunteers' (especially the postdocs from the EU Network). This had two consequences : more time than anticipated was needed for the preliminary drafting of the report and, secondly, it should not be considered as a *design report* but rather as a *feasibility study.* This latter is motivated by the fact that in Europe, no decision has been taken yet concerning the possible realization of the ELFE (Electron Facility For Europe) project. Several options are open, such as ELFE@DESY wherein a 25 GeV electron beam (from the TESLA facility) could be injected in the existing HERA ring which, in its turn, would be converted to a stretcher ring; another recent option concerns ELFE@CERN which implies the construction of a JLab-like 25.3 GeV electron accelerator using the LEP superconducting cavities which will soon become available (a last option is still to have a new, dedicated ELFE facility constructed, but such possibility seems rather unlikely). However, both first options require different solutions for the production of a real photon beam : in the first option, its seems appropriate to make use of the technique of the 'backscattering of laser light', while the second one could take advantage of the coherent bremsstrahlung process. Finally, one last disadvantage of not having a clear view on the technical lay-out of the desired electron accelerator facility implies that we could not make precise estimates of the various parameters that will determine the characteristics of the photon beam. Consequently, we have kept both options open and we have investigated in a more general way the feasibility of incorporating a real photon project in the planned facilities, fulfilling the requirements as imposed by some (selected) experiments.

It is for these reasons that this report should rather be considered as a 'collection' of individual contributions wherein one or more aspects of the an-

ticipated facility are studied. Nevertheless, it will give us the possibility to formulate recommendations which should be taken into consideration whenever ELFE should be realized.

10 July 2000

This work is supported in part by the 'Training and Mobility of Researchers' network of the European Union HaPHEEP (Contract number FMRX-CT96-0008, coordinated by Dr. J.-M. Laget, Saclay, France)

0.2 General Introduction

G.Anton and R. Van de Vyver

At present, there exists a relatively large and active community inside Europe which aims at the profound study of hadronic physics with high energy electromagnetic probes. The goal of this research is the ultimate understanding of the structure of and the interactions between hadrons like nucleons and mesons.
This issue is also strongly supported by NuPECC in its report *Nuclear Physics in Europe : Highlights and Opportunities*, [1] stating **'As a new initiative, a high luminosity and high duty cycle electron facility of at least $\sqrt{s} = 7GeV$ ($E > 25GeV$ for fixed target experiments) should be built'**; consequently, it seems clear that the nuclear physics community should take the initiative for the realization of such accelerator facility.

The physics case for this so-called ELFE machine *Electron Laboratory for Europe* has been discussed on several occasions [1, 2, 3, 4, 5]. Feasibility studies for such proposed ELFE facility have also been performed; this resulted in the presentation to the DESY Scientific Council on November 6, 1997 of the option *ELFE@DESY*. In this solution ELFE could form an integral part of the TESLA project : making use of the 27 GeV TESLA (pulsed) injector together with the HERA ring operating in stretcher mode, one could produce an extracted continuous electron beam of at most a few tens of μA.
Another possibility consists in the construction of a dedicated ELFE machine using the LEP superconducting cavities; in this *ELFE@CERN* option, a 25.3 GeV continuous electron beam, with a current of about 100 μA, would be available. The accelerator concept is similar to the JLab facility (Newport News, USA) and its specific design characteristics have been thoroughly studied, recently resulting in an extensive 'Conceptual Design Report' [6].

One of the objectives of the 'Training and Mobility of Researchers' Network HaPHEEP, sponsored by the European Union [7] is precisely to help in preparing the future of electromagnetic hadron physics in Europe. This includes the detailed study of the physics issues by which the proposed accelerator facility is justified, together with the exploration of its various experimental aspects. One suggestion consists in a feasibility study of constructing and operating a *high-energy, high-intensity polarized* **real** *photon beam.* Real photons as a research tool, as compared to the virtual photon probe, has its specific merits (see also Section 1.1) : there are no initial and final state interactions of the electron involved, it is complementary to DIS, results at the real photon point often put stringent constraints on the models, its spin structure is much simpler and, in many cases, one has to deal with simpler detection systems and/or targets.

At this point it should be stressed that there exists a long tradition of real photon research in Europe : experimental groups from institutes all over the continent were or are engaged in experiments at the existing electron facilities, such as MAMI in Mainz (Germany), ELSA in Bonn (Germany) and the GRAAL project in Grenoble (France).
Consequently, within the context of the Network, an informal working group was formed in collaboration with specialists from several other nuclear physics institutes. This group met at various occasions and organized dedicated workshops at Grenoble (France, April 1998) and Erlangen (Germany, February 1999) with the ultimate aim to put the acquired knowledge, ideas and suggestions together in this report.

The decision to advocate the installation of a real photon beam line at the anticipated ELFE machine was strenghtened by the similar plans at the anticipated 12 GeV electron facility at JLab [8]; here, one aims at the study of the photoproduction of 'unusual mesons'. Consequently, the idea of extending the useful energy domain up to about 20 GeV looked particularly appealing to us.

This report contains three main chapters, centering on :

- the motivation for physics with real photons
- some proposed experiments
- the technical requirements and options for such project

The practical organization of each chapter will be discussed at its beginning. In a special section at the end of this report, some conclusions will be drawn. As the various contributions contained in this report, stem from different authors and were submitted at moments which were widely spread in time, some overlap between them could not be prevented. In order to avoid a further delay in finishing this report, we opted for a straightforward putting together of the individual papers and only minor changes/adaptations were made by the editors.

Bibliography

[1] Nuclear Physics European Collaboration Committee-Report, Eds. J. Vervier *et al.*, December 1997

[2] Proc. of the Workshop on 'The Future of Nuclear Physics in Europe with Polarized Electrons and Photons', Orsay, France (July 1990), Eds. J.-P. Didelez and G. Tamas

[3] Proc. of the Open Workshop on 'Hadronic Physics with a Continuous Electron Beam of 15 GeV', Orsay, France (February 1992), Ed. J.-F. Mathiot

[4] Conference Proceedings of 'The ELFE Project, an Electron Laboratory for Europe', Mainz, Germany (7-9 October 1992), Eds. J. Arvieux and E. De Sanctis, ISBN 88-7794-060-3 (1993)

[5] Proc. of the Second ELFE Workshop on Hadronic Physics : 'Prospects of Hadron and Quark Physics with Electromagnetic Probes', Saint Malo, France (23-27 September 1996), Eds. N. d'Hose, B. Frois, P.A.M. Guichon, B. Pire and J. Van de Wiele, *Nucl. Phys.* **A622** (1997)

[6] ELFE at CERN, K. Aulenbacher *et al.*, CERN 99-10, Ed. H. Burkhardt (06 December 1999), ISBN 92-9083-154-5

[7] EU-TMR Network 'Hadronic Physics with High Energy Electromagnetic Probes' (HaPHEEP), Contract number FMRX-CT96-0008 (01 September 1996 - 31 August 2000)

[8] Design Report of the Hall D Project, R. Clark *et al.*, Thomas Jefferson National Accelerator Laboratory - TJNAF (August 1999)

Chapter 1

Physics Motivation

1.1 Introduction

S. Boffi, R. Jakob, J.-M. Laget

1.1.1 Probing hadronic substructure !

Although, since the advent of Quantum Chromodynamics (QCD) in the early 70's we do have a renormalizable quantum field theory at hand to describe strong interactions, we still have to face the fact that there is no rigorous analytical explanation for the confinement of partons in hadrons. The theoretical link between the elementary quark and gluon fields of the quantum field theory and the objects observed in the detectors of a real experiment, i.e. baryons and mesons, is still missing. Despite the celebrated and undeniable successes of QCD in the perturbative domain, and despite a number of serious attempts and approaches to unravel the non-perturbative features of QCD, it is fair to say that one of the main goals of QCD is not yet achieved: *an explanation of hadronic substructure within the field theory starting from first principles.*

Fortunately, the missing information on hadron substructure can be cast in a well-defined form of certain hadronic matrix elements of parton field operators, and measured in a number of hard processes. The unambiguous extraction of the values of the matrix elements from experiment thereby relies on factorization theorems, which ensure that we indeed measure process-independent properties of hadrons and not just information specific to the process under consideration. The phenomenological exploration of hadron structure via experiments is an indispensable prerequisite for the finalization of the theoretical task: the full understanding of strong interactions including confinement phenomena. The more complete the experimental mapping of different aspects of the hadron substructure can be carried out, the better will be the guide-line for any theoretical attempt.

In order to probe the internal structure of hadrons we use processes involving a hard scale which defines the resolution; the harder the scale the smaller the distances which can be resolved. Traditionally, the hadron structure is explored in reactions with highly virtual photons (or with Z-, and W-bosons of the weak interaction) where the virtuality (or invariant mass), Q^2 to give it a name, provides this scale. The totally inclusive deep inelastic scattering (DIS) process is the archetype of all hard scattering processes to investigate the substructure of the nucleon. From it we learned about the existence of partons inside the nucleon, later identified as quarks and gluons, and still most information on the properties of nucleon matter originates from DIS data.

Similarly, for exclusive quantities, like e.g. elastic form factors or transition form factors, the kinematic region of high virtuality of the probing photon yields the information on the quark and gluon degrees of freedom, i.e. on the substructure of hadrons on the partonic level. The real photon limit, on the

other hand, links the form factors to static hadronic properties like charges, charge radii and magnetic moments. This is a well-known example where the real photon limit provides information at the kinematical boundaries of a certain quantity. It goes without saying that the range of intermediate virtualities is of strong interest as it reveals the transition from soft physics, governed by bound state properties of hadrons, to the hard scattering of quarks and gluons.

In this report we are interested in the strict limit of zero virtualities. Particularly in reactions induced by high energy real photons, a wealth of information on hadronic substructure can be obtained which is complementary to the one obtained from the high virtuality processes. The kinematic domains of DIS and the elastic scattering are schematically indicated in Fig. 1.1.1 as a function of the photon virtuality Q^2 and the energy ν. For comparison the kinematic region of real photon induced reactions is shown, which is defined by $Q^2 = 0$ and, at the same time represents the $x = 0$ limit to DIS. From the kinematical considerations alone it is evident that real photon induced reactions provide information on quantities close to their kinematical boundaries as will be exemplified in detail in the following contributions in this Chapter.

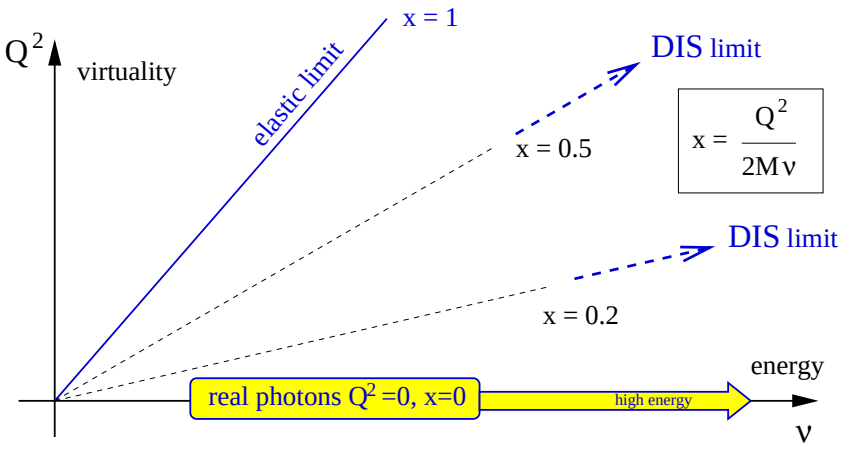

Figure 1.1.1: Kinematic domains of high energy real photon induced reactions in comparison with DIS and elastic scattering.

1.1.2 Why to use high energy real photons ?

A **High energy** of the photon beam is mandatory in exploring the hadronic substructure in reactions induced by real photons. The high energy provides the hard scale necessary for a resolution down to small distances at the level of partonic, i.e. quark and gluon degrees of freedom.

A **High intensity** of the real photon beam will allow sufficient accuracy in the determination of inclusive quantities like for instance the gluon polarization ΔG and, moreover, will give access to exclusive observables like cross sections of wide angle Real Compton Scattering or exclusive vector meson production,

which otherwise would be difficult to determine because of too small counting rates.

A polarized beam, preferably with the options of linear and circular polarization is crucial, since many of the physics cases discussed in the following depend on the measurement of particular asymmetries.

In comparison with processes involving highly virtual photons, **real photon induced reactions** have some technical advantages and bring new insights in our understanding of the structure of hadronic matter:

- Two different aspects of hadronic substructure are accessible:

  the substructure of nucleons
  On the one hand, in processes with large momentum transfer the structure of the hadronic target is probed by the highly energetic real photon down to small scales, where parton degrees of freedom are effective. Typical examples for this type of reactions are Real Compton Scattering (RCS) and photoproduction of mesons both at wide angles (i.e. around 90°).

  the substructure of photons
  On the other hand, a real photon reveals a hadronic substructure itself in form of quarkonium states, i.e. effective mesonic degrees of freedom. This hadronic component of the photon plays an important role, for instance in diffractive meson production at low momentum transfer.

  Varying the momentum transfer t allows to explore the transition between the diffractive regime (low t) and the hard scattering regime (large t).

- The spin structure of real photon amplitudes is simpler than the one of virtual photon amplitudes, since the photon can only be transversely polarized. A combined use of polarized photon beams and polarized targets allows a full determination of the helicity amplitudes.

- The determination of the cross sections at the real photon point appears to be a strong constraint on models.

There are some principal technical advantages as well:

- The energy of a real photon beam can reach the maximum energy of a given electron accelerator and allows to reach kinematical domains inaccessible to electrons.

- The real photon beam is a (relatively) clean beam and its degree of polarization is potentially high. The good spatial separation between the tagger and the target allows to deal with mono-energetic photons individually interacting with the target, whereas with virtual photons one has

always to rely on the one-photon approximation. The degree of polarization of the virtual photon depends on the degree of polarization of the electron beam which hardly reaches 70-80%, whereas for instance with laser-light backscattering one can obtain almost 100% polarization.

- Real photon induced experiments can make use of thicker targets, since there is no problem of deteriorating the energy resolution by multiple scatterings in the target like for electron scattering. This fact (partly) makes up for the effect of the lower initial flux on the luminosity.

All these particular features justify thorough experimental and theoretical investigations in the real photon limit to unravel the internal structure of hadrons.

1.1.3 Which processes ? (Organization of the Section)

The relevant real photon induced processes for the investigation of the hadron substructure can be identified. This Chapter on the physics motivation is organized accordingly, thereby grouping together contributions which address the same class of reactions:

• We start with four contributions on **photoproduction of vector mesons**. In these reactions the hadronic content of the real photon plays a crucial rôle.

In Section 1.2 N.N. Nikolaev discusses the possibility to use a joint analysis of LT asymmetries for ground state and excited vector mesons to determine D-wave and 2S-wave assignments of the $\rho'(1480)$ and $\rho'(1700)$ and of the $\omega'(1420)$ and $\omega'(1600)$ mesons, respectively. To this end the diffractive production of longitudinally polarized mesons induced by a linearly polarized photon beam has to be measured.

A new idea is presented by N.N. Nikolaev in Section 1.3, where he proposes to access the skewed version of the g_2 spin structure function in diffractive vector meson production by circularly polarized photons scattering on transversely polarized protons. Unitarity (diffraction) driven spin effects at small x offer a breaking mechanism of the Wandzura-Wilczek relation and lead to a violation of the Burkhardt-Cottingham sum rule.

In Section 1.4 H.J. Pirner discusses the exclusive photoproduction of J/ψ mesons near the threshold. A Van der Waals type force, expected from phenomenological considerations, would lead to an observable enhancement of the threshold cross section. The high energy resolution of a real photon beam is an indispensable prerequisite for the fine scanning of the cross section near the threshold. A more extensive addendum to this contribution has been submitted by J.-M. Laget as presented in Section 1.5.

In vector meson photoproduction at high energies the direct excitation of a hybrid $q\bar{q}g$ state, which is assumed to mix with a $2S$-excitation state to form

the physical ρ' and ρ'', can be identified by its decay characteristics, as outlined by H.J. Pirner in Section 1.6.

• Two contributions consider the physics of **Real Compton Scattering** at high energies and (moderately) large momentum transfer.

Polarization observables in high energy Real Compton Scattering (RCS) at large momentum transfer will give an important indication whether soft or hard mechanisms contribute dominantly. In Section 1.7 R. Jakob sketches how RCS, in particular via the measurement of polarization observables, can play a key role in elucidating the transition from 'soft physics' to 'hard physics' dynamical scenarios, one of the most controversely debated questions in the physics of hard exclusive reactions.

A large momentum transfer in high energy RCS serves as the relevant scale in a systematic light-cone expansion to unravel higher twist effects as demonstrated by M. Maul in Section 1.8.

• There is one contribution on the subject of **Color Transparency**.

In Section 1.9 J.M Laget also addresses the question of the dominance of hard scattering in exclusive reactions, which would be signalled by the onset of Color Transparency (CT). Reactions induced by photons in few body systems, as for instance the reaction $D(\gamma, p\pi^-)p$ in the energy range $4 < E_\gamma < 10$ GeV, or exclusive production of ϕ and J/ψ vector mesons on few body systems, have clear advantages in the search for CT effects.

• The theory part continues with three contributions about possible measurements of the **Gluon polarization** ΔG and on the **Spin Content of the Nucleon**.

On behalf of the APOLLON collaboration, M. Düren presents in Section 1.10 the physics motivation for the proposal to measure photoproduction of charmed hadrons, in particular the J/ψ meson. APOLLON was originally designed in 1996 to measure the polarisation of gluons in the nucleon. In addition it allows detailed studies of charm production close to threshold.

S. Alekhin, V. Borodulin, A. Çelikel, M. Kantar, and S. Sultansoy in Section 1.11 focus on the same quantity, the gluon polarization, and propose to go to much higher energies using the beam of a possible Next Linear Collider (NLC), for instance TESLA.

In Section 1.12 B. Seitz and K. Helbing discuss helicity dependent photo absorption measurements at $Q^2 = 0$ as a unique tool to investigate the nucleon spin structure. These measurements provide new constraints on Regge theory. Furthermore, the high energy behaviour of the integrand of the GDH sum rule, which is strongly connected to the Ellis-Jaffe and Bjorken sum rules, will help to clarify the important questions concerning the spin distributions inside the nucleon.

Finally, the potential of what is called *the inverse deeply virtual Compton scattering* process is discussed in Section 1.13 by *M. Diehl, M. Düren and G. Anton.* It holds the promise to access the same skewed parton distributions as in DVCS and it certainly deserves further detailed study.

1.1.4 Conclusion :

In this report we collected a number of theoretical contributions by different authors elucidating the wealth and richness of the field of hard reactions induced by high energy real photons. Rather different aspects are briefly addressed in those contributions (the technical details may be found in the references at the end of each subsection). Despite of the diversity of the contributions, they all have in common that information on hadron substructure, either on nucleons or on the hadron content of the real photon itself, is investigated which is not available in this form from hard processes involving highly virtual photons.

It is exactly the complementarity of the obtainable information which makes the field of high energy real photon physics valuable, and in fact indispensable, for the long-term project of mapping out our knowledge on confinement phenomena, a task which certainly requires all experimental information available. Therefore, from the theoretical point of view the additional option of performing experiments with high energy real photon induced processes at an existing or future electron accelerator facility represents a chance not to be missed.

1.2 Spin-dependent Diffractive Vector Meson Production

N.N. Nikolaev

The ground state vector mesons $V = \rho^0, \omega, \phi, J/\Psi, \Upsilon$ are believed to be the S-wave, spin-triplet $q\bar{q}$ states of the Standard Model hadronic spectroscopy. The radially excited vector states are well established only in heavy quarkonia: $\psi(2S; 3686)$, $\Upsilon(2S; 10233)$, $\Upsilon(3S, 10270)$, $\Upsilon(4S, 10580)$. The only solid candidate for the D-wave angular excitation is $\Psi(3772)$. In the light quarkonia, the D-wave vs. $2S$-wave assignment of the $\rho'(1480)$ and $\rho'(1700)$ and of the $\omega'(1420)$ and $\omega'(1600)$ mesons has not been resolved yet. Furthermore, there has been much speculation that one of the ρ' states has a strong admixture of the hybrid $q\bar{q}g$ state [1].

The dominant QCD mechanism of photoproduction can be viewed as elastic scattering of the the color dipole $q\bar{q}$ state of the photon off the target nucleon followed by the projection of the scattered state onto the vector meson. This QCD mechanism implies the diagonalization of the scattering matrix in the color dipole basis and is embodied in the color dipole factorization [2, 3]

$$A(\gamma^* \to V) = \int d^2\mathbf{r} dz \Psi_V^\dagger(\mathbf{r}, z) A_{cd}(x, \mathbf{r}) \Psi_{\gamma^*}(\mathbf{r}, z)\,, \tag{2.1}$$

where Ψ_{V,γ^*} are color dipole distribution amplitudes and $A_{cd}(x, \mathbf{r})$ is the color dipole-nucleon scattering amplitude. The QCD properties of Ψ_{γ^*} and of $A_{cd}(x, \mathbf{r})$ are well known [4], and color dipole factorization offfers a fascinating possibility of the Q^2 dependent scanning of the radial wave function of vector mesons [2, 3]. For instance, the wave function of the S states has a radial node and the node effect leads to a strong suppression of the $2S$ state production which is lifted at large Q^2. This prediction [2, 3, 5] has been confirmed at HERA [6].

The recent QCD theory of s-channel helicity conservation breaking vector meson production [7, 8] has revealed a strong dependence of helicity-flip amplitudes on the wave function of vector mesons. Especially interesting finding [8] is a strong enhancement of helicity-flip in diffractive production of D-wave vector mesons as compared to $1S$ state production, which derives from a sensitivity of spin-flip effects to Fermi motion of quarks in vector mesons [9]. This enhancement holds way beyond the pQCD domain and different spin properties of real photoproduction of S- and D-wave states offers a unique hold on the D-wave vs. $2S$-wave assignment of the $\rho'(1480)$ and $\rho'(1700)$ and of the $\omega'(1420)$ and $\omega'(1600)$ mesons.

For the isolation of s-channel helicity conservation breaking LT interference effects it is sufficient to have linearly polarized photon beams with tagged polarization plane. One must look for the production of longitudinally polarized vector mesons and isolate the LT interference cross section. Within the diffraction cone the expected LT asymmetries are from several to dozen per cent for

2S states and to several dozen per cent for D states. Barring the abnormally strong node effect in the 2S production case (the possibility which needs further scrutiny), the LT spin asymmetries for the 2S and D wave state will be of opposite sign. The LT asymmetry grows rapidly to about 100 per cent at the photon-to-vector-meson momentum transfer $\sqrt{t} \sim 1$ GeV. Consequently, the joint analysis of the LT asymmetry in photoproduction of the ρ and the two ρ' states would allow identification of the $2S$ and D wave ρ' states.

Bibliography

[1] A Donnachie and Yu.S. Kalashnikova, e-Print Archive: hep-ph/9901334

[2] N.N. Nikolaev, *Comments Nucl.Part.Phys.* **21**, 41 (1992)

[3] B.Z.Kopeliovich, J.Nemchik, N.N.Nikolaev and B.G.Zakharov, *Phys. Lett.* **B309** (1993) 179; B.Z.Kopeliovich, J.Nemchik, N.N.Nikolaev and B.G.Zakharov, *Phys. Lett.* **B324** (1994) 469.

[4] N.N.Nikolaev and B.G. Zakharov, *Z. Phys.* **C53**, 331 (1992); *JETP* **78**, 598 (1994); *Z. Phys.* **C64** (1994) 631.

[5] J.Nemchik, N.N.Nikolaev, E.Predazzi and B.G.Zakharov, *Z. Phys.* **C75** (1997) 71; J. Nemchik, N.N.Nikolaev, E.Predazzi, B.G.Zakharov and V.R.Zoller, *J.Exp.Theor.Phys.* **86** (1998) 1054.

[6] H1 Collab., C.Adloff et al., *Phys. Lett.* **B421** (1998) 385

[7] E.V.Kuraev, N.N.Nikolaev and B.G.Zakharov, *JETP Lett.* **68**, 667 (1998)

[8] I.P.Ivanov and N.N.Nikolaev, *JETP Letters* **69**, 268 (1999)

[9] B.G. Zakharov, *Yad. Fiz.* **49**, 1386 (1989); *Sov. J. Nucl. Phys.* **49**, 860 (1989); B.Z. Kopeliovich and B.G. Zakharov, *Phys. Lett.* **B226**, 156 (1989).

1.3 The Real Photoproduction Window at Skewed g_2 Spin Structure Function and Burkhardt-Cottingham Sum Rule Violation and Breaking of Wandzura-Wilczek Relation

N.N. Nikolaev

The combination $g_{LT}(x,Q^2)=g_1(x,Q^2)+g_2(x,Q^2)$ of familiar spin structure functions g_1 and g_2 of deep inelastic scattering (DIS) is related to the absorptive part of amplitude $A_{\mu\rho,\nu\lambda}(\mathbf{\Delta}=0)$ of forward (T) transverse to (L) longitudinal photon scattering accompanied by the target nucleon spin-flip,

$$\sigma_{LT}=\frac{1}{(Q^2+W^2)}\mathrm{Im}A_{-1-\frac{1}{2},L+\frac{1}{2}}(\mathbf{\Delta}=0)=\frac{4\pi^2\alpha_{em}}{Q^2}\cdot\frac{4m_p}{\sqrt{Q^2}}\cdot x^2 g_{LT}(x,Q^2)\,, \tag{3.1}$$

where $\mathbf{\Delta}$ is the momentum transfer and $\mu,\nu=\pm1,L$ and $\rho,\lambda=\pm\frac{1}{2}$ are helicities of particles in $\gamma^*_\nu p_\lambda\to\gamma^*_\mu p'_\rho$ scattering, Q^2,W^2 and $x=Q^2/(Q^2+W^2)$ are standard DIS variable. The motto of high energy QCD – the quark helicity conservation, the common wisdom that high energy scattering is spin-independent, some model considerations [1] including [2] the vanishing one-pomeron exchange contribution to $A_{-1-\frac{1}{2},L+\frac{1}{2}}(\mathbf{\Delta}=0)$, all suggest that the corresponding spin asymmetry $A_2=\sigma_{LT}/\sigma_T$ vanishes in small-x limit of DIS. Burkhardt and Cottingham [2] argued that because neither pomeron nor high lying reggeon exchanges contribute to $A_{-1-\frac{1}{2},L+\frac{1}{2}}(\mathbf{\Delta}=0)$, then unsubtracted (superconvergent) dispersion relation holds for this Compton scattering amplitudes. Precisely superconvergence has been the principal assumption behind the much discussed BC sum rule [2]

$$\int dx g_2(x,Q^2)\propto\int_{Q^2/2}^{\infty}d\nu\mathrm{Im}A_2(Q^2,\nu,\mathbf{\Delta}=0)=0\,, \tag{3.2}$$

for thorough reviews see [3, 4, 5, 6].

The case of the helicity amplitude $A_{-1-\frac{1}{2},L+\frac{1}{2}}(\mathbf{\Delta})$ is quite tricky. On the one hand, QCD motivated considerations strongly suggest a nonvanishing pomeron spin-flip in diffractive nucleon-nucleon scattering [7]. On the other hand, recent studies have shown that the s-channel helicity nonconserving (SCHNC) LT interference cross section σ^D_{LT} of diffractive DIS [8] and related SHCNC spin-flip amplitudes of diffractive vector meson production do not vanish [9, 10] at small x. Consequently, the QCD pomeron exchange can contribute to off-forward $A_{-1-\frac{1}{2},L+\frac{1}{2}}(\mathbf{\Delta})$ at $\Delta\neq0$, but the pomeron exchange factorization enforces the forward zero, $A_{-1-\frac{1}{2},L+\frac{1}{2}}(\mathbf{\Delta})\propto\mathbf{\Delta}^2$ and the vanishing σ_{LT} in one-pomeron exchange approximation.

By the unitarity relation, the opening of diffractive DIS channel $\gamma^*p\to p'X$ affects the elastic scattering amplitude. The best known unitarity effect is

Gribov's absorption or shadowing correction [11] to one-pomeron exchange. Besides simple shadowing, for spinning particles unitarity corrections can give rise to new spin amplitudes absent in one-pomeron exchange and, specifically, lift the forward kinematical zeros. A good example is a recent derivation [12] of a rising tensor structure function $b_2(x,Q^2)$ for DIS off spin-1 deuterons, which breaks the Close-Kumano sum rule [13].

Recently it has been shown [14] that the unitarity mechanism leads to about x-independent spin asymmetry A_2 and scaling and steeply rising $g_{LT}(x,Q^2)$ at small x,

$$g_{LT}(x,Q^2) \sim \frac{G^2(x,\overline{Q}^2)}{x^2}, \tag{3.3}$$

where $G(x,Q^2) = xg(x,Q^2) \sim \left(\frac{1}{x}\right)^{\delta_g}$ is the conventional unpolarized gluon structure function of the target nucleon and $\overline{Q}^2$ is flavour dependent scale to be specified below. It invalidates the Burkhardt-Cottingham sum rule. The found small-x rise of diffraction driven $g_{LT}(x,Q^2)$ is steeper than given by the Wandzura-Wilczek relation [15]under conventional assumptions on small-x behaviour of $g_1(x,Q^2)$:

$$x^2 g_{LT}^{WW}(x,Q^2) = x^2 \int_x^1 \frac{dy}{y} g_1(y,Q^2)\,, \tag{3.4}$$

and diffraction mechanism offers a long sought breaking of the suspect Wandzura-Wilczek relation.

The nucleon spin-flip defines a brand new skewed gluon distribution [16, 17], without going into details we only state that anomalous dimensions which control the small-x dependence of this skewed structure function are identical to those for unpolarized gluon distribution. The numerical estimates for unitarity driven g_{LT} depend on the the spin-flip parameter in the pomeron-nucleon vertex which, incidentally, is of great interest for the polarimetry of stored proton beams and for the whole spin physics program at RHIC [18]. The conservative estimate [14] for g_{LT} based on the Nikolaev-Pronyaev-Zakharov results for SCHNC LT interference in diffractive DIS is shown in fig. 1.3.1 at the moment we can not exclude even one order in magnitude larger effect. To the extent that different parameterization of g_1 have been fitted to the same experimental data, all available parameterizations of g_1 give approximately the same WW integral, the WW curve shown in fig. 1 is for the parameterization [19]. The diffractive mechanism takes over at $x \lesssim 10^{-3}$.

The diffractive production of vector mesons by circular polarized photons on transverse polarized proton target offer a direct experimental window at skewed version of $g_{LT}(x,\xi,Q^2)$ at $\xi = x \approx \frac{m_\rho^2}{W^2}$ and $Q^2 \approx m_\rho^2$. Because the unitarity driven $g_{LT}(x,\xi,Q^2)$ is the scaling function of Q^2, the experimental evaluations of $g_{LT}(x,\xi,Q^2)$ at even such a soft scale will be sufficient to confirm the existence of the unitarity mechanism. The experimental signal for the unitarity mechanism will be the helicity amplitude $A^V_{0-\frac{1}{2},+1+\frac{1}{2}}(\mathbf{\Delta})$ which does

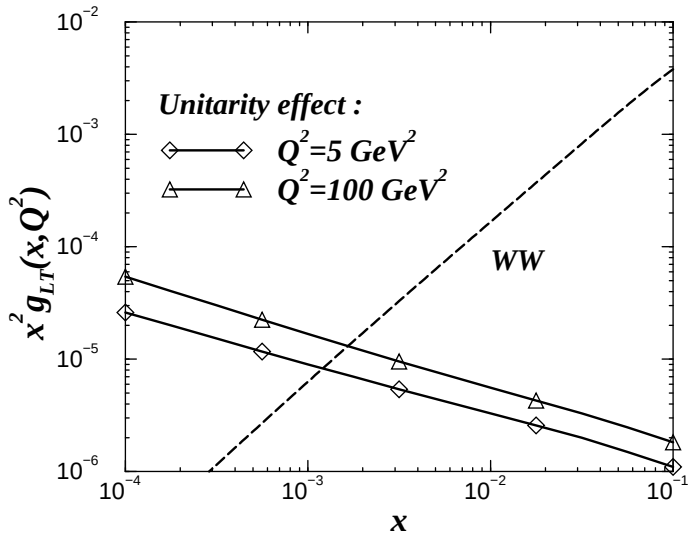

Figure 1.3.1: *The conservative estimate assuming* $r_5(0) = -0.1$ *for the unitarity driven* $x^2 g_{LT}^{(U)}(x, Q^2)$ *vs. the expectation from WW relation (the dashed curve) for GS [19] parameterization for* $g_1(x, Q^2)$*. The difference between the curves for* $Q^2 = 5$ GeV^2 *(diamonds) and* $Q^2 = 100$ GeV^2 *(triangles) is due to the charm contribution at large* Q^2*.*

not vanish in the forward direction $\Delta = 0$. Such a real photoproduction data can fix the pomeron-nucleon spin-flip coupling and constrain the evaluations of $g_{LT}(x, \xi = 0, Q^2)$ for polarized DIS.

The above discussed transverse spin asymmetry and tensor spin asymmetry discussed earlier in [12] fall into a brand new family of unitarity (diffraction) driven spin effects which, in the opposite to the common wisdom, persist in high energy and/or small-x limit and change completely our ideas on small-x behaviour of spin effects. The polarized photoproduction of ρ mesons on polarized protons is the optimal process for testing the existence of diffractive mechanism for g_{LT}.

Bibliography

[1] J. Bartels, B.I. Ermolaev and M.G. Ryskin, *Z. Phys.* **C70**, 273 (1996); *Z. Phys.* **C72**, 627 (1996); B.I. Ermolaev and S.I. Troian, e-Print Archive: hep-ph/9703384; B. Ermolaev, R. Kirschner and L. Szymanowski, e-Print Archive: hep-ph/9806439.

[2] H.Burkhardt and W.N.Cottingham, *Ann. of Phys. (USA)*, **56**, 453 (1970)

[3] B.L.Ioffe, V.A.Khoze and L.N.Lipatov, Hard Processes, North Holland (Amsterdam-Oxford-New York-Tokyo), 1984.

[4] R.L.Jaffe, *Comm. Nucl. Part. Phys.* **19**, 239 (1990)

[5] M. Anselmino, A. Efremov and E. Leader, *Phys. Rept.* **261**, 1 (1995) Erratum-ibid. **281**, 399-400 (1997)

[6] B. Lampe and E. Reya, **MPI-PHT-98-23**, e-Print Archive: hep-ph/9810270.

[7] B.G. Zakharov, *Yad. Fiz.* **49**, 1386 (1989); *Sov. J. Nucl. Phys.* **49**, 860 (1989); B.Z. Kopeliovich and B.G. Zakharov, *Phys. Lett.* **B226**, 156 (1989).

[8] N.N. Nikolaev, A.V. Pronyaev and B.G.Zakharov, e-Print Archive: hep-ph/9812212, *Phys. Rev.* **D** (1999) in print.

[9] E.V.Kuraev, N.N.Nikolaev and B.G.Zakharov, *JETP Lett.* **68**, 667 (1998)

[10] I.P.Ivanov and N.N.Nikolaev, *JETP Letters* **69**, 268 (1999)

[11] V.N.Gribov, *Sov.Phys. JETP* **29** (483) 1969

[12] N.N. Nikolaev and W. Schafer, *Phys. Lett.* **B398**, 245 (1997) Erratum-ibid. **B407**, 453 (1997).

[13] F.E. Close and S. Kumano, *Phys. Rev.* **D42**, 2377 (1990).

[14] I.P. Ivanov, N.N. Nikolaev, A.V. Pronyaev and W. Schafer, **FZJ-IKP-TH-99-08**, e-Print Archive: hep-ph/9903228

[15] S.Wandzura and F.Wilczek, *Phys. Lett.* **B72**, 195 (1977)

[16] A.V. Radyushkin, *Phys. Lett.* **B385**, 333 (1996)

[17] X. Ji, *Phys. Rev.* **D55**, 7114 (1997)

[18] N.H. Buttimore et al., e-Print Archive: hep-ph/9901339.

[19] T. Gehrmann and W.J. Stirling, *Phys. Rev.* **D53**, 6100 (1996)

1.4 J/ψ Photoproduction - I

H.J. Pirner

In several papers [1, 2] the proposition has been made that the interaction between charmonium and the nucleon is dominated by a real gluon exchange interaction. This type of short range Van der Waals force leads to an attractive potential between the J/ψ and the nucleon. There is a also a phenomenological speculation by Brodsky [3] that the anomaly in spin observables namely the polarization assymetry A_{NN} observed at Brookhavenat $p_{lab} = 122\,\mathrm{GeV}$ [4] has its origin in bound states formed close to threshold of the NNJ/ψ system.

Photoproduction of J/ψ near threshold would be an ideal experiment to follow up such experimental hints. In contrary to the expected phase space behaviour for the heavy meson production, states below threshold coming from the attractive van der Waals interaction would give an enhancement of the threshold cross section similar to the pn cross section near threshold.

The observation of a real gluonic potential between color neutral states would open up the possiblity to trace part of the nucleon nucleon interaction to color forces.

Bibliography

[1] M. Luke, A.V. Manohar, M.J. Savage, Phys. Lett. B288 (1992) 355, hep-ph/9204219.

[2] S.J. Brodsky, G.A. Miller, Phys. Lett. B412 (1997) 125, hep-ph/9707382.

[3] S.J. Brodsky, G. de Teramond, Phys. Rev. Lett. 60 (1988) 1924.

[4] G.R. Court et al., Phys. Rev Lett. 57 (1986) 507.

1.5 J/ψ Photoproduction - II

J.-M. Laget

The threshold regime of charmonium and open charm production opens up a new window into QCD dynamics, particularly multiquark, gluonic and hidden colour correlations in nucleons and nuclei. In contrast to diffractive charm production at high energy which tests the behaviour of the gluon structure functions at small x, charm production near threshold tests the structure of the target near $x = 1$ and its short range behaviour.

This has to do with the kinematics of the reaction products. For J/ψ production on the nucleon, the threshold energy is $E_\gamma = 8.20$ GeV and, due to the large mass of the charmed quark ($m_c \approx 1.5$ GeV), the $c\bar{c}$ fluctuation of the photon travels over $l_c \cong 2E_\gamma/4m_c^2 = 0.36$ fm (see Fig. 1.5.1). The large mass of the charmed quark also imposes a small transverse size $r_\perp \sim 1/m_c = 0.13$ fm of this fluctuation. The minimum value allowed for the momentum transfer is large ($t_{min} \sim 1.7$ GeV^2 at the very threshold, ~ 0.6 GeV^2 at $E_\gamma = 10$ GeV). Thus, charm production near threshold implies a small impact parameter ($b \sim 1/\sqrt{-t} \sim 0.2$ fm). All the five valence quarks (the two heavy charm quarks in the probe and the three light quarks in the target) must be in the same small interaction volume.

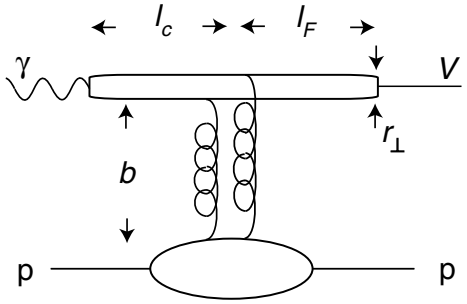

Figure 1.5.1: *The characteristic time scales in J/ψ production on proton.*

Consequently, all the quarks must be involved in the reaction mechanism. On nucleon targets, this implies that three gluon exchange may take over from two gluon and one gluon exchange, and open the way to the study of correlations between valence quarks. Relying on the short distance ($x \sim 1$) behaviour of hadronic matter [1, 2], inferred from properties of perturbative QCD, the charm production cross section can be cast in a simple form [3]. For two gluon exchange the cross section of the $\gamma p \to J/\psi\, p$ takes the form:

$$\frac{d\sigma}{dt} = \mathcal{N}_{2g} v \frac{(1-x)^2}{R^2 \mathcal{M}^2} F_1(\frac{t}{4})(s-m^2)^2 \qquad (5.1)$$

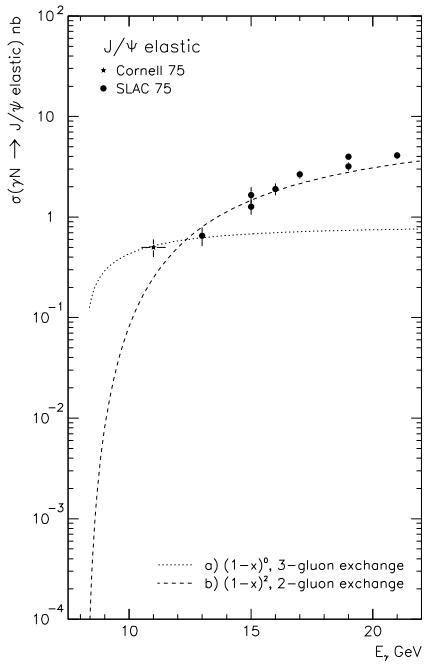

Figure 1.5.2: *Variation of the cross sections of J/ψ photoproduction near threshold, for two or three gluon exchange mechanisms.*

while for three gluon exchange it reads :

$$\frac{d\sigma}{dt} = \mathcal{N}_{3g} v \frac{(1-x)^0}{R^4 \mathcal{M}^4} F_1(\frac{t}{9})(s-m^2)^2 \tag{5.2}$$

where $x \approx (2m\mathcal{M} + \mathcal{M}^2)/(s-m^2)$ and $\mathcal{M}$ is the mass of the $c\bar{c}$ pair. The relative weight of the multiply connected terms is controlled by the interquark separation $R \simeq 1/m_c$. The extra powers of $1/\mathcal{M}$ arise from the higher twist hard processes (see Ref. [4]). $F_1(t)$ is the isoscalar proton form factor; its argument takes into account that the momentum transfer is shared between two or three valence quarks in the proton. This implies that the t distribution for the three gluon exchange cross section is flatter than for two gluon exchange cross section. The $(s-m^2)^2$ term stems from the coupling of the incoming photon to the $c\bar{c}$ pair (see, for instance, Ref. [5]) and compensates the same term in the phase space $v = 1/16\pi(s-m^2)^2$. The normalization coefficient $\mathcal{N}$ is determined assuming that each channel saturates the experimental cross section measured at Stanford [6] and Cornell [7] around $E_\gamma = 12$ GeV. As depicted in Fig. 1.5.2, such a conjecture is consistent with the scarce existing data [6, 7, 8], but clearly calls for a more comprehensive determination of the J/ψ photoproduction cross section between threshold and, let say, 20 GeV.

On few body targets, each exchanged gluon may couple to a coloured quark cluster and reveal the hidden color part of the nuclear wave function, a domain of short range nuclear physics where nucleons lose their identity. The existence of such hidden colour configurations are predicted by QCD evolution equa-

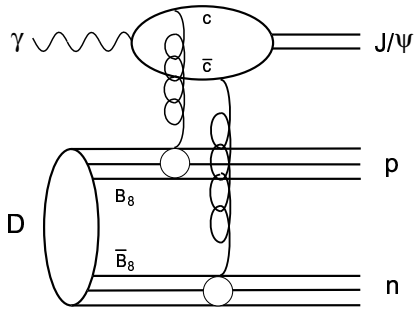

Figure 1.5.3: *The simplest diagram to reveal hidden color state in deuterium [10].*

tions [9]. It is striking that in $\gamma d \to J/\psi\ pn$ the $|B_8\overline{B_8}>$ hidden colour state of the deuteron couples so naturally by two gluons to the $J/\psi\ pn$ final state [10], as depicted in Fig. 1.5.3. Such a contribution may dominate subthreshold production, since the high momentum of the nucleon suppresses quasi free mechanisms. On deuterium the threshold for J/ψ production is ~ 5.65 GeV, while on heavy nuclei the threshold is simply the J/ψ mass 3.1 GeV.

Near threshold, the formation length (during which the $c\bar{c}$ pair evolves into a J/ψ, after its interaction with a nucleon)

$$l_F \cong \frac{2}{m_{\psi'} - m_{J/\psi}} \left[\frac{E_{J/\psi}}{2m_c}\right] \cong 0.11 E_\gamma \tag{5.3}$$

is around 1 fm, closer to the nucleon size than to the nucleus size. This is the ideal situation to determine the scattering cross section of a full sized charmed meson on a nucleon, contrary to higher energies which rather give access to the nuclear interaction of a compact $c\bar{c}$ pair. The study of the A dependence of the J/ψ photoproduction cross section at SLAC at 20 GeV [11] gave $\sigma_{J/\psi} = 3.5 \pm 0.8 \pm 0.5$ mb. However, a large calculated background was substracted and the lack of information on the J/ψ kinematics prevented to disentangle its coherent and incoherent photoproduction. The study of hadroproduction gave $\sigma_{J/\psi} \approx 7$ mb. But after correction for energy loss of the incoming hadron and for coherence effects this value went down to $\sigma_{J/\psi} \approx 3.6$ mb. All this calls for a new measurement of J/ψ photoproduction on several nuclei in the range of energy $E_\gamma \approx 10$ GeV, with a good identification and determination of the J/ψ momentum.

Even though the $c\bar{c}$ pair is created with rather high momentum at threshold, it may be possible to observe reactions where the pair is captured by the target nucleus, forming "nuclear-bound quarkonium" [12]. This process should be enhanced in subthreshold reactions. There is no Pauli blocking for charm quarks in nuclei, and it has been estimated that there is a large attractive Van der Waals potential binding the pair to the nucleus [13]. The discovery of such qualitatively new states of matter would be a major success.

Besides possible applications in connected domains (for instance, the knowledge of the J/ψ N scattering in the search for Quark-Gluon plasma), all these studies select gluonic exchange mechanisms between hadrons or quark clusters. The observation of the gluonic potential between colour neutral states is of utmost importance as it would open up the possibility to trace part of the Nucleon-Nucleon interaction at short range to colour force. Experiments are mandatory to explore this virgin frontier of our knowledge.

Bibliography

[1] P. Hoyer, Nucl. Phys. A622 (1997) 284c.

[2] S.J. Brodsky, et al. Nucl. Phys. B369 (1992) 519.

[3] S.J. Brodsky, E. Chudakov, P. Hoyer and J.M. Laget, in preparation.

[4] E.L. Berger and S.J. Brodsky, Phys. Rev. Lett. 42 (1979) 940.

[5] J.M. Laget, preprint hep-ph/0003213, March 2000.

[6] Camerini et al., Phys. Rev. Lett. 35 (1975) 483.

[7] B. Gittelman et al., Phys. Rev. Lett. 35 (1975) 1616.

[8] R. Anderson et al., SLAC-PUB-1741 *Invited talk presented at Int. Conf. on Production of Particles with New Quantum Numbers, Wisconsin U., Madison, Apr. 22-24, 1976.*

[9] S. J. Brodsky, C. Ji and G. P. Lepage, Phys. Rev. Lett. 51 (1983) 83.

[10] J.M. Laget and R. Mendez-Galain, Nucl. Phys. **A581** (1995) 397.

[11] R.L. Anderson et al., Phys. Rev. Lett. 38 (1977) 263.

[12] S.J. Brodsky, G.F. de Teramond and I.A. Schmidt, Phys. Rev. Lett. 64 (1990) 1924.

[13] M. Luke, A.V. Manohar and M.J. Savage, Phys. Lett. B288 (1992) 355.

1.6 ρ' Photoproduction

H.J. Pirner

We have calculated a non-perturbative QCD calculation of diffractive ρ, ρ' photo- and leptoproduction in [1]. The incoming photon dissociates into a $q\bar{q}$ which scatters on the nucleon and transforms into a vector meson state. The scattering amplitude is calculated in the model of the stochastic vacuum (Heidelberg Pomeron). Asuming that the ρ' and ρ'' are mixed states of an active $2S$-excitation and a hybrid $q\bar{q}g$ state which cannot be excited diffractively in lowest order QCD, we obtained good agreement with the existing data. The genuine quark model states are the $2S$- and $2D$-excitations. The $2S$-state couples to the photon strongly, whereas the $2D$-state has a vanishing wave function at the origin and consequently only a small relativistically induced coupling to the photon. Also diffraction proceeds mostly without angular momentum transfer, so the production of the $2D$-state is suppressed. In the paper below we have used a simplified ansatz for the vector meson states. We employ the nonrelativistic notation $1S$- and $2S$- as a short hand notation for light cone wave functions which in the nonrelativistic limit have this character predominantly. Our ansatz for the physical vector meson states has the following form:

$$|\rho(770)\rangle = |1S\rangle \tag{6.1}$$

$$|\rho(1450)\rangle = \cos\theta\ |2S\rangle + \sin\theta\ |rest\rangle \tag{6.2}$$

$$|\rho(1700)\rangle = -\sin\theta\ |2S\rangle + \cos\theta\ |rest\rangle \tag{6.3}$$

Here the state $|rest\rangle$ describes the $|2D\rangle$ and hybrid $|h\rangle$ states whose coupling to the photon are suppressed and which we neglect in our approach. The wave function of the photon has the usual perturbative form, but it includes a running quark mass $m(Q^2)$ to take into account chiral symmetry breaking and confinement at large distances in an approximate way. The data could be improved, however. Especially the markedly different spectrum in the $\pi^+\pi^-$ mass for photoproduction and e^+e^--annihilation is a strong sign of such a hybrid state. At higher energies the direct production of the hybrid should be possible and the observation of its characteristic decay discussed also in the above paper.

Bibliography

[1] G. Kulzinger, H.G. Dosch, H.J. Pirner, Eur. Phys. J. C7 (1999) 73, hep-ph/9806352.

1.7 Real Compton Scattering : Soft vs. Hard Mechanisms

R. Jakob

Historically, the Compton process, i.e. the elastic scattering of photons off charged particles, has provided an early evidence for the particle nature of light, and thus given rise to the concept of photons as quantums of the electromagnetic field [1]. In the near future, the Compton scattering of high energy real photons off protons may give an answer to one of the most controversely debated questions in the last decade: the question whether exclusive processes at intermediate large momentum transfer proceed dominantly via 'soft' or 'hard' reaction mechanisms.

1.7.1 The Controversy

The Hard Scattering Approach

It is generally accepted that exclusive processes at asymptotically large momentum transfer, Q, are correctly described within the framework of the hard scattering approach (HSA) as developed in the late 70's [2, 3, 4, 5].

The basic principle of the HSA is the factorization of the overall scattering amplitude into a hard, perturbative scattering amplitude of partons, calculable within perturbative QCD, and soft non-perturbative distribution amplitudes (DAs), which encode the information on the structure of the hadrons. The DAs being hadron wave functions integrated over transverse degrees of freedom depend on the light-cone momentum fractions of the partons inside the hadron, and give the probability amplitude to find a certain momentum configuration.

Exclusive processes, as described in the HSA, have two characteristics very distinct from the ones of comparable inclusive reactions:

- At large momentum transfer only the lowest Fock state contributes dominantly to exclusive processes, i.e. for instance the Fock-state with three valence quarks in the proton. Contributions from higher Fock states are suppressed by powers of Λ/Q (where Λ is a typical hadronic scale $\lesssim 1\,\mathrm{GeV}$).

- The overall momentum transfer in the process has to be shared internally by the exchange of a sufficient number of gluons between the partons which have to build up a hadron in the final state. A typical internal momentum transfer squared has the generic form $xy\,Q^2$, i.e. the product of two momentum fractions, say x and y, with the square of the external momentum transfer Q^2. Since the calculation of the amplitude involves an integral over the full range $0 \leq \{x, y\} \leq 1$ of all momentum fractions,

contributions from the end-point regions are unavoidable, where internal gluons become soft.

Criticism of Applications of the HSA at Moderately Large Momentum Transfer

The calculation of exclusive quantities at intermediate momentum transfer within the framework of the HSA, in particular of the elastic form factors of pions and of nucleons in the regions of available data, has been criticised on account of severe internal inconsistencies [6]:

1. The perturbative contributions calculated in the HSA are well below the data, unless strongly asymmetric end-point concentrated DAs are used. Leading to fair agreement with experiment those DAs, however, enhance the contributions picked up in the soft end-point regions. The contradictory situation emerges that the main part of the results originates from kinematic regions where the basic assumptions of the formalism, as for instance the one-gluon-exchange approximation, are unreliable.

2. As well, the neglect of the direct overlap of soft wave functions, the so-called Feyman mechanism, is not justified. With model assumptions on the transverse momentum dependence of the wave functions those contributions can be calculated for a comparison, and turn out to be of the same order (as for the pion form factor [7, 8]), or even significantly larger (as for the electromagnetic form factors of the nucleon [9, 10]) than the hard scattering contribution.

Another point has to be added to this list:

3. In all calculations in the HSA the running strong coupling is treated in an effective way: by setting the argument to some fixed scale, by introducing a gluon mass term, by freezing of the coupling to some fixed value at small scales, ... or similar ad-hoc prescriptions.

It has to be emphasized that the above points of criticism to the application of the HSA, as severe as they are, rely on numerical considerations in a certain range of intermediate momentum transfer, say a few GeV^2, depending on the quantity considered (e.g., $Q^2 \lesssim 10\,\mathrm{GeV}^2$ for the pion form factor $F_\pi(Q^2)$; $Q^2 \lesssim 30\,\mathrm{GeV}^2$ for the magnetic form factor of the proton $G_M^p(Q^2)$). In the asymptotic limit $Q^2 \to \infty$ all objections against the assumed dominance of the hard scatttering mechanism vanish. The question *where* the transition from 'soft' to 'hard' mechanisms actually takes place has to be investigated in phenomenological studies, and finally will be decided by the outcome of experiments.

The Modified HSA

The difficulties in the application of the HSA were overcome in a modified version of this approach [11]. The main ingredients of the modified HSA (mHSA) are (without going into details here; for a recent review see [12]):

- transverse parton momenta in the hard partonic scattering amplitude,
- Sudakov type form factors comprising radiative gluonic corrections (double logarithms resummed to all orders of the strong coupling),
- gluon virtualities as arguments of the running strong coupling,
- intrinsic transverse momentum dependence of the soft wave functions in form of a phenomenological model (constrained by electromagnetic charge radii and the probability limit $P \leq 1$ valid for any state) [7].

In the mHSA perturbative calculations are rendered self-consistent in the sense that most of the contributions picked up in integrations are truely from hard regions, and the singularities from (the one-loop pQCD form of) the running coupling are regularized, since contributions from soft end-point regions are sufficiently suppressed by transverse momentum effects and Sudakov factors. The price to pay is that results calculated in the mHSA are significantly below the data for momentum transfers where data are available. The mHSA results for the quantity $Q^2\,F_\pi(Q^2)$ fall short roughly by a factor 2-3 compared to data [7, 13, 8]; the results for $Q^4\,G_M^p(Q^2)$ are almost an order of magnitude smaller than the data [14, 9]. In fact, this outcome is not surprising, since it simply reflects the observation that the standard HSA gets unreliable large contributions from soft regions.

Scaling Behavior according to Dimensional Counting Rules

A strong argument in favor of the dominance of the hard scattering mechanism is the observation that many exclusive quantities show a scaling behavior in approximate agreement[1] with dimensional counting rules as predicted for the contributions from hard scattering. The question naturally arises, why this scaling behavior shows up, when the hard scattering mechanism is not the dominant one ?

A tentative explanation for this puzzling situation was given in [15], where scaling behavior is argued to be mimicked over a large range of momentum transfer by a broad maximum of contributions the scaling quantities get from a soft mechanism, calculated as the overlap of soft wave functions. Since, the

[1] The agreement is less good, if one looks for logarithmic scale dependences (eventually to large powers as, for instance, in the elastic proton-proton scattering) originating from the evolution of the wave functions and from the running of α_s, which are additionally predicted by the HSA, but not seen in the data.

position and shape of the broad maximum is linked to the transverse size of hadrons, it is not accidentally that various different exclusive quantities show a similar effect.
Since both, soft and hard physics contributions reveal (approximate) scaling behavior, this experimental observation, unfortunately, has little conclusive power to decide which mechanism is the dominant one in a certain range of momentum transfer. As argued below, polarisation observables in the Real Compton Scattering with high energy photons, however, are sensitive to the different mechanisms.

1.7.2 RCS in the Hard Scattering Approach

Two groups, Vanderhaeghen, Guichon and Van de Wiele [16], and Brooks and Dixon [17], recently recalculated the real Compton Scattering off protons at large momentum transfer. Discrepancies between the results obtained in two previous works [18, 19] were the motivation to take special care of the numerical treatment of the integration of propagator singularities.

Assuming the dominance of the hard scattering mechanism the authors of [16] proposed to fit the lowest coefficients of an expansion of the proton distribution amplitude to meet the cross section data with the results of the leading order pQCD calculation. It was demonstrated that the accuracy of the fitting procedure depends on the number of angular settings, and can be improved significantly when an initial state photon asymmetry is measured.

The authors of [17], on the contrary, conluded from a comparison of their leading order pQCD calculation for RCS at high momentum with the corresponding results for the elastic form factors: *"... Thus, it seems unlikely that the elastic proton form factor and the Compton scattering amplitudes are both described by pQCD at presently accessible energies, ..."*.

The concept of 'universality' of DAs thus invalidates a project of determining the proton DA from RCS data alone. On the other hand, the question of identifying the dominant contribution to the process at momentum transfers corresponding to the presently available energies becomes even more important. Only experiments which lead to data with higher accuracy than the existing rather old ones and which extend the kinematical regions to significantly higher energies are appropriate to settle the issue.

1.7.3 RCS in the Soft Physics Approach

As shown in [21, 10] at intermediate large momentum transfer the Real Compton Scattering off protons in the soft physics approach approximately factorizes into a hard parton-photon subprocess and a soft proton matrix element de-

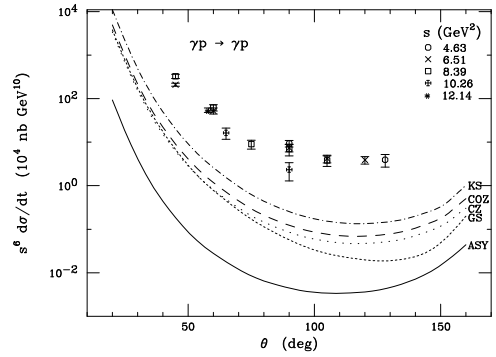

Figure 1.7.1: *The unpolarised scaled cross section for different DAs. The Figure is taken from [17] comparing the results of the pQCD calculation with the available data from [20].*

scribed by new form factors specific to Compton scattering [2]. The unpolarised cross section reads

$$\frac{\mathrm{d}\sigma}{\mathrm{d}t} = \frac{2\pi\alpha_{em}^2}{s^2}\left[-\frac{u}{s}-\frac{s}{u}\right]\left\{\frac{1}{2}\left(R_V^2(t)+R_A^2(t)\right)-\frac{us}{s^2+u^2}\left(R_V^2(t)-R_A^2(t)\right)\right\}, \tag{7.1}$$

where the new form factors, $R_V(t)$ and $R_A(t)$, are certain moments of skewed parton distributions (SPD), and can be represented by an overlap of light-cone wave functions, in direct analogy to Feynman's end-point mechanism for the ordinary electromagnetic form factors. Like the latter ones also the new Compton form factors depend on the invariant momentum transfer squared $|t|$ only. This is a strict prediction of the soft physics approach which can be checked experimentally.

The soft physics approach, as realized in the overlap representation, is complementary to the hard perturbative one. It is argued, however, that for large angle Compton Scattering the soft contribution, although formally representing a power correction to the asymptotically leading perturbative one, dominates at experimentally accessible momentum transfer. The onset of the dominance of the hard scattering is expected at much larger momentum transfer.

Assuming a Gaussian form for the transverse momentum dependence and a common transverse size parameter for all Fock-states the new Compton form factors can be related to the inclusive parton distribution functions [21, 10]. Evaluating the form factors from a global parameterization of distribution functions, as for instance given by GRV [24], one finds in the soft physics approach results for the Compton cross section in fair agreement with the admittedly old data [20].

[2] The approximate factorization relies on both scales, $-t$ and $-u$, being at least moderately large. At a photon energy of 12 GeV that may be reached at an upgraded JLab facility [22] and at c.m. scattering angles around 90° the kinematical conditions for the soft physics approach would be satisfied. Still higher energies, perhaps accessible at ELFE [1], would be even better.

An improvement can be obtained by treating the Fock-states separately. In Fig. 1.7.2 results for the cross section are shown, which are obtained by an explicit modeling of the lowest three Fock states (qqq, $qqq\,g$, and $qqq\,\bar{q}q$) and the GRV parameterization as input for all higher Fock states (for details see [10]).

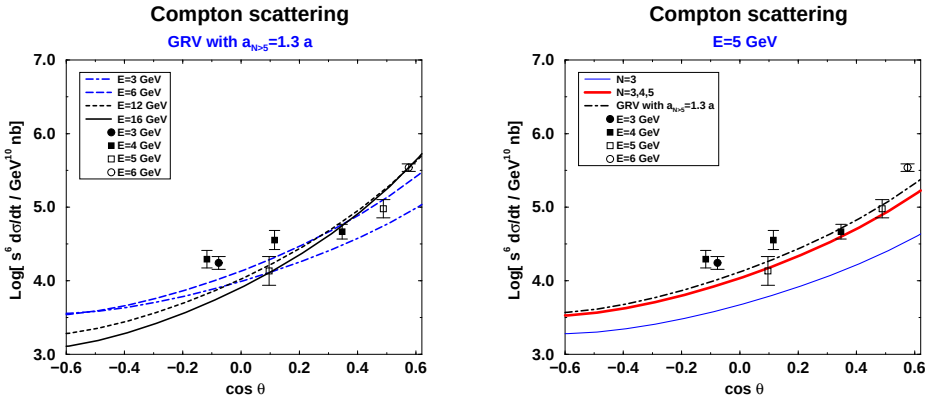

Figure 1.7.2: *The Compton cross section scaled by* s^6 *versus* $\cos\theta$*, where* θ *is the scattering angle in the c.m. Data, for* $-t$, $-u \geq 2.5$ GeV^2 *only, are taken from Ref. [20]. Left: Model predictions obtained from an explicit model of lowest three Fock states and the GRV parameterization [24] for various photon energies in the laboratory frame. Right: Model predictions decomposed into separate Fock state contributions at a photon energy of 5 GeV.*

1.7.4 RCS in the Diquark Model

In [25] the wide angle Real Compton Scattering was calculated within the framework of the diquark model, in which protons are viewed as being built up by quarks and diquarks. The calculation is a particular version of the HSA, but the model combines in an effective way perturbative QCD with non-perturbative elements – the diquarks which represent quark-quark correlations in the proton wave function modeled as quasi-elementary constituents. In this sense the calculation in [25] combines features of the pQCD contribution with some aspects of the soft physics approach.

1.7.5 Initial state helicity correlation $A_{\rm LL}$

Of particular interest is the initial state helicity correlation

$$A_{\rm LL}\,\frac{{\rm d}\sigma}{{\rm d}t} \;=\; \frac{1}{2}\left(\frac{{\rm d}\sigma(\mu=+1,\nu=+1/2)}{{\rm d}t} - \frac{{\rm d}\sigma(\mu=+1,\nu=-1/2)}{{\rm d}t}\right) \qquad (7.2)$$

where μ, ν are the helicities of the incoming photon and proton, respectively. In the soft physics approach $A_{\rm LL}$ takes the form

$$A_{\rm LL} \frac{{\rm d}\sigma}{{\rm d}t} = \frac{2\pi\alpha_{em}^2}{s^2} R_V(t) R_A(t) \left(\frac{u}{s} - \frac{s}{u}\right) \tag{7.3}$$

such that measurements of both the cross section and the helicity correlation A_{LL} allows one to isolate the two form factors experimentally.

Result for $A_{\rm LL}$ in the different approaches are shown in Fig. 1.7.3 (taken from [17]). The large variations of the predictions clearly show that $A_{\rm LL}$ is a well-suited indicator to identify the dominant mechanism.

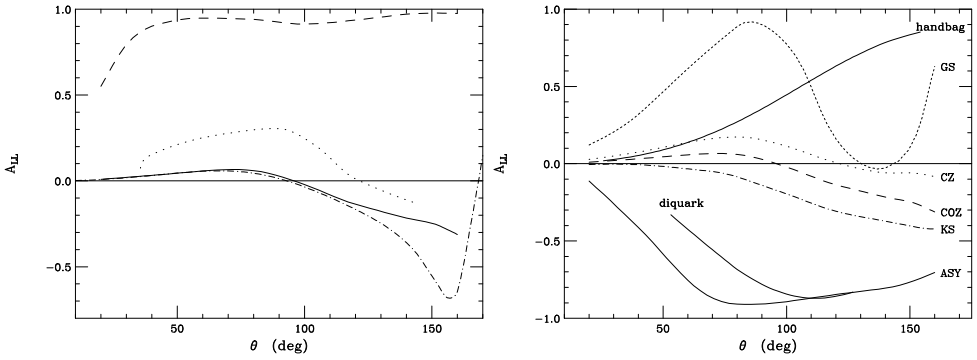

Figure 1.7.3: *Predictions for the initial state helicity correlation A_{LL} (figures taken from [17]). Left: Results obtained in the different calculations within the HSA (dotted line:[18], dashed line:[19], dot-dashed line:[16], and solid line:[17]) obtained using the same (COZ) distribution amplitudes as input. Right: Comparison of results obtained with different DAs (COZ, CZ, KS, GS, ASY) /[17] and the results obtained in the diquark model [25] and within the soft physics approach [15] (labeled as 'handbag').*

1.7.6 Conclusion

The theoretical understanding of hard exclusive reactions has made enormous progress, in which the RCS process plays a key rôle. Still the pending problem of identifying the dominant contributions at intermediate momentum transfers has to be overcome. Experimental information is urgently needed; the measurement of the cross section and helicity correlations, in particular the correlation $A_{\rm LL}$, of RCS at high energies and large momentum transfer will allow us to find answers. Certainly, insight in the crucial issue of identifying the dominant mechanism will give a new impetus to the whole field.

Bibliography

[1] A.H. Compton, Phys. Rev. 22 (1923) 409.

[2] V.L. Chernyak, A.R. Zhitnitsky, V.G.Zerbo, JETP Lett. **26** 594 (1977);
V.L. Chernyak, A.R. Zhitnitsky, Phys. Rept. **112** 173 (19984).

[3] A.V. Efremov, A.V. Radyushkin, Phys. Lett. **B94** 245 (1980).

[4] G.P. Lepage and S.J. Brodsky, Phys. Rev. **D22** 2157 (1980).

[5] A. Duncan, A.H. Mueller, Phys. Rev. **D21** 1636 (1980).

[6] N. Isgur and C.H. Llewellyn Smith, Nucl. Phys. **B317** 526 (1989);
A.V. Radyushkin, Nucl. Phys. **A532** 141c (1991).

[7] R. Jakob, P. Kroll, Phys. Lett. **B315** 463 (1993);
Phys. Lett. **B319** 545(E) (1993).

[8] N.G. Stefanis, W. Schroers, H.C. Kim, Phys. Lett. **B449** 299 (1999) and hep-ph/9812280.

[9] J. Bolz, P. Kroll, Z. Phys. **A356** 327 (1996).

[10] M. Diehl, T. Feldmann, R. Jakob and P. Kroll, Eur. Phys. J. **C8** 409 (1999).

[11] J. Botts, G. Sterman, Nucl. Phys. **B325** 62 (1989);
H.-N. Li and G. Sterman, Nucl. Phys. **B381** 129 (1992).

[12] N. G. Stefanis, Eur. Phys. J. direct **C7** 1 (1999).

[13] R. Jakob, P. Kroll, M. Raulfs, J. Phys. **G22** 45 (1996);
P. Kroll, M. Raulfs, Phys. Lett. **B387** 848 (1996).

[14] J. Bolz, R. Jakob, P. Kroll, M. Bergmann, N.G. Stefanis,
Z. Phys. **C66** 267 (1995).

[15] M. Diehl, T. Feldmann, R. Jakob, P. Kroll, Phys. Lett. **B460** 204 (1999).

[16] M. Vanderhaeghen, P.A.M. Guichon, J. Van de Wiele,
Nucl. Phys. **A622** 144c (1997).

[17] T. Brooks and L. Dixon, hep-ph/0004143.

[18] G.R. Farrar, H. Zhang, Phys. Rev. **D41** 3348 (1990),
Phys. Rev. **D42** 2413(E) (1990).

[19] A. Kronfeld, B. Nižić, Phys. Rev. **D44** 3445 (1991);
Phys. Rev. **D46** 2272(E) (1992).

[20] M.A. Shupe *et al.*, Phys. Rev. **D19** 1921 (1979).

[21] A.V. Radyushkin, Phys. Rev. **D58** 114008 (1998).

[22] A.M. Nathan, hep-ph/9807397.

[23] *ELFE at CERN*, K. Aulenbacher *et al.*, CERN Report 99-10, Ed. H. Burkhardt (06 December 1999), ISBN 92-9083-154-5

[24] M. Glück, E. Reya and A. Vogt, Z. Phys. **C67** 433 (1995);
Eur. Phys. J. **C5** 461 (1998).

[25] P. Kroll, M. Schürmann, P.A.M. Guichon, Nucl. Phys. **A598** 435 (1996).

1.8 Higher-Twist Effects in Real Photon Compton Scattering

M. Maul

In this contribution we describe in the case of large angle real photon Compton scattering a systematic light-cone expansion. The terms obtained in this way are analogous to an expansion of leading and higher twist in terms of the well known operator product expansion in deep inelastic scattering.

Naturally, higher-twist contributions arise as corrections in hard QCD processes in inverse powers of a natural scale of the reaction. In deep inelastic electron proton scattering, for example, this scale is set by the momentum transfer Q^2. The situation in real photon Compton scattering is more difficult. For the reaction $\gamma(q) + P(P) \to \gamma(q') + P(P')$, where q, q' denote the momenta of incoming and outgoing photon and P, P' the momenta of incoming and outgoing proton the scales are set by the three Mandelstam variables $s = (P+q)^2$, $t = (q-q')^2$, $u = (P-q')^2$. For large angle real photon Compton scattering all three have to be large to ensure the hardness of the propagators and factorization. The essential approximation for this process is, that the parton momenta p and p' are nearly identical to the momenta of their parent hadron [1], i.e. $p = P$ and $p' = P'$. We can then describe the large angle real photon Compton scattering in terms of a hard scattering amplitude and a set of integrated double distributions, which only depend on t. In leading order only the twist-2 distribution is involved which is defined analogously to the ordinary double distributions using axial gauge by [2]:

$$\begin{aligned} & \langle P', S' | \bar{q}_a(0) \hat{z} q_a(z) | P, S \rangle \\ = \; & \bar{u}(P', S') \hat{z} u(P, S) \left(e^{-i(pz)} F_a(t) - e^{i(p'z)} \bar{F}_a(t) \right) + \cdots \quad . \end{aligned} \tag{8.1}$$

Here F_a is an integrated vector double distribution for quarks with flavor a and $\bar{F}_a$ the corresponding double distribution describing the antiquarks. There exists also a tensor double distribution which is not essential for our considerations here, and therefore we will omit it for the further discussion. We can consider the expression above as the first term in a light cone expansion around the point $z^2 = 0$. In order to get hold of the twist-4 effects we have to expand this result up to the next order, i.e for example:

$$\begin{aligned} & \langle P', S' | \bar{q}_a(0) \gamma_\mu q_a(z) | P, S \rangle \\ = \; & \bar{u}(P', S') \gamma_\mu u(P, S) \left(e^{-i(pz)} F_a(t) - e^{i(p'z)} \bar{F}_a(t) \right) \\ & + \bar{u}(P', S') \gamma_\mu \hat{u}(P, S) z^2 \left(e^{-i(pz)} F_a^{(1)}(t) - e^{i(p'z)} \bar{F}_a^{(1)}(t) \right) \end{aligned}$$

$$+\cdots \tag{8.2}$$

Here $F_a^{(1)}$ is an integrated twist-4 double distribution for quarks with flavor a and $\bar{F}_a^{(1)}$ is the corresponding integrated double distribution for the antiquarks. One can explain those higher-twist contributions in terms of higher Fock states of the double distribution and they correspond to diagram (c) in Fig. 1.8.1. The second source of higher-twist contributions arise via the expansion of the propagator in the handbag diagram (see diagram (b) in Fig. 1.8.1). This expansion has been calculated in [3] and, up to the order we need, it is given by:

$$\langle T(q(z)\bar{q}(0))\rangle = i\frac{\hat{z}\Gamma[d/2]}{2\pi^2(-z^2)^{d/2}} + i\frac{\Gamma[d/2-1]}{16\pi^2(-z^2)^{d/2-1}}\int_0^1 dv[\bar{v}\hat{z}\sigma + v\sigma\hat{z}]G(vz) \tag{8.3}$$

These contributions lead to direct twist-4 quark gluon quark correlators and can be parameterized to the lowest order in the expansion in z as follows:

$$\begin{aligned} & \langle P', S'|\bar{q}_a(0)\gamma_\mu G_{\alpha\beta}(vz)q_a(z)|P,S\rangle \\ = \;& \bar{u}(P',S')\gamma_\mu\sigma_{\alpha\beta}u(P,S)\left(e^{-i(pz)}F_a^{(G)}(t,v) - e^{i(p'z)}\bar{F}_a^{(G)}(t,v)\right) \quad . \\ & +\cdots \end{aligned} \tag{8.4}$$

The descriptions given above are the parameterizations for a vector current. In the same way we find contributions for the axial vector current. In the framework of deep inelastic scattering those contributions correspond to longitudinally polarized parton distributions. In this case they contribute to the unpolarized cross sections. Their parameterization reads as follows:

$$\begin{aligned} & \langle P', S'|\bar{q}_a(0)\gamma_\mu\gamma_5 q_a(z)|P,S\rangle \\ = \;& \bar{u}(P',S')\gamma_\mu\gamma_5 u(P,S)\left(e^{-i(pz)}G_a(t) + e^{i(p'z)}\bar{G}_a(t)\right) \\ & +\bar{u}(P',S')\gamma_\mu\gamma_5 u(P,S)z^2\left(e^{-i(pz)}G_a^{(1)}(t) + e^{i(p'z)}\bar{G}_a^{(1)}(t)\right) \\ & +\cdots \end{aligned} \tag{8.5}$$

The corresponding parameterization of the quark gluon quark correlator reads:

$$\begin{aligned} & \langle P', S'|\bar{q}_a(0)\gamma_\mu\gamma_5 G_{\alpha\beta}(vz)q_a(z)|P,S\rangle \\ = \;& \bar{u}(P',S')\gamma_\mu\gamma_5\sigma_{\alpha\beta}u(P,S)\left(e^{-i(pz)}G_a^{(G)}(t,v) + e^{i(p'z)}\bar{G}_a^{(G)}(t,v)\right) \quad . \\ & +\cdots \end{aligned} \tag{8.6}$$

We write down for our kinematics the expression for the amplitude for real photon Compton scattering: In principle all the twist-4 double distributions

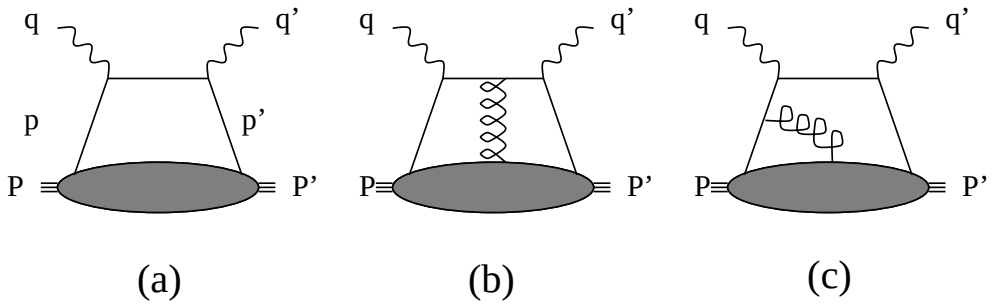

Figure 1.8.1: *Diagrams for the Compton scattering process: Leading oder contribution: diagram (a); twist-4 contribution resulting from the expansion of the propagator in a background field: diagram (b); twist-4 contribution resulting from higher Fock states of the double distribution: diagram (c).*

are accessible by the method of the QCD sum rule calculation in the same way this has already been performed for the pion wave function [4]. Calculating the T-product for the amplitude:

$$T_{\mu\nu} = i \int d^4z \langle P', S'|T[j_\mu(z) j_\nu(z)]|P, S\rangle; \quad j_\mu(z) = \sum_a i e_a \bar{q}_a(z) \gamma_\mu q_a(z) \tag{8.7}$$

yields an expression in which two momenta for the denominator in the propagator occur:

$$p_1 = p + q; \qquad p_2 = p' - q \tag{8.8}$$

and we obtain the resulting expressions in an expansion $1/s$ and $1/u$:

$$T_{\mu\nu} = \sum_a e_a^2 (t_a^{\mathrm{tw}-2} + t_a^{\mathrm{tw}-4} + \cdots) \quad . \tag{8.9}$$

The twist-2 part consists of the integrated twist-2 double distributions and reads:

$$\begin{aligned} t_a^{\mathrm{tw}-2} &= \frac{1}{4}\bar{u}(P', S')\gamma_\sigma u(P, S)\left[\frac{1}{s}\left(F_a(t)A_{1\nu\mu} + \bar{F}_a(t)A_{1\mu\nu}\right)\right. \\ &\qquad \left. + \frac{1}{u}\left(F_a(t)A_{2\mu\nu} + \bar{F}_a(t)A_{2\nu\mu}\right)\right] \\ &- \frac{1}{4}\bar{u}(P', S')\gamma_\sigma\gamma_5 u(P, S)\left[\frac{1}{s}\left(G_a(t)A_{1\nu\mu5} - \bar{G}_a(t)A_{1\mu\nu5}\right)\right. \\ &\qquad \left. + \frac{1}{u}\left(G_a(t)A_{2\mu\nu5} - \bar{G}_a(t)A_{2\nu\mu5}\right)\right] \\ &+ \cdots \end{aligned} \tag{8.10}$$

Here and in the following we use the notations:

$$A_{i\mu\nu} = \mathrm{tr}[\gamma_\mu \hat{p}_i \gamma_\nu \gamma_\sigma]$$

$$\begin{aligned} A_{i\mu\nu 5} &= \mathrm{tr}[\gamma_\mu \hat{p}_i \gamma_\nu \gamma_\sigma \gamma_5] \\ B_{i\mu\nu}(v) &= \mathrm{tr}[\gamma_\mu (\bar{v}\hat{p}_i \sigma_{\alpha\beta} + v\sigma_{\alpha\beta}\hat{p}_i)\gamma_\nu \gamma_\sigma] \\ B_{i\mu\nu 5}(v) &= \mathrm{tr}[\gamma_\mu (\bar{v}\hat{p}_i \sigma_{\alpha\beta} + v\sigma_{\alpha\beta}\hat{p}_i)\gamma_\nu \gamma_\sigma \gamma_5] \quad . \end{aligned} \tag{8.11}$$

for the twist-4 contributions we get:

$$\begin{aligned} t_a^{\mathrm{tw-4}} &= \bar{u}(P',S')\gamma_\sigma u(P,S)\left[\frac{1}{s^2}\left(F_a^{(1)}(t)A_{1\nu\mu} + \bar{F}_a^{(1)}(t)A_{1\mu\nu}\right)\right. \\ &\qquad \left. + \frac{1}{u^2}\left(F_a^{(1)}(t)A_{2\mu\nu} + \bar{F}_a^{(1)}(t)A_{2\nu\mu}\right)\right] \\ &- \bar{u}(P',S')\gamma_\sigma\gamma_5 u(P,S)\left[\frac{1}{s^2}\left(G_a^{(1)}(t)A_{1\nu\mu 5} - \bar{G}_a^{(1)}(t)A_{1\mu\nu 5}\right)\right. \\ &\qquad \left. + \frac{1}{u^2}\left(G_a^{(1)}(t)A_{2\mu\nu 5} - \bar{G}_a^{(1)}(t)A_{2\nu\mu 5}\right)\right] \\ &- \frac{1}{16}\bar{u}(P',S')\gamma_\sigma\sigma_{\alpha\beta}u(P,S)\int_0^1 dv \\ &\quad \times\left[\frac{1}{s^2}\left(F_a^{(G)}(t,v)B_{1\nu\mu}(v) + \bar{F}_a^{(G)}(t,v)B_{1\mu\nu}(v)\right)\right. \\ &\qquad \left. + \frac{1}{u^2}\left(F_a^{(G)}(t,v)B_{2\mu\nu}(v) + \bar{F}_a^{(G)}(t,v)B_{2\nu\mu}(v)\right)\right] \\ &+ \frac{1}{16}\bar{u}(P',S')\gamma_\sigma\gamma_5\sigma_{\alpha\beta}u(P,S)\int_0^1 dv \\ &\quad \times\left[\frac{1}{s^2}\left(G_a^{(G)}(t,v)B_{1\nu\mu 5}(v) - \bar{G}_a^{(G)}(t,v)B_{1\mu\nu 5}(v)\right)\right. \\ &\qquad \left. + \frac{1}{u^2}\left(G_a^{(G)}(t,v)B_{2\mu\nu 5}(v) - \bar{G}_a^{(G)}(t,v)B_{2\nu\mu 5}(v)\right)\right] \\ &\quad + \cdots \end{aligned} \tag{8.12}$$

In this sense one can develop an expansion in powers of $1/s$ and $1/u$ in analogy to the $1/Q^2$-expansion in deep inelastic scattering besides the fact, that the operators are sandwiched between different nucleon states with different momentum and spin.

Bibliography

[1] M. Diehl, T. Feldmann, R. Jakob, P. Kroll, `hep-ph/9903268`

[2] A. V. Radyushkin Phys. Rev. D **59**, 014030 (1999).

[3] I. I. Balitsky, V. M. Braun Nucl. Phys. B **311**, 541 (1989).

[4] V. M. Braun and I. B. Filianov, Z. Phys. C **48**, 239 (1990).

1.9 Color Transparency in Few Body Systems

J.-M. Laget

(This text is an excerpt from Ref. [1])

In Hadronic Physics, one of the key question is: At which momentum transfer hard scatterings dominate the reaction amplitudes? The onset of Color Transparency may prove to be the most direct way to answer it: it may well depend on each channel.

It may occur earlier in Photoproduction of Mesons. The reason is that these channels lie in between Deep Inelastic Scattering (DIS) and Elastic Scattering (Form Factors). In DIS the energy transfer is large enough to break-up the target, making a hard scattering description good enough at momentum transfers as low as $Q^2 \simeq 1$ GeV^2. On the contrary, the energy transfer is vanishing in form factor measurements, rending questionable a hard scattering description at low momentum transfers, in the range of few GeV^2. In exclusive mesons production reactions, both the energy and the momentum transfers are large enough to allow for a perturbative treatment in the momentum transfer range of few GeV^2.

The concept of "Color Transparency" follows from the underlying structure of QCD: interactions between "white" objects depend on their transverse size. A hard scattering of the probe produces recoiling particles with small transverse size, whose the subsequent interactions in Nuclear Matter are reduced. There is no doubt that Color Transparency should occur. The question is where and when.

The idea is to select one of the simplest configurations of a nucleon (or a hadron) in a nucleus and to see how it evolves toward its asymptotic wave function. The study of the interaction of the outgoing hadron with the nuclear medium, as a function of the size of the nucleus, will give us informations on the corresponding evolution. However, the characteristic scale of the evolution should be larger, or comparable, to the size of the largest nuclei.

To date there are no convincing evidences for Color Transparency. The reason is that most of the attempts were performed in quasi elastic kinematics. In the A(e,e'p) reactions, for instance, it is very likely that the values of Q^2 are too low to observe color transparency in the quasi-free kinematics channels, where the energy of the ejected nucleon T_p and the photon four-momentum are not independent ($T_p = Q^2/2M$). In the range of reasonable values of Q^2, for which the cross section does not vanish, the life time of the small object is of the order of the distance between nucleons rather than the nuclear radius. For instance, at the highest $Q^2 = 6$ GeV^2 where data exist, the energy of the outgoing proton is only 3 GeV and its characteristic evolution distance is no

more than 1.5 fm, closer to the internucleonic distance rather to the size of the nucleus.

The way to overcome this difficulty is to study reactions induced by photons in few body systems: Exclusive reactions allow to adjust the formation length of the hadron to the distance between nucleons. The kinematics should be chosen such that the interactions of the emerging hadron with a second nucleon are maximal. This occurs when the produced hadron propagates on-shell (triangular logarithmic singularity). A clear signal for color transparency would be the suppression of final state interactions when the momentum transfer increases.

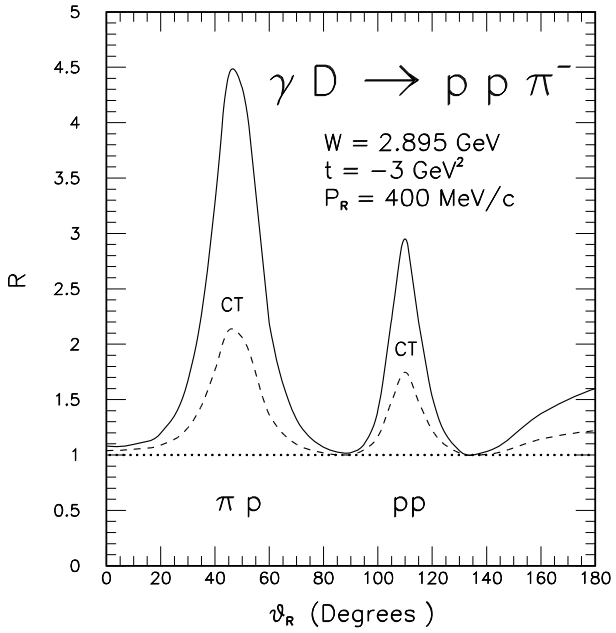

Figure 1.9.1: *Ratio of the total to the quasi-free cross section of the $D(\gamma, \pi^- p)p$ reaction against the angle of the recoiling proton whose the momentum is kept constant at 400 MeV/c. The peak at the left corresponds to πp rescattering, while the peak at the right corresponds to pp rescattering. The full lines and dashed lines include hadron rescattering without and with color transparency effect, respectively. The dotted curves correspond to the quasi-free process.*

A good example is the reaction $D(\gamma, p\pi^-)p$ in the energy range $4 < E_\gamma < 10$ GeV. For real photons the momentum transfer t, between the incoming photon and the outgoing pion, sets the size of the interaction volume. As can be seen in Fig. 1.9.1, the on shell rescattering peaks corresponding to πp or pp interactions are clearly separated. At the top of each peak, the rescattering amplitude is dominated by low momentum components of the deuteron wave function and on mass shell elementary reaction amplitudes (see Ref. [2]): Such a Logarithmic singularity has already been observed at lower energies [3]. The rescattering amplitude is therefore on solid grounds. Furthermore, the elementary reaction $n(\gamma, \pi^-)p$ is almost flat, in the range of t around 3 to 10 GeV^2, and exhibits,

around $\theta_\pi = 90°$, a scaling behavior which is a necessary condition for hard scatterings. Here, the nucleon cross section is well reproduced by a model based on the exchange of saturating Regge trajectories [4].

Figs. 1.9.2 and 1.9.3 show the evolution of the cross-sections at the top of the πp rescattering peak against the recoil momentum P_R and the momentum transfer t, respectively. The expected effect of Color Transparency is clearly apparent. A toy model, based on a geometrical expansion of the mini configuration of the ejected hadron, has been used and is meant as a guide: Only experiment will tell us what is the relevant nature of the process which governs its evolution and formation.

This situation is more comfortable than in the more classical study of quasi elastic scattering of electrons from heavy nuclei, where one look for a change of a flat level of attenuation of the outgoing nucleon, instead of the evolution of a well defined peak.

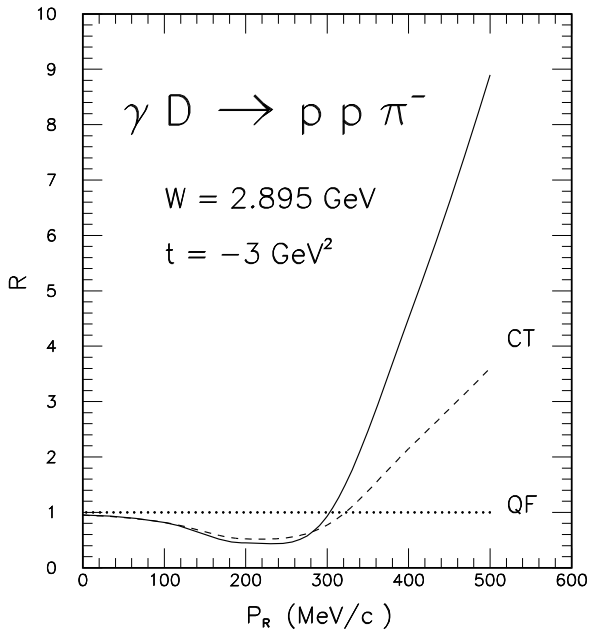

Figure 1.9.2: *Ratio of the total to the quasi-free cross section of the $D(\gamma, \pi^- p)p$ reaction against the momentum of the recoiling proton, at the top of the πp rescattering peak. The full lines and dashed lines include πp scattering without and with color transparency effect, respectively. The dotted curves correspond to the quasi-free process.*

Counting rate estimates show that this channel is already accessible in the CLAS detector at CEBAF, in the range of t around 3 to 5 GeV^2, with $N_\gamma \simeq 10^7 s^{-1}$. A beam of real photons of 10 GeV, with $N_\gamma \simeq 10^8 s^{-1}$, would be ideal to map out the t dependence up to 10 GeV^2. Above, the cross sections are decreasing too fast (as s^{-7}), making the measurement almost impossible.

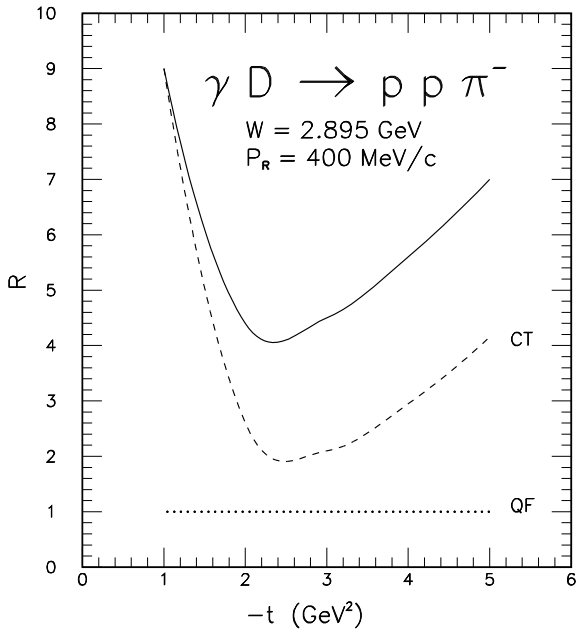

Figure 1.9.3: *Same as in Fig. 1.9.2, but against the momentum transfer.*

Exclusive Vector Mesons production on few body systems is certainly very promising. It allows to prepare a pair of quarks, with an adjustable transverse size, and to study its interaction with a nucleon in well defined kinematics. Furthermore, the coherence time (during which the incoming photon oscillates into a $q\overline{q}$ pair) and the formation time (after which this pair recombines into the final meson) can be adjusted independently to the internucleonic distance. Such a study may end up with a better understanding of the formation of vector mesons in cold hadronic matter, and is complementary to the study of vector meson production in heavy ion collisions. Although more work has to be done to put it on the same footing as the previously discussed channels, the strategy will follow the same lines: the elementary cross sections are of same order of magnitude.

A special emphasis should be put on ϕ and J/Ψ mesons production: not only these narrow states are more easy to identify, but their flavor content, different from that of the ground state of cold hadronic matter, makes them a promising probe.

Bibliography

[1] J.-M. Laget, "What can we learn with 10 GeV Photons?". Proceedings of the Workshop CEBAF at 8+ GeV. June 1998.

[2] J.-M. Laget, Phys. Rep. 69 (1981) 1.

[3] P.E. Argan et al., Phys. Rev. Lett. 41 (1978) 86.

[4] M. Guidal, J.-M. Laget and M. Vanderhaeghen, Phys. Lett. B400 (1997) 6; Nucl. Phys. A627 (1997) 645; Phys. Rev. C57 (1998) 1454.

1.10 Photoproduction of Charmed Hadrons and the Polarization of the Gluon

M. Düren

In 1997 the APOLLON *(=Asymmetries of POLarized Light On Nucleons)* experiment has been proposed with the aim to provide the world's first high statistics measurement of the gluon spin distribution of the nucleon at large x. The experiment was designed to run at HERA in parallel with the other experiments. Running five experiments at HERA would however be an overcomittment of the ring and therefore the experiment was not approved at that time.

Nowadays, the importance of a precision measurement of the gluon polarisation is widely recognized. HERMES has presented a first result of a direct measurement of the gluon polarisation and it has upgraded its detector for further measurements. New experiments to measure the gluon polarisation with high precision have been approved, in particular at RHIC and COMPASS. It has been argued, that the energy of APOLLON is not large enough to unambiguously relate the measured asymmetry to the polarisation of the gluon. The measurement of the gluon polarisation is experimentally difficult and all of the experiments have certain drawbacks. To turn the argument around, one can argue that APOLLON is just in the right energy regime to study the higher order corrections and verify that these are understood. If the corrected APOLLON results are consistent with the results of the high energy experiments, then one can really be confident that one understands the gluon polarisation. In any case, the importance of the gluon polarisation justifies to cross check the results with a further experimental method. APOLLON provides a high statistics measurement at a region of large x which is difficult to reach by the other experiments. The only competing photoproduction experiment, the proposed E-156 experiment at SLAC, has been turned down as the beamline was given to another experiment.

Even if priorities of physics motivations might change over the years, what remains is that APOLLON measures a uniquely clean physics process, namely the production of charmed hadrons (especially J/ψ) from polarised real photons off a polarised nucleon. This process is of high interest, not only in view of the gluon polarisation. Charm production close to threshold can give new insights as described in Section 1.4 by H.J. Pirner. Compared to quasi-real electroproduction, photoproduction has significant experimental advantages. Large luminosities and polarisations can be easily achieved and the detector does not suffer from large background due to low angle electron scattering, Bremsstrahlung and Moller scattering as in the case of electroproduction.

The APOLLON proposal fits in an ideal way into the programme of a high intensity, high energy, polarised photon beam at ELFE. The full proposal is presented in the Appendix (Chapter 5). It is still in its original version as written for HERA, but will be updated as soon as the boundary conditions of ELFE are better defined.

1.11 A Search for Nucleon Spin Content with a High Energy Real γ Beam

S. Alekhin, V. Borodulin, A. Çelikel, M. Kantar, S. Sultansoy

A decade ago combined SLAC and EMC data for the first moment of polarized structure function of proton $g_1^p\left(x,Q^2\right)$ led to a rather small value,

$$\int_0^1 g_1^p\left(x,Q^2\right)dx = 0.126 \pm 0.01 \tag{11.1}$$

In the naive parton model, assuming the validity of Bjorken sum rule

$$\int_0^1 \left[g_1^p\left(x,Q^2\right) - g_1^n\left(x,Q^2\right)\right]dx = \frac{1}{6}\frac{g_A}{g_V} \tag{11.2}$$

and of the SU(3) analysis, this result led to following values

$$\Delta u = 0.78 \pm 0.06, \quad \Delta d = -0.47 \pm 0.06, \quad \Delta s = -0.19 \pm 0.06 \tag{11.3}$$

for the polarized quark moments. Since then, measurements have shown that only about 25 % of the spin is carried by valence quarks and much of the remaining spin must be due to the gluons which hold the proton together and to angular momentum of quarks and gluons,

$$\frac{1}{2} = \frac{1}{2}\Delta\Sigma + \Delta G + \Delta l_z \tag{11.4}$$

where

$$\Delta\Sigma = \Delta u + \Delta d + \Delta s \quad . \tag{11.5}$$

In order to measure gluon contribution to nucleon spin, we must select a process where the familiar lowest order graphs of deep inelastic scattering from a single quark are suppressed. Analysis of the experimental data shows that there is no significant charm content in nucleus, therefore J/Ψ and open charm production processes seem to be the most promising candidates for measurement of polarized gluon distribution.

Uncertainty in the measurement of asymmetry varies linearly with the beam polarization, in this respect using almost monochromatic and fully polarized Compton backscattered laser photon has a great advantages over coherent bremsstrahlung from a diamond crystal.

Proposals to measure gluon polarization using Compton backscattered photons are considered in a number of papers. Electron beam from linac type accelerator as a source of real photon beam was proposed in [2]. For the same purpose, ring type electron beam is considered in [3]. Finally, a possible experiment at DESY has been investigated in details (APOLLON Project[4]).

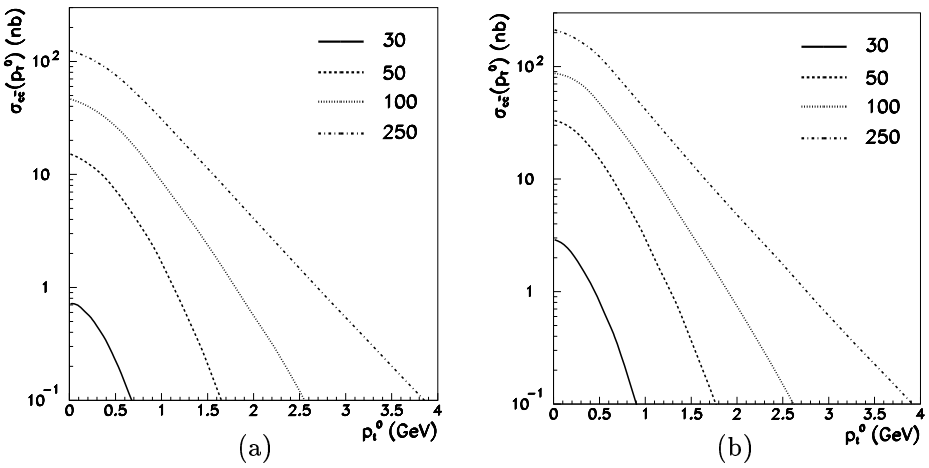

Figure 1.11.1: *The distribution of the inclusive D^*-meson production $\sigma_{D^*\,X}(p_t \geq p_t^0)$ versus p_t^0 for different electron energies: $E_e = 30$ GeV - solid line, $E_e = 50$ GeV - dashed line, $E_e = 100$ GeV - dotted curve, $E_e = 250$ GeV - dashed-dotted line. The c-quark mass is 1.5 GeV/c^2 (a), 1.3 GeV/c^2 (b).*

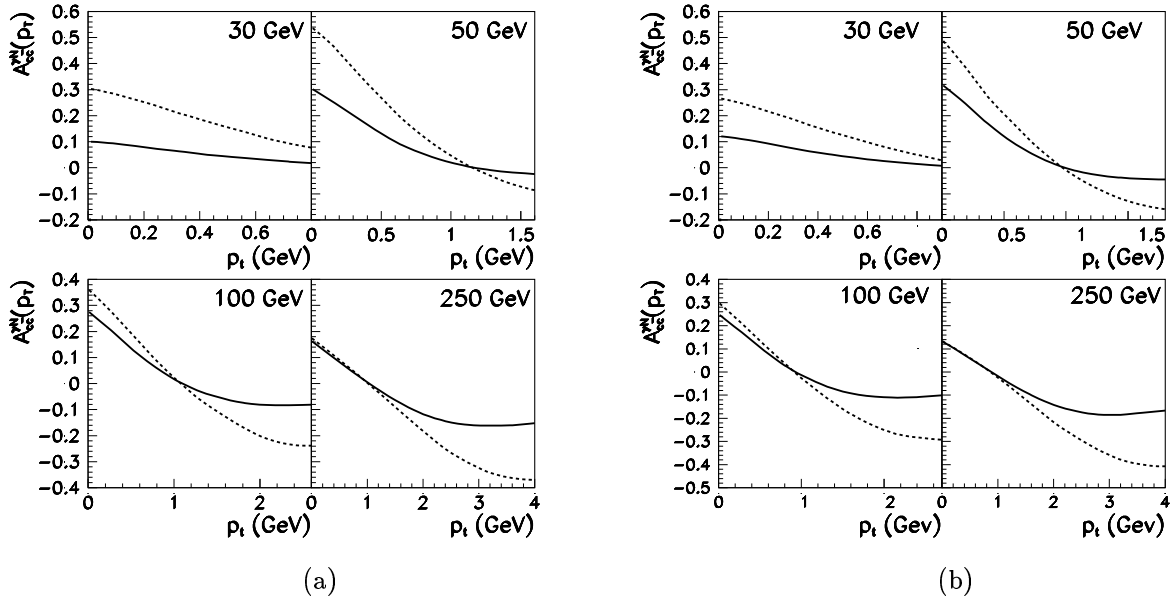

Figure 1.11.2: *The differential asymmetry $A_{D^*}^{\gamma N}(p_t)$ of the D^* meson production versus p_t for the c-quark mass 1.5 GeV/c^2 (a) and 1.3 GeV/c^2 (b). The solid (dashed) line corresponds to the set A (B) of polarized gluon density [1].*

Unfortunately, neither SLAC nor HERA or ELFE electron beam energies are high enough to provide unambiguous interpretation of gluon polarization. Among the existing electron beams LEP2 would be the most suitable if we could use it for this purpose.

On the other hand, multi-hundred GeV electron beams will be available at NLC's in coming decade. High energy real gamma beam will be obtained from NLC electron beam using Compton backscattering for $\gamma\gamma, \gamma e, \gamma p$ and γ-nucleus colliders. These photon beams can also be used to investigate nucleon spin structure.

The advantage of using photon beam from TESLA is exhibited in [5] where open-charm photoproduction is analysed for various machines. Fig. 1.11.1 shows the distribution of inclusive D^* meson production $\sigma_{D^*X}(p_t \geq p_t^0)$ versus p_t^o for different electron energies. In Fig. 1.11.2, the differential asymmetry $A_{D^*}^{\gamma N}(p_t)$ of D^* meson production versus p_t is presented. Here, leading order QCD calculation has been done. Next to leading order corrections [6] are quite sizeable at SLAC and DESY energies.

Bibliography

[1] T. Gehrmann and W.J. Stirling, DTP/95/82, hep-ph/9512406.

[2] S.I. Alekhin, V.I. Borodulin and S. Sultanov,
Int. J. of Mod. Phys. A 8 (1993) 1603.

[3] S. Ataǧ et al., Nucl. Instr.and Meth. A 381 (1996) 23

[4] M. Duren, Proceedings of the workshop, Zeuthen 1997, p 414.

[5] S. Alekhin, V. Borodulin, A. Celikel, M. Kantar, S. Sultansoy, hep-ph/9811418

[6] I. Bojak and M. Stratmann, DTP/98/22, hep-ph/9804353
and DTP/98/36, hep-ph/9807405

1.12 Asymmetries in Total Real Photo Absorption

B. Seitz and K. Helbing

Helicity dependent photo absorption measurements at $Q^2 = 0$ provide a unique tool to investigate the nucleon spin structure. They provide new constraints on Regge theory and to trajectories connected to polarization observables. Furthermore, the high energy behavior of the integrand of GDH sum rule which is strongly connected to the Ellis Jaffe and Bjorken sum rules will be investigated.

In this contribution we review the physical relevance and discuss in Chapter 2 of this report the experimental options for such measurements in the energy region of about 3 to 30 GeV.

1.12.1 Introduction

Several experiments in the resonance region concerning polarized total photo absorption are planned or underway at laboratories like MAMI, ELSA, TJNAF, GRAAL, LEGS and SPring 8. In contrast, this paper describes the physical motivation and the experimental feasibilities to investigate these phenomena at energies of up to $\simeq$ 30 GeV.

At the real photon point ($Q^2 = 0$) for photon energies above the resonance region perturbative quantum chromo dynamics (pQCD) as well as effective models like the constituent quark model (CQM) lack of predictive power. In the resonance region or at high Q^2 in deep inelastic scattering (DIS) a vast multitude of phenomena can be understood in terms of e.g. valence and sea quarks or partons and gluons. On the other hand there is no such description of the underlying dynamics for the region of high energy real photo absorption.

Essentially there are Regge theory and sum rules like the Gerasimov-Drell-Hearn (GDH) sum rule which provide predictions for the kinematic domain in question (see figure 1.12.1). Both Regge theory and the GDH sum rule can be derived on very general grounds by application of fundamental principles like causality and analycity of the scattering amplitude. This is accompanied by the disadvantage that the predictions are more of a 'summarizing' character: Regge theory indicates the asymptotic behavior for high energies while the GDH sum rule is connected to an integral over the whole energy range.

Nevertheless, there are multiple connections to the regions where perturbative field theories are available. Working at a possible boundary of the concept of strong interaction and field theory in general is a challenging feature as well.

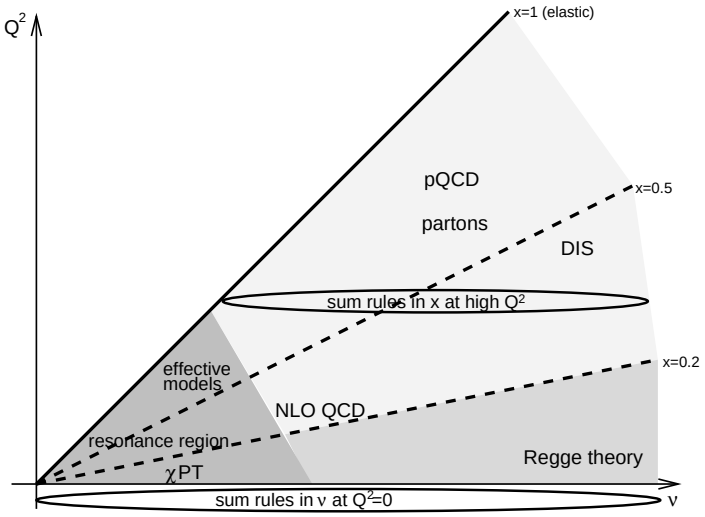

Figure 1.12.1: *Kinematic regions and available descriptions*

1.12.2 Physical Motivation

To measure the energy dependence of the difference of the helicity dependent photo absorption cross sections $\sigma_{3/2}$, $\sigma_{1/2}$ (photon and nucleon spin parallel vs antiparallel) is one of the main motivations for the proposed experiment. Complementary data to the experiments in the energy regime of the resonances and to data from deep inelastic scattering could help to clarify the important questions concerning the spin distribution inside the nucleon.

This section shows the relevance of such a measurement on its own but also its connection to the resonance region and to deep inelastic scattering.

Regge theory

For a long time since the 1970's Regge theory has been considered to be superseded by QCD. Nowadays, it has regained significant relevance — especially in regions were QCD fails due to its limited "radius" of convergence Regge theory very often provides the missing link.

The early ideas in the 1960's like the "bootstrapping" mechanism of the generation of all hadrons which are composed of each other[3] or like the assumption of a confining potential and the observation that many hadrons can be categorized to by trajectories (see figure 1.12.3) have indeed been superseded by a more quantitative understanding of these phenomena in terms of QCD and the quark parton model.

Today, the justification of Regge theory is its correct description of the

[3] in a sense the first preliminary quark or parton model

characteristics of a variety of processes like diffractive scattering where QCD partially fails.

> Regge theory [...] incorporates many of the most complicated confinement aspects of QCD. [Coll 84]

It has been shown, that the spin averaged total cross section at highest energies is dominated by the Pomeron while at energies above the resonance region data can be described by the ρ, ω trajectory [Donn 92]:

$$\sigma_T(s) \simeq c_1 \cdot s^{\alpha_R(0)-1} + c_2 \cdot s^{\alpha_P(0)-1} \tag{12.1}$$

All unpolarized total cross sections can be fitted with the same values for $\alpha_R(0)$ and $\alpha_P(0)$ (see figure 1.12.2). Observations of this kind lead to a revival of Regge theory.

Generally, in Regge language the structure of the dynamics can be calculated by means of rather simple function theory. In addition, using the idea to replace the sum over partial waves by a contour integral in the complex plane of the angular momentum generalized to complex values. The resulting expression for the scattering amplitude thus is based on fundamental assumptions:

$$A(s,t) = \gamma_{AC}(t)\gamma_{BD}(t)\frac{\exp[-i\pi\alpha(t)] + \mathcal{S}}{\sin\pi\alpha(t) \cdot \Gamma(\alpha(t))}\left(\frac{s}{s_0}\right)^{\alpha(t)} \quad , \tag{12.2}$$

where $\mathcal{S} = \pm 1$ is called the 'signature'. This formulation of the scattering amplitude exhibits the following features:

- $t \geq 0$: When $\alpha(t)$ passes through an integer the factor $[\sin\pi\alpha(t)]^{-1}$ produces resonance poles in t which can be understood as t-channel intermediate states of definite squared mass t and spin $\alpha(t)$. The sums of these states are called Reggeons.[4]
- $t \leq 0$, fixed: The energy dependency of the cross section shows a power behavior $d\sigma/dt = \frac{1}{s^2}\left|A(t,s)\right|^2 \sim f(t) \cdot s^{2\alpha(t)-2}$
- The coupling is factorized γ_{AC}, γ_{BD}.

In the language of field theory Regge trajectories can be understood as the exchange of multiple bound states. In the case of e.g. the ρ-trajectory (see figure 1.12.3) the exchange of all mesons with $I^G(J^{PC}) = 1^+(\text{odd}^{--})$ has to be considered. Obviously it is impossible to calculate such an exchange of bound states within QCD from first principles since this would require a solution to the QCD confinement problem, which is out of reach at the moment.

In eq. (12.1) $\alpha_R(0)$ and $\alpha_P(0)$ denote the intercepts of the ρ, ω-trajectory[5] and the intercept of the Pomeron-trajectory ($t = 0$). The values for these

[4] $[\sin\pi\alpha(t)]^{-1}$ is sometimes even called the Reggeon propagator.

[5] These trajectories happen to be approximately exchange-degenerate.

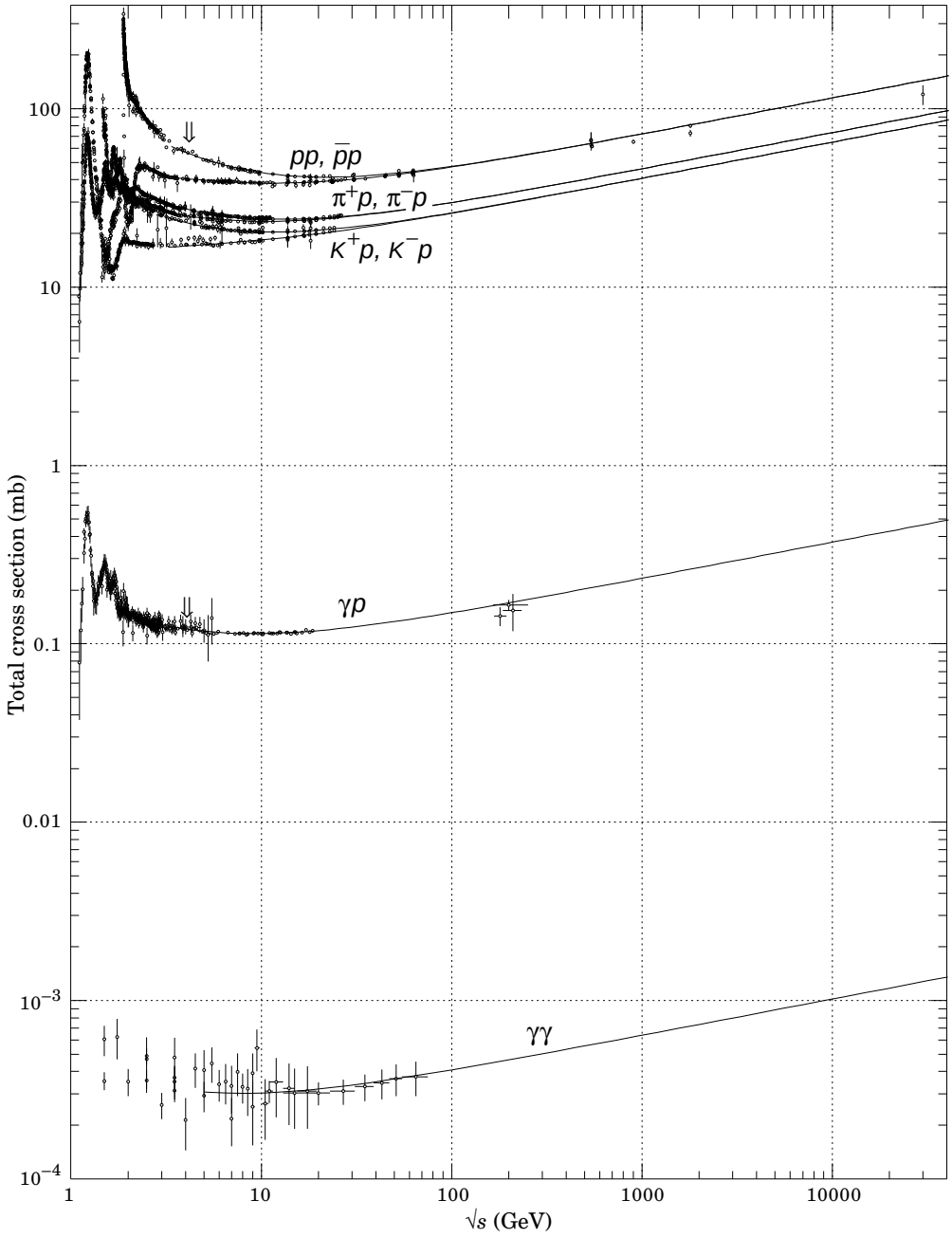

Figure 1.12.2: *Summary of hadronic, γp and $\gamma\gamma$ total cross sections [Comp 98].*

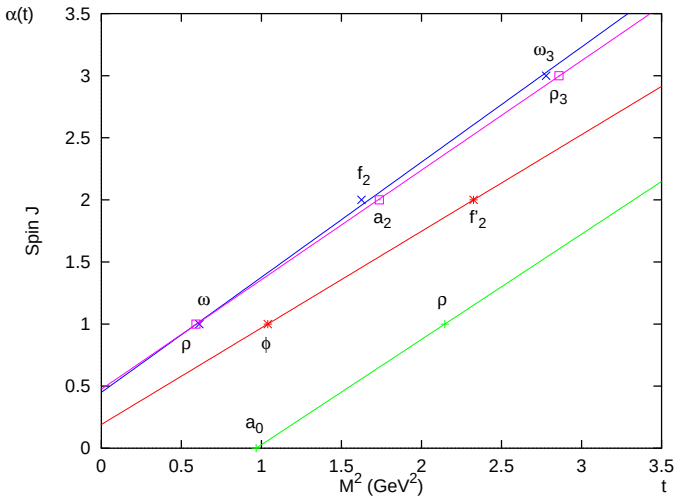

Figure 1.12.3: *Mesons on trajectories*

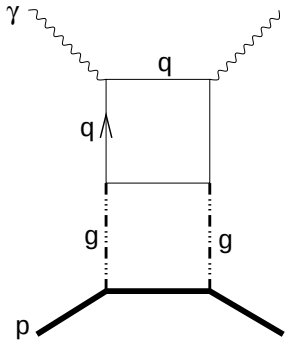

Figure 1.12.4: *Two-gluon exchange model of the Pomeron*

intercepts are $\alpha_R(0) = 0.53$ and $\alpha_P(0) = 1.08$. The value for the ρ, ω-trajectory strikingly matches the value that can be extracted when drawing a line through all mesons having the same quantum numbers like the ρ and ω respectively (see figure 1.12.3).

Whereas the origin of ρ, ω-trajectory seems to be well understood, this is not the case for the Pomeron-trajectory. The given quantum numbers are $I^G(J^{PC}) = 0^+(\text{even}^{++})$ which are the same as for vacuum. The derivation of the Pomeron effects in the framework of QCD is still a problem lacking a complete solution. In the simplest picture the Pomeron is only a two-gluon exchange as shown in figure 1.12.4. But this exchange can only roughly describe the effects observed in "hard" processes and how to relate the Pomeron to an approach in a non-perturbative QCD-based model is still unclear.

While the Pomeron trajectory dominates the high energy behavior of the total photo absorption cross section it does not contribute to the difference. In addition Pomeron cuts (the exchange of multiple reggeons) do not contribute

at the real photon point since poles and cuts coincide at $t = 0$ while Pomeron cuts could contribute at high t. Thus Pomeron cuts are not discussed further.

The lowest lying trajectories that determine the high energy behavior of the cross section difference [Clos 94] are the a_1 (isovector) and the f_1 (isoscalar) Regge trajectories giving rise to

$$\left(\sigma_{1/2} - \sigma_{3/2}\right)^{p+n} \sim s^{\alpha_{f_1}(0)-1} \ , \quad \left(\sigma_{1/2} - \sigma_{3/2}\right)^{p-n} \sim s^{\alpha_{a_1}(0)-1} \tag{12.3}$$

Concerning the mesons associated to these two trajectories only very little is known. Only the $a_1(1260) : I^G(J^{PC}) = 1^-(1^{++})$ and the $f_1(1285) : I^G(J^{PC}) = 0^+(1^{++})$ are known for sure. The f_3 has not been seen at all; for the a_3 it was believed to have evidence for having a mass of 2050 MeV. But the evidence was weak and thus it is no longer listed by the particle data group.

Again, like in the case of the ρ and ω the a_1 and f_1 trajectories are assumed to be approximately exchange degenerate. Moreover, they are also assumed to be degenerate with those trajectories of opposite signature. Nevertheless, the corresponding mesons on these trajectories $I^G(J^{PC}) = 1^+(2^{--})$ and $0^+(2^{--})$ aswell have not been found.

Taking the $a_3(2050)$ for serious the a_1- and f_1-trajectories would roughly have the universal slope of about 0.9 GeV^{-2} like those plotted in figure 1.12.3. On the other hand, the fact that no other meson of these trajectories has been observed might indicate that their masses could be much higher and thus the slope might be smaller.

Regarding the spin structure function g_1 supports this hypothesis. In the parton picture g_1 can be understood as the difference of valence and sea quark $(q, \bar{q})$ distributions with respect to their polarization $(\uparrow, \downarrow)$.

$$g_1 = \frac{1}{2} \sum_f e_f^2 \left(\Delta q_f + \Delta \bar{q}_f\right), \quad \Delta q_f = q_f^{\uparrow} - q_f^{\downarrow} \tag{12.4}$$

Given the relation of g_1 to the difference of total virtual photo absorption[6]

$$\sigma_{1/2}(\nu, Q^2) - \sigma_{3/2}(\nu, Q^2) = \frac{16\pi^2\alpha}{2m\nu - Q^2} \left(g_1(x, Q^2) + \frac{Q^2}{\nu^2}\, g_2(x, Q^2) \right) \tag{12.5}$$

$$\simeq \frac{16\pi^2\alpha}{2m\nu - Q^2} \cdot g_1(x, Q^2) \quad \text{at low } Q^2 \tag{12.6}$$

the connection to Regge trajectories is (see eq. (12.2)):

$$g_1^N(x, Q^2) \sim \beta(Q^2) \cdot x^{-\alpha_{a_1, f_1}(0)} \tag{12.7}$$

As an example figure 1.12.5 shows the g_1 data as function of x at $Q^2 = 5$ GeV^2. The values for the Regge intercept α that can be extracted from g_1 at $x < 0.1$ on the proton (and the neutron) have a large uncertainty and range from 0.2 to 0.7

[6] with $\nu = \left(s - M^2\right)/2M$, $x = Q^2/2M\nu$

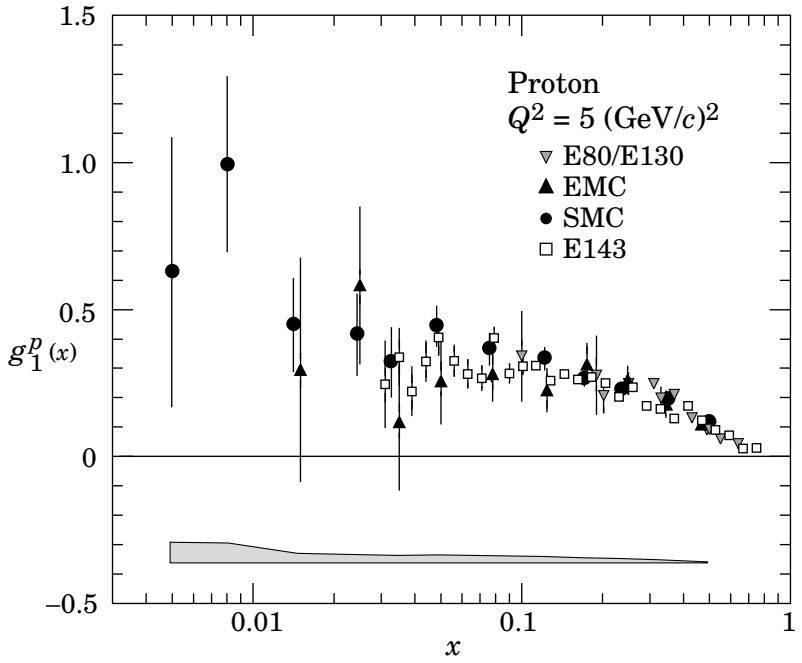

Figure 1.12.5: *The spin-dependent structure function $g_1(x)$ of the proton*

Another way to estimate α from polarized deep inelastic scattering data is to regard the photo absorption cross section asymmetry

$$A_1 = \frac{\sigma_{1/2}(\nu, Q^2) - \sigma_{3/2}(\nu, Q^2)}{\sigma_{1/2}(\nu, Q^2) + \sigma_{3/2}(\nu, Q^2)} \sim s^{\alpha - \alpha_P} \simeq s^{\alpha - 1} \tag{12.8}$$

The advantage of this method is that the unpolarized structure function F_2 is not needed to extract A_1 from the data as is in the case of g_1. Consequently the errors esp. at small x (large ν) are smaller (see figure 1.12.6). The value of the Regge intercept of the f_1 and the a_1 meson from these data range roughly from 0.3 to 0.6 where the Pomeron intercept contributes a significant systematic error.

Figure 1.12.7 compares the different assumptions. Clearly the data from polarized deep inelastic scattering indicate a much smaller slope than the universal one. Moreover, this would be a contradiction the (small) evidence for the a_3-meson having a mass of about 2 GeV. According to the DIS data the masses of the a_3 meson and the f_3 meson should be of the order of 3 GeV.

The direct measurement of the energy evolution of the spin dependent real photo absorption cross sections to large energies is one of the most important challenges for the future, where a start can be made with the experiment presented here. Such a measurement would provide the asymptotic high energy behavior of $\sigma_{3/2} - \sigma_{1/2}$. Thus a precise value for for the Regge intercept could be deduced which would an input of high interest to the physics of the spin distribution of sea quarks and to g_1 at low x. The systematic error of the mea-

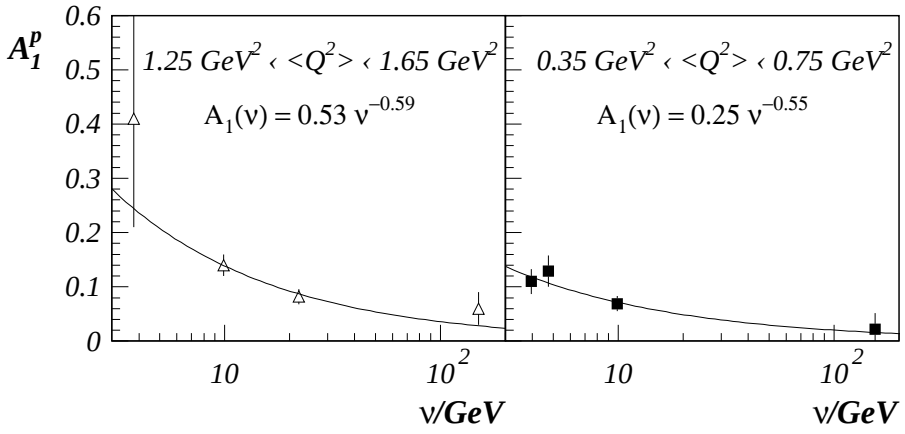

Figure 1.12.6: *Fit to the asymmetry in total virtual photo absorption [Stei 96]*

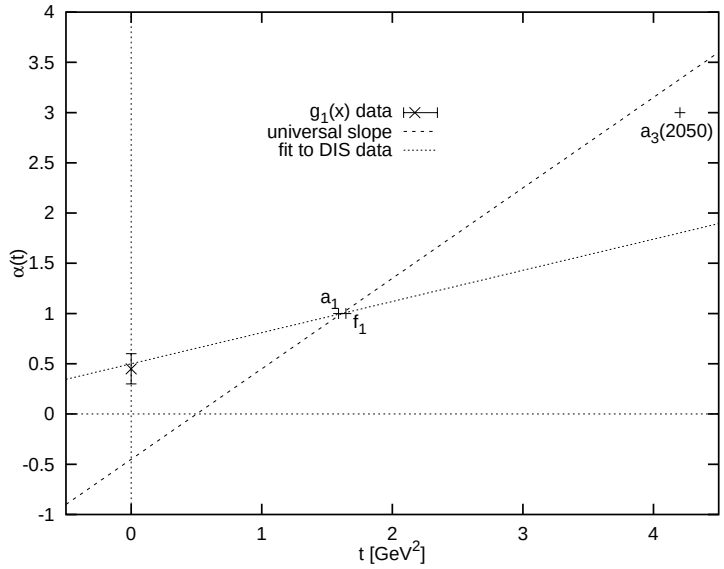

Figure 1.12.7: *Possible a_1,f_1 trajectories*

surement of the GDH integral at MAMI and ELSA would be reduced (see 1.12.2). In addition we would obtain predictions for the masses of the mesons lying on the a_1 and f_1 trajectory and it could be clarified whether there is another trajectory deviating from the universal slope apart from the Pomeron-trajectory.

The Gerasimov-Drell-Hearn sum rule

The Gerasimov – Drell – Hearn (GDH) sum rule relates the difference of the helicity dependent photo absorption cross sections on the nucleon to a ground state property, the anomalous magnetic moment κ_N. Although it has been derived from general principles as early as 1966, an experimental verification is still pending.

The structure of the GDH sum rule connecting dynamic and static properties of the nucleon makes it an ideal testing ground for nucleon models. Since the sum rule is derived under very general assumptions, it gives strong constraints to these models; as it connects dynamic and static properties, it provides a stringent test for theoretical predictions.

The GDH sum rule can be regarded as the $Q^2 = 0$ limit of the Ellis – Jaffe and Bjorken sum rules, i.e. a Q^2 evolution of these latter sum rules should converge against the GDH value for $Q^2 \to 0$. Present experimental data at higher momentum transfer and theoretical predictions both pose important questions to experiment and theory alike, especially because this transition can be regarded as the transition from pQCD to the non perturbative regime.

Through an energy weighted integral the GDH sum rule [Gera 66], [Drel 66] connects the helicity dependent photo absorption cross sections $\sigma_{3/2}, \sigma_{1/2}$ to a ground state property of the nucleon, its anomalous magnetic moment κ_N:

$$-\frac{2\pi^2 e^2 \kappa^2}{M^2} = \int_0^\infty \frac{\sigma_{1/2} - \sigma_{3/2}}{\nu} d\nu, \tag{12.9}$$

where e^2 is the fine structure constant, M the Nucleon mass and ν the energy of the incident photon in the lab system.

The sum rule is derived from the Compton scattering amplitude in forward direction using dispersion relations and the optical theorem. In this procedure, only general physical principles like Lorentz and gauge invariance, causality, relativity and unitarity are used. Therefore, it is independent of particular models for strong interactions.

1.12.2.2.1 Dispersion theoretic derivation

To understand the GDH sum rule, its importance and its connection to the sum rules of DIS, one of its derivations will be briefly outlined. As stated before,

the GDH sum rule (eq. 12.9) is derived from the Compton forward scattering amplitude of a real photon on a nucleon. This scattering amplitude $T(\nu, \theta = 0)$ can be written between the initial and final nucleon Pauli spinors χ_i and χ_f:

$$T(\nu, \theta = 0) = \chi_f^\dagger [\vec{\epsilon_f}^* \cdot \vec{\epsilon_i} f(\nu) + i\vec{\sigma} \cdot (\vec{\epsilon_f}^* \times \vec{\epsilon_i}) g(\nu)] \chi_i \tag{12.10}$$

where $f(\nu)$ and $g(\nu)$ are the spin non–flip and spin flip amplitudes, $\vec{\epsilon_f}$ and $\vec{\epsilon_i}$ denote the polarization vectors of the initial and final photon and $\vec{\sigma}$ is the spin of the nucleon. The amplitudes $f(\nu)$ and $g(\nu)$ can be expanded into a power series, where the leading terms are given by low energy theorems based on Lorentz and gauge invariance [Low 54],[Gell 54]:

$$f(\nu) = -\frac{e^2}{M} + (\alpha_N + \beta_N)\nu^2 + \mathcal{O}(\nu^4) \tag{12.11}$$

$$g(\nu) = -\frac{e^2 \kappa_N^2}{2M^2}\nu + \gamma_N \nu^3 + \mathcal{O}(\nu^5) \tag{12.12}$$

The first term in the expansion of $f(\nu)$ is the Thomson limit, the second term is the contribution of the nucleon's scalar polarizabilities.

Similarly, the leading term in $g(\nu)$ is given by the anomalous magnetic moment κ_N, the next order is the vector polarizability of the nucleon. Note, that because of crossing symmetry $f(\nu)$ must be even under the transformation $\nu \to -\nu$, whereas $g(\nu)$ must be odd. The two independent amplitudes $f(\nu)$ and $g(\nu)$ can be determined by an experiment using circularly polarized photons and a polarized nucleon target with spin parallel and antiparallel to the initial photon momentum.

In the CMS frame, this defines the helicity states 3/2 and 1/2. The optical theorem relates the imaginary part of an amplitude to the corresponding photo absorption cross section:

$$Im[T_{3/2,1/2}(\nu)] = \frac{\nu}{4\pi}\sigma_{3/2,1/2}(\nu) \tag{12.13}$$

Now, using the separation $T_{3/2} = f - g$ and $T_{1/2} = f + g$ and an unsubtracted dispersion relation, one obtains:

$$Re[g(\nu)] = \frac{2\nu}{\pi} P \int_{\nu_{thr}}^{\infty} \frac{d\nu'}{\nu'^2 - \nu^2} \frac{\nu'}{4\pi} \frac{\sigma_{1/2} - \sigma_{3/2}}{2} \tag{12.14}$$

The use of an unsubtracted dispersion relation relies on the reasonable hypothesis that $|g(\nu)| \to 0$ as $\nu \to 0$. Since the threshold energy is of the same order as the pion mass, the expression (eq. 12.14) can be expanded into a power series as well. Comparing the resulting series with the low energy expansion (eq. 12.12), one easily obtains the GDH sum rule (eq. 12.9).

The no–subtraction hypothesis is the only questionable assumption in deriving the GDH sum rule, but Regge arguments tell, that the GDH integral converges [Bass 97],[Coll 78].

Table 1.12.1: *Different predictions for the isospin decomposition of the GDH sum rule based on multipole analysis. All values are given in μb*

		[Karl 73]		[Work 92]	[Sand 94]		GDH
	$N\pi\pi$	$N\pi$	total	$N\pi$	$N\pi$	total	
I^{VV}	49	170	219	176	178	227	218.5
I^{SS}	1	2	3	-0.9 -0.4	-3	-2	0.3
I^{VS}	15	24	39	19	50	65	-14.7
proton			261			289	204.1
neutron			183			160	233.5

Apart from this classical way to derive the GDH sum rule, a number of other ways exist,which lead to the same result [Pant 98].

1.12.2.2.2 Multipole Predictions for the GDH Sum Rule

Up to the present, the GDH sum rule has never been verified experimentally. Various experiments in the resonance region will test its validity up to $E_\gamma = 3.5$ GeV. These experiments will check the predictions of the various multipole analysis (see e.g. [Sand 94]) for unpolarized single pion photo production as well as contributions from strangeness production and the onset of vector meson dominance.

Present predictions from exclusive single pion photo production fail to reproduce the GDH value, which is of inclusive nature, for proton and neutron alike.

These discrepancies become even more apparent, when an isospin separation is made [Karl 73]:

$$I^{VV} = \frac{2\pi^2 e^2 \kappa_V^2}{4M^2} = \int_{\nu_0}^{\infty} \frac{\sigma_{3/2}^{VV} - \sigma_{1/2}^{VV}}{\nu} d\nu \qquad (12.15)$$

$$I^{SS} = \frac{2\pi^2 e^2 \kappa_S^2}{4M^2} = \int_{\nu_0}^{\infty} \frac{\sigma_{3/2}^{SS} - \sigma_{1/2}^{SS}}{\nu} d\nu \qquad (12.16)$$

$$I^{VS} = \frac{2\pi^2 e^2 \kappa_V \kappa_S}{2M^2} = \int_{\nu_0}^{\infty} \frac{\sigma_{3/2}^{VS} - \sigma_{1/2}^{VS}}{\nu} d\nu \qquad (12.17)$$

Here the isovector–isovector (eq. 12.15) and isoscalar-isoscalar (eq. 12.16) predictions seem to agree reasonably well with the GDH value, but the isovector–isoscalar (eq. 12.17) prediction fails to reproduce the GDH value even in sign (see table 1.12.1).

For a more detailed review of the nucleonic aspects of the GDH sum rule and the contribution of different resonances and multipoles, the paper by Drechsel

[Drec 95] is strongly recommended.

1.12.2.2.3 Suggested Modifications to the GDH Sum Rule

The GDH sum rule (eq. 12.9) is derived by relying on fundamental physical properties of the Compton scattering amplitude in the forward direction. Furthermore, the validity of an *unsubtracted* dispersion relation for the spin dependent part $g(\nu)$ of this amplitude (eq. 12.10) is assumed.

In deriving the sum rule, there is no reason why this assumption should not hold. However, this assumption implies that for photon energies high enough, the total absorption cross section should become independent of the initial helicity state.

The test of the helicity dependent behavior of the cross section at high energies, i.e. the test of the no–subtraction assumption is one of the most important motivations for the proposed experiment.

The validity of an unsubtracted dispersion relation requires not only the sufficiently fast vanishing of the *imaginary* part of $g(\nu)$ for the integral to converge, but the real part has to vanish too, i.e. $g(\infty) = 0$. This was noted as early as in 1968, when the necessity of modifications to Compton scattering sum rules based on dispersion relations was discussed [Abar 68],[Fox 69]. In these works, the existence of an additional pole at $J = 1$ in the angular momentum plane at higher energies was predicted. Using invariant Compton scattering amplitudes (see e.g. [Lvov 97] for a recent description of the formalism), this pole would appear as a fixed pole at $t = 0$ in the asymptotic amplitude $A_4^{as}(\nu, t)$, which governs spin dependent compton scattering in forward direction above the resonance region. If this pole was the third component of an isovector, the problem for the $(p - n)$ difference (eq. 12.17) could be solved if [Petr 95]

$$\frac{8\pi^2}{M} a_4^p(0) = -\frac{8\pi^2}{M} a_4^n(0) \approx 66\mu b \tag{12.18}$$

Starting from the same ideas Chang et.al. [Chan 94] calculated a possible modification of eq. 12.9 based on current algebras. The predicted fixed poles can be attributed to non–trivial terms in the associated current commutators. The convergence of the GDH sum rule would imply, that the charge densities commute with each other. In contrast to this, it is claimed [Chan 92] that the vacuum expectation value of the triple commutator of charge densities generated by quark fields does not vanish, but is proportional to the number of colors carried by these fields. This modifies (eq. 12.9) to

$$\frac{2\pi^2 \alpha \kappa_{p,n}^2}{M^2} + S_{p,n} = \int_0^\infty \frac{\sigma_{\frac{3}{2}} - \sigma_{\frac{1}{2}}}{\nu} d\nu \tag{12.19}$$

These authors claim that the isovector – isoscalar discrepancy found in the evaluation of the traditional form of eq. 12.9 gives a hint that S does not

vanish. After applying their formalism they predict for the difference $S_p - S_n$:

$$S_p - S_n = \frac{e^2 G_A^{(3)}}{3F_\pi^2} = 137\mu b \tag{12.20}$$

with $G_A^{(3)} = 1.25$ being the Gamov–Teller β–decay constant and $F_\pi = 93$ MeV. This value would bring the predictions from the multipole analysis into qualitative agreement with the GDH prediction. Considering the fundamental nature of the GDH sum rule and its importance as a non perturbative limit of pQCD predictions, together with the discrepancies found in the predictions for the resonance region, these modifications would – if justified by the experiments– lead to serious doubts on our understanding of the electromagnetic structure of nucleons.

The proposed experiment would provide complementary data to the low energy experiments at Mainz and Bonn thus reducing the systematic error on the GDH sum rule value significantly.

1.12.2.3 Connection to DIS

The cross section of inclusive electron–nucleon scattering can be expressed by the product of the lepton tensor $L^{\mu\nu}$:

$$L^{\mu\nu} = \sum_{s'} \bar{u}(k,s)\gamma^\mu u(k',s')\bar{u}(k',s')\gamma^\nu u(k,s) \tag{12.21}$$

and the hadron tensor $W^{\mu\nu}$:

$$k_0' \frac{d\sigma}{d\Omega_e'} = \frac{2m}{s-m^2}\frac{\alpha^2}{Q^4} L^{\mu\nu} W_{\mu\nu} \ , \quad Q^2 = -(k-k')^2, \ s = (p+k)^2 \tag{12.22}$$

with k and p being the 4-momentum of the incoming electron and nucleon resp. and k' denoting the momentum of the outgoing electron. The hadron tensor describes the internal structure of the nucleon. Since this structure cannot (yet) be obtained in general by application of QCD, this hadron tensor is parameterized by four scalar, dimensionless structure functions.

For the absorption of transversely polarized virtual photons by longitudinally polarized nucleons with total spin 3/2 and 1/2 ($\sigma_{3/2}^T$, $\sigma_{1/2}^T$) the result of this tensor product reads:

$$\sigma_{3/2}^T = \frac{8\pi^2\alpha}{2m\nu - Q^2}\left(F_1(x,Q^2) - g_1(x,Q^2) + \frac{Q^2}{\nu^2}g_2(x,Q^2)\right) \tag{12.23}$$

$$\sigma_{1/2}^T = \frac{8\pi^2\alpha}{2m\nu - Q^2}\left(F_1(x,Q^2) + g_1(x,Q^2) - \frac{Q^2}{\nu^2}g_2(x,Q^2)\right) \tag{12.24}$$

It is the achievement of Anselmino et. al. [Anse 89] to note a strong connection between the weighted integral over the difference $\sigma_{3/2} - \sigma_{1/2}$ (dropping index T) to the first moment $\Gamma_1 = \int g_1(x)dx$ of g_1 which is linked to the Bjorken and Ellis–Jaffe sum rules in the scaling limit:

$$I(Q^2) = \frac{m^2}{8\pi^2\alpha} \int\limits_{Q^2/2m}^{\infty} d\nu(1-x)\frac{\sigma_{1/2}(x,Q^2) - \sigma_{3/2}(x,Q^2)}{\nu} \tag{12.25}$$

$$= \frac{2m^2}{Q^2} \int\limits_0^1 dx \left(g_1(x,Q^2) - \frac{4m^2x^2}{Q^2} g_2(x,Q^2) \right) \quad \text{for } Q^2 \neq 0 \tag{12.26}$$

At high Q^2 in the scaling region the second term of eq. 12.26 containing g_2 is negligible. Hence we obtain

$$I(Q^2) = \Gamma_1 \cdot 2m^2/Q^2 \quad . \tag{12.27}$$

The GDH sum rule provides an important constraint on the spin structure of the composite nucleon. It is complementary to the important Bjorken [Bjor 66] and Ellis–Jaffe [Elli 74] sum rules which relate the first moment of the nucleon's spin structure function $g_1(x, Q^2)$ to the axial coupling:

$$\Gamma_1^p - \Gamma_1^n = \frac{1}{6}\frac{g_A}{g_V}(1 - \alpha_S(Q^2) \pm \ldots) \simeq 0.19 \quad . \tag{12.28}$$

New interest in the GDH sum rule has not only been inspired by its technical feasibility, but even more by the so called spin problem of the nucleon. The spin problem consists of two parts.

The first is the x_{Bj} dependence of the spin structure function $g_1(x)$. Here, neither the behavior a, $x_{Bj} \approx 1$, nor its behavior at very low x_{Bj} is completely known experimentally or theoretically. Furthermore, the experimental values found for the first moment of g_1 indicate that a naive parton picture where the spin of the nucleon consists of the valence quark contribution fails. The problem of this so called spin crisis is still to be solved and has been widely discussed in literature.

Planned activities like the COMPASS, APOLLON or HERA upgrades, aim at a further understanding of these problems.

Secondly, the spin structure function g_1 depends on x_{Bj} and on Q^2: $g_1 = g_1(x, Q^2)$.

Therefore Γ_1 has a Q^2 dependence. For $Q^2 > 5\text{GeV}^2$, the experimental values of the first moment of g_1 seems to be in reasonable agreement with the theory, but for $Q^2 \to 0$, theory and experiment begin to diverge.

It was noted by Anselmino et.al. [Anse 89] that (eq. 12.9) can be interpreted as the $Q^2 = 0$ limit of the Ellis – Jaffe and Bjorken sum rules.

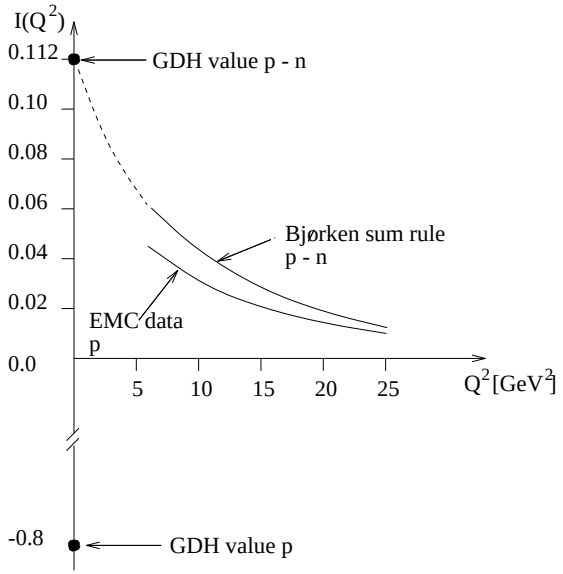

Figure 1.12.8: *GDH predictions compared to DIS sum rules*

This clearly shows the second part of the spin problem. Looking at the data (even when ignoring the predictions of the Ellis – Jaffe sum rule), $g_1(x, Q^2) > 0$ for Q^2 as low as a few GeV^2, g_1 is small and has a *positive* sign (see figure 1.12.8).

However, the $Q^2 = 0$ limit given by the GDH sum rule predicts a large value with a *negative* sign. This becomes even more complicated when looking at the proton neutron difference. Here the data not only seem to support the Bjorken sum rule, but the Q^2– evolution seems also to agree with the value predicted by the GDH sum rule indicating that the dramatic changes cancel in the $(p - n)$ difference.

Only experiments at low Q^2 like those proposed at TJNAF and at the photon point ($Q^2 = 0$) could help to disentangle this intriguing situation and shed some light on the transition for pQCD to the non–perturbative regime[Ma 97].

Acknowledgments

We would like to thank G.Anton, M.Düren, M. Schumacher and R. Van de Vyver for many interesting and fruitful discussions.

Bibliography

[Abar 68] H. D. I. Abarbanel, M. L. Goldberger: Phys.Rev. **165**(1968) 1594

[Anse 89] M. Anselmino et. al.: Sov. J. Nucl. Phys. **49**(1989) 136

[Bass 97] S.D. Bass: Mod. Phys. Lett. **A12**, (1997) 1051

[Bjor 66] J. D. Bjorken: Phys. Rev. **148**(1966) 1467

[Coll 78] P.D.B. Collins:*Regge theory and High Energy Physics*, Cambridge UP 1978

[Coll 84] P.D.B. Collins, A.D. Martin:*Hadron interactions*, Bristol 1984

[Comp 98] Courtesy of the Compas group, IHEP, Protvino, Russia, April 1998

[Chan 92] L.N. Chang, Y. Liang: Phys. Rev. **D 45**(1992) 2121

[Chan 94] L.N. Chang et. al.: Phys. Lett. **B 329**(1994) 514

[Clos 94] F.E. Close, R.G. Roberts: Phys. Lett. **B 336**(1994) 257

[Drel 66] S.D. Drell, A.C. Hearn: Phys. Rev. Lett. **16**(1966) 908

[Drec 95] D. Drechsel: Prog. Part. Nucl. Phys **34**(1995) 181

[Donn 92] A. Donnachie, P.V. Landshoff: Phys.Lett. **B296**(1992) 227

[Elli 74] J. Ellis, R. Jaffe: Phys. Rev. **D 9**(1974) 1444

[Fox 69] G. C. Fox, D. Z. Freedman: Phys. Rev. **182**(1969) 1628

[Gell 54] M. Gell–Mann, M. L. Goldberger: Phys. Rev. **96**(1954) 1433

[Gera 66] S. B. Gerasimov: Sov. J. Nucl. Phys. **2**(1966) 430

[Karl 73] I. Karliner: Phys. Rev. **D 7**(1973) 2717

[Low 54] F. Low: Phys. Rev **96**(1954) 1428

[Lvov 97] A.I. L'vov, V.A. Petrunkin, M. Schumacher: Phys. Rev. **C 55**(1997) 359

[Ma 97] W. X. Ma et. al.: **nucl–th/9712036**

[Pant 98] R. Pandtförder Thesis, Uni Bonn 1998

[Petr 95] V. A. Petrunkin: Contribution of fixed pole in Compton scattering amplitude on nucleon and generalised GDH sum rule; unpublished, Göttingen 1995

[Sand 94] A. M. Sandorfi et. al.: Phys. Rev **D 50**(1994) R6681

[Stei 96] A. STEINMETZ: The high energy contribution to the Drell-Hearn-Gerasimov sum rule of the proton, SMC 96/13

[Work 92] R. L. WORKMAN, R. A. ARNDT: Phys. Rev **D 45**(1992) 1789

1.13 Inverse Deeply Virtual Compton Scattering

M. Diehl, M. Düren, G. Anton

DVCS

One of the prime goals of ELFE is the in-depth study of skewed parton distributions (SPDs). As discussed in the ELFE report (Sect. 2.1.1) [1], their large information content offers a unique possibility to explore the dynamics of quarks and gluons in the nucleon and in other hadrons. A key process sensitive to SPDs is deeply virtual Compton scattering (DVCS),

$$e + p \;\; \rightarrow \;\; e + \gamma^* + p \;\; \rightarrow \;\; e + \gamma + p, \tag{13.1}$$

shown in fig. 1.13.1(a). Its main feature, compared with deeply virtual meson production, is that it competes with the calculable Bethe-Heitler process. The interference between the two offers a unique possibility to explore the virtual Compton process $\gamma^* + p \to \gamma + p$ at amplitude level. This interference term can be accessed either by single spin asymmetries or by reversing the lepton beam charge.

The measurement of DVCS is a challenge for experiment: it requires high energy, high luminosity, and one has to be able to select exclusive events where the scattered nucleon stays intact. Details of how the process will be measured in the electron beam program of ELFE are discussed in Sect. 3.1 of ref. [1].

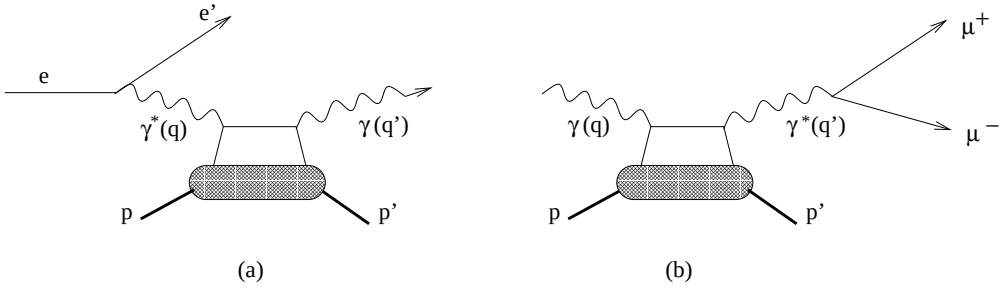

Figure 1.13.1: *The reversed version of the DVCS handbag diagram (a) is shown as diagram (b): a real photon scatters off a quark in the proton. In this exclusive channel, a virtual photon is produced which decays e.g. into a muon pair. The shaded blobs denote the skewed parton distributions.*

$\overline{\text{DVCS}}$

There is a 'sister process' to DVCS, where instead of the transition from a spacelike γ^* to a real γ one has the scattering of a real γ into a timelike γ^*,

which subsequently decays into a lepton pair, e.g., into $\mu^+\mu^-$:

$$\gamma + p \;\rightarrow\; \gamma^* + p \;\rightarrow\; \mu^+\mu^- + p. \tag{13.2}$$

We will call this process *inverse deeply virtual Compton scattering* ($\overline{\text{DVCS}}$). In the kinematical limit of large photon virtuality $Q'^2 = q'^2$, large squared c.m. energy $s = (p+q)^2$, and small invariant momentum transfer $t = (p-p')^2$ to the proton, this process factorizes in the same way as DVCS [2]. Fig. 1.13.1(b) shows the corresponding Feynman diagram.

Just like deeply virtual Compton scattering, $\overline{\text{DVCS}}$ interferes with a calculable Bethe-Heitler contribution, shown in fig. 1.13.2. It turns out that in the kinematical limit of $\overline{\text{DVCS}}$ the Bethe-Heitler contribution is large, so that the best access to $\overline{\text{DVCS}}$ is via the interference of the two processes. Different parts of the interference term can be extracted from the cross section: single spin asymmetries are sensitive to the imaginary part of the Compton amplitude $\gamma + p \rightarrow \gamma^* + p$, whereas the charge asymmetry in the angular distribution of μ^+ and μ^- projects out the real part of this amplitude. Notice that this charge asymmetry is the analogue of the beam charge asymmetry in DVCS, which can only be accessed at the expense of having both electron and positron beams. In contrast, the charge asymmetry in $\overline{\text{DVCS}}$ is readily measured in the final state. In the factorization regime there is a close connection of the amplitude

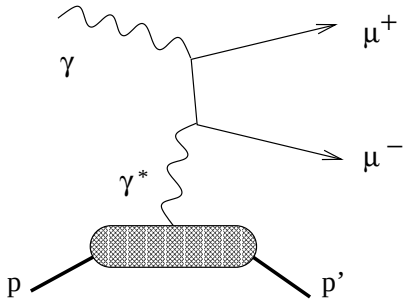

Figure 1.13.2: *The Bethe-Heitler pair production diagram interferes with $\overline{DVCS}$.*

for DVCS at given values of the photon virtuality Q^2 and Bjorken's variable x_B with the amplitude for $\overline{\text{DVCS}}$ at the corresponding values of Q'^2 and

$$\tau = \frac{Q'^2}{s}, \tag{13.3}$$

which acts as a scaling variable in the reversed process.

The values of Q^2 resp. Q'^2 where the factorization regime is reached may well be different, a situation that is well-known in the comparison of processes with spacelike and timelike photons. Judging from the experience gained in Drell-Yan muon pair production at hadron colliders and from hadron production in e^+e^- collisions, one can expect to see leading-twist dominance in $\overline{\text{DVCS}}$ for photon virtualities both below and above the J/ψ mass.

To conclude, the $\overline{\text{DVCS}}$ process allows one to experimentally access the same skewed parton distributions as the DVCS process, however using completely different experimental techniques. A detailed comparison of the scaling regimes of DVCS and $\overline{\text{DVCS}}$ will be of interest by itself, and provide strong consistency checks on the theoretical description and the extraction of the SPDs. The information on the real part of the Compton amplitude, which one can obtain from the angular distribution of the lepton pair in $\overline{\text{DVCS}}$, is not accessible in DVCS without both electron and positron beams, a feature not foreseen in the ELFE setup presented here.

Bibliography

[1] M. Anselmino, V. Braun, E. De Sanctis, *et al.*, **in** ELFE (Electron Laboratory For Europe) - Physics Motivations (draft version, 16 June 2000)

[2] J.C. Collins, L. Frankfurt and M. Strikman, Phys. Rev. **D56** (1997) 2982
J.C. Collins and A. Freund, Phys. Rev. **D59** (1999) 074009

Chapter 2

Experiments

2.1 Introduction

G. Anton, N. d'Hose and R. Van de Vyver

After the theoretical framework presented in the previous part, in this chapter the experimental conditions are described which are required for the realization of some typical experiments. The detailed requirements for the photon beam and the detectors will be touched upon in the last section (Detector Considerations).

This chapter is organized as follows :
In a first section, *J. Hössl together with N. d'Hose and G. Tamas* describe the experimental study of the 'real Compton scattering process'. This seems to be the most demanding experiment due to the very small cross sections involved. This measurement was originally proposed to be performed at the HERA facility at DESY/Hamburg in the context of the ELFE@DESY option, making use of a laser back scattering photon beam. Undoubtly such experiment could also be performed at a more dedicated electron accelerator facility like ELFE@CERN; because of the required high photon flux, it seems appropriate in the latter case to make use of coherent bremsstrahlung. This measurement will necessarily make use of a large acceptance detector for both photons and recoil protons in order to be able to distinguish this RCS process from competitive reactions such as photoproduction of π^0. The resolution in angle and momentum should be thus good that a clear separation between these final states is possible.
This chapter continues with a paper by *B. Seitz and K. Helbing* on 'Asymmetries in total real photo absorption' (the physics motivation has been presented in Section 1.12). This subject is ultimately connected with a study of the spin structure of the nucleon. The experiment also requires a large angle detector with high efficiency but with rather low resolution. As a total cross section is measured the photon flux can be relatively low.
In the next contribution by *M. Düren*, for which the theoretical motivation has been given in Section 1.10, the reader is referred to the Appendix where the full proposal of the 'Apollon project' can be found. This experiment aimes at the measurement of the polarization asymmetry of J/ψ photoproduction. Practically, the experiment could be carried out with a laser backscattered real photon beam (produced at the HERA ring) and using a muon pair spectrometer, placed behind the fixed, polarized target, in which the leptonic decay of the J/ψ channel will be detected.
Follows then a short contribution by *M. Diehl, M. Düren and G. Anton* on the basic requirements for an inverse deeply virtual Compton experiment, the motivation of which has been discussed in Section 1.13.
Finally, this chapter is concluded by a short section on 'Detector Considerations' (*G. Anton, N. d'Hose, K. Helbing and R. Van de Vyver*) in which some detection systems which are 'virtually' on the market and of which some might be needed for the realization of the proposed experiments, are briefly reviewed.

However, no conclusion concerning the choice of the detection system is drawn as there still exist too many unknowns with respect to the lay-out of the anticipated ELFE facility and to the priority of the various proposals.

2.2 Measurement of Real Compton Scattering and Vector Meson Photoproduction at High Energies

Jürgen Hößl, N. d'Hose and G. Tamas

The study of Real Compton Scattering (RCS) seems to be one of the most demanding experiments. Consequently, an adequate detector system for the measurement of this RCS process at a photon energy of 12 GeV has been studied. Detailed simulations prove the ability to extract the RCS events from a much larger background mainly from π^0 photoproduction. In addition the feasibility to measure simultaneously π^0, η, ω and Φ photoproduction is investigated.

2.2.1 Introduction

(This introduction been adapted from a study of 'Real Compton Scattering for ELFE at DESY' by N. d'Hose & G. Tamas)

The motivation for this RCS project has been presented in Sections 1.7 and 1.8. It may suffice to repeat that the RCS process represents a fundamental exclusive reaction which will provide us with new insights into the internal structure of the nucleon.

Real Compton Scattering has been extensively studied in the resonance region at photon energies up to 1 GeV, and in the diffractive regime (small θ_{CM}) at high photon energies. Just a few results at large scattering angle and high energy are available. Apart from data up to 2 GeV [1], [2], only measurements exist up to 6 GeV, performed at the Cornell Electron synchrotron [3]. These data show a behaviour of $d\sigma/dt$ in $f(\theta_{CM})s^{-n}$ where $n = 6.4 \pm 0.3$ which nearly indicates in this energy domain ($E_\gamma = 2 - 6$ GeV) the scaling law for the pQCD regime.

It is proposed to measure Real Compton scattering in the hard regime, at large s and t, even if Q^2=0. Consequently, θ_{CM} has to be large ($\simeq 90°$), so it has to be investigated from $\cos\theta_{CM} = 0.6$ to -0.6. Given

$$s = M_p^2 + 2M_p E_\gamma$$

$$t = -\frac{(s - M_p^2)^2}{2s}(1 - \cos\theta_{CM}),$$

the kinematical region studied in this experiment is summarized in Table 2.2.1.

E_γ (GeV)		8	10	12
s (GeV^2)		15.9	19.6	23.4
t (GeV^2)	($\cos\theta_{CM}$=0.6)	-2.8	-3.6	-4.3
	($\cos\theta_{CM}$=0)	-7.1	-9.0	-10.8
	($\cos\theta_{CM}$=-0.6)	-11.3	-14.3	-17.3

Table 2.2.1: *Kinematical domain for the Real Compton scattering experiment*

2.2.2 Requirements for the Detector System

A measurement of Real Compton Scattering (RCS) at photon energies between 8 and 12 GeV (around 90° in the CM-system: -0.6< $cos\theta_{CM}$ <0.6) imposes a lot of requirements on the detector system resulting from the ability of kinematics reconstruction and background separation.

In the above mentioned kinematic range both the photon and the proton from the RCS process are emitted in the laboratory frame at forward angles between 11 and 50 degrees. For kinematic reconstruction we therefore need a granular forward detector capable to distinguish between photon and proton hits.

The main background one has to deal with for RCS at high energies is π^0 photoproduction, which has a much larger cross section in the CM range around 90°. It can be parameterized as :

$$\frac{d\sigma/dt(\gamma p \to p\pi^0)}{d\sigma/dt(\gamma p \to p\gamma)} = \frac{1000\ GeV^2}{3s} \quad ([3])$$

Techniques applied in former RCS experiments [3, 1, 2] at energies between 2 and 6 GeV making use of the slightly different kinematics of RCS and π^0 photoproduction and the coplanarity of the RCS process can not be utilized at energies as high as 12 GeV as can be seen from table 2.2.2.

Therefore, it is necessary to identify the π^0 via both decay photons which should give separate hits in the detector. Because of the small angles between the two decay photons (e.g. 1.6° at 12 GeV and $\cos\theta_{cm}$=0.6, compare table 2.2.3) for symmetric π^0 decays, a high resolution 2π calorimeter is required. Special attention has to be paid to avoid one photon escaping from the detector system without detection. This can happen either if a photon escapes through unavoidable gaps or if the energy of the photon is below the detection threshold. For the first case it is essential to have a good energy resolution to recognize the missing photon by the missing energy deposit, for the second case a low threshold is required. A further difficulty associated with the latter case is, that for very asymmetric π^0 decays, which produce a low energy and a high energy photon, the high energy photon is emitted very close to the π^0 direction

perfectly faking an RCS event.

A further serious background component is η photoproduction: It has a large decay branching ratio (about 40%) into two photons. In contrary to π^0, symmetric η decays are no problem, because of the four times larger opening angle between the decay photons. As for the π^0, asymmetric decays of the η can simulate RCS events due to the very similar kinematics at 12 GeV at least at foreward angles (compare table 2.2.2).

Other reaction channels cause no complications, because they either lead to multiphoton events or contain more than one charged particle. A trigger, which accepts only events with one photon and one charged particle, will effectively suppress these reaction channels.

2.2.3 Proposed Set-up

For the photon detection we propose a high resolution 2π calorimeter consisting of about 3500 $PbWO_4$ crystals arranged in an rotational symmetry (47 rings) around the beam axis with 2π coverage (compare figure 2.6.3). Each of the crystals is orientated towards the center of the target station. The planned dimensions of the individual crystals vary between 9x9 cm^2 at 90 degree and 5x5 cm^2 at forward direction in diameter with a length between 25 cm and 33cm. The granularity of the proposed calorimeter increases in forward direction to guarantee separation of the two photons from π^0 decay as can be seen from table 2.2.3. π^0 decay photons do not hit the same or adjacent crystals. The overall length and diameter of the calorimeter are 350 cm and 250 cm respectively. A rescaling of the detector and crystal size to different dimensions, which would be more appropriate for running at a specific machine or scenario, will in principle not change the simulation results quoted below. (We simulated also a calorimeter with dimensions 300 cm $\times$ 150 cm [4] and obtained similar results.)

The advantage of $PbWO_4$ is the very short radiation length of 0.89 cm, the moliere radius of 2.2 cm and the large density of 8.28 gcm^{-3}. Figure 2.2.2 shows the extension of an electromagnetic shower in $PbWO_4$ induced by a 10 GeV photon compared to other commonly used material. Due to the small radiation length a crystal length of 25 cm is sufficient for $PbWO_4$. In addition $PbWO_4$ is a fast scintillator (about 10ns) with sufficient lightoutput (200 photons per MeV) and a high radiation hardness ($10^6 Gy$) allowing an operation at high photon fluxes.

In order to identify different reactions and reconstruct the kinematics of events, it is necessary to distinguish hits from charged particles and photons in the calorimeter. For that purpose a scintillating fibre vertex detector around the target provides the measurement of charged particles. This detector consists of two cylindrical layers (14 cm and 30 cm in diameter) around the target, each layer contains two sublayers of crossed scintillating fibres (angles against cylinder axis: $\pm 18^\circ$ for the inner layer, $\pm 22.5^\circ$ for the outer layer). The alignment of

the scintillating fibres on the two sublayers can be seen from figure 2.6.3. This geometry allows to reconstruct the crossing point of a charged particle in each of the two layers separately. From these points the track of the particle can be reconstructed. Each of the 1500 fibres has a thickness of 2mm providing a good position resolution and a length of 68cm for the inner and 115cm for the outer layer. The proposed fibre detector allows an identification of charged particles with an efficiency of more than 99.9%, determination of the number of charged particles produced in the process, reconstruction of interaction point within the target at a precision level of 1 cm, and determination of the impact point of charged particles in the photon calorimeter. Thus it is possible to discriminate between charged and neutral clusters in the calorimeter.

2.2.4 Performance – Simulation Results

A detailed simulation study was carried out to examine the performance of the proposed set-up and prove the ability to discriminate RCS events against background at a photon energy of 12 GeV. In addition we investigated the capability to measure different meson photoproduction reactions at high energies. For a most realistic simulation the following reaction channels

- $\gamma + p \rightarrow \gamma + p$
- $\gamma + p \rightarrow \pi^0 + p$
- $\gamma + p \rightarrow \pi^+ + n$
- $\gamma + p \rightarrow \eta + p$
- $\gamma + p \rightarrow \rho^0 + p$
- $\gamma + p \rightarrow \omega + p$
- $\gamma + p \rightarrow \eta' + p$
- $\gamma + p \rightarrow \Phi + p$

and effects

- tagging resolution of 0.1%

- energy resolution of $PbWO_4$ crystals: $\frac{3\%}{\sqrt{EinGeV}}$
- energy threshold: 30MeV for single crystal, 50MeV for cluster
- finite length of liquid hydrogen target: 28cm
- cross sections for different reactions (rough approximation for some channels because of lack of data and/or calculations at 12GeV)

were taken into account simultaneously.

General Performance

The scintillating fibre detector identifies charged particles produced in a reaction with Θ-angles between 10 and 90 degrees and allows to determine the tracks and impact points of these particles in the calorimeter.

Due to inactive cladding around each fibre (3% of fibre diameter) and threshold effects a detection efficiency of 95.6% [5] can be achieved for each of the four sublayers. This gives a detection efficiency of 99.8% for each layer (consisting of two sublayers) and an inefficiency of the whole fibre detector (two layers) of only 4×10^{-6}.

For track reconstruction the crossing points of the particle through both layers are required. This is only possible if each one of the four sublayers has triggered and leads to a track recognition efficiency of 83.5%. For reconstructed tracks the interaction point within the liquid hydrogen target along the target axis can be determined with an error (all quoted errors within this paper are 1σ-values) of 0.8cm and the error for the Θ-angle of the charged particle varies between 0.35° (at 11°) and 0.95° (at 85°). This precision allows to determine exactly the crystal that has been hit by the charged particle. A complication arises in the reconstruction of clusters induced by high energy recoil protons (up to 9GeV for RCS at 12GeV for our CM range), because of hadronic interactions of the proton in the $PbWO_4$ crystals (hadronic interaction length of about 20cm). This leads to deposition of energy in many crystals. Therefore only about 80% of the proton clusters can be reconstructed properly.

Energy and angle of photons produced in reactions either directly (as for example in RCS) or by decay of particles, are measured in the $PbWO_4$ calorimeter. For the Θ-angle an accuracy between 0.2° (at 11°) and 0.5° (at 50°) is achieved substantially better than the granularity of the calorimeter due to averaging over the crystals of a cluster. The good energy resolution of the crystals ($\frac{3\%}{\sqrt{EinGeV}}$) and the complete 2π geometry of the calorimeter permit the identifi-

cation of different exclusive meson photoproduction channels by invariant mass technique as will be shown in section 2.2.4.

Real Compton Scattering

To prove the capability to measure RCS at 12 GeV the above quoted reaction channels were taken into account in a Monte Carlo simulation (GEANT) trying to sort out the RCS events from the other channels.

For the kinematic reconstruction of the 2-body RCS process the measurement of two variables out of (E_γ,P'_p,θ'_p,E'_γ,θ'_γ) is sufficient. With the proposed setup in combination with the tagging system, we are able to measure (E_γ, θ'_p, ϕ'_p, E'_γ, θ'_γ, ϕ'_γ), which allows the efficient background suppression due to overdetermination of the kinematics.

The identification and reconstruction philosophy for RCS events consists in searching for two cluster events in the calorimeter, where one of these is identified as a charged cluster using the scintillating fibre detector and the other is a neutral cluster. Cuts on missing energy and topology of the photon (neutral) cluster (i.e. maximum energy in one single crystal of the cluster compared to total cluster energy) are applied to suppress those π^0 and η photoproduction events, where one photon is missing or the two photon hits are close together faking one cluster. The reaction $\gamma + p \rightarrow \pi^+ + n$ is suppressed by cuts on missing energy, because a neutron converts only a fraction of it energy to visible energy compared to a photon. ρ^0, ω, η' and Φ photoproduction events can be eliminated completely from the sample applying the above mentioned cuts, because they either lead to multicharged and/or multineutral final states or – in the case of the η' – have large mass and small $\gamma\gamma$- decay branchings.

In the remaining sample there survives – apart from RCS events – a certain fraction of π^0 and η events. The simulation indicates, that for the RCS experiment signal to background ratios of better than one (apart for the most backward CM bin) can be achieved, although the cross section for π^0 and η photoproduction at 12 GeV are about an order of magnitude higher than for RCS. For forward bins RCS can be measured almost without background (signal to background ratio better than 10), because the cross section ratio for RCS to π^0 photoproduction becomes more advantageous at forward angles and less decay photons from asymmetric π^0 decay are below detection threshold. The detailed result of the simulation is shown in table 2.2.4. An essential requirement according to the simulation is the low photon detection threshold of 50MeV. The remaining irreducable π^0 and η background can be determined from the precise simultaneous measurement of these channels using events with two neutral and one charged cluster in the calorimeter (see section 2.2.4).

Using the data between 2 and 6 GeV published in ref. [3] and pQCD scaling laws ($\frac{d\sigma}{dt} = s^{-6} f(\Theta_{CM})$), it is possible to make a rough RCS count rate estimate

ΔN for the different CM scattering angle bins:

$$\Delta N = \Phi_\gamma \times n_p \times \frac{d\sigma}{dt} \times \frac{dt}{dcos\Theta_{CM}} \times \Delta cos\Theta_{CM}$$

with

$$\Phi_\gamma \quad tagged\ photon\ flux$$

$$n_p \quad target\ protons\ per\ cm^2$$

$$\frac{d\sigma}{dt} \quad differential\ cross\ section$$

$$\frac{dt}{dcos\Theta_{CM}} = \frac{(s - m_p^2)^2}{2s}$$

$$\Delta cos\Theta_{CM} \quad width\ of\ CM\ bins$$

Assuming the number of tagged photons to be $10^8 s^{-1} GeV^{-1}$ at 12 GeV, operating a 28 cm liquid hydrogen target ($\rho = 0.07 g/cm^3$, $n_p = 1.2 \times 10^{24} cm^{-2}$) and the above proposed detector system, the count rates for the different bins with $\Delta cos(\theta_{cm}) = 0.2$ are given in the table 2.2.5.

It should be noticed, that with a 2π forward detector, all bins are measured simultaneously. In a measuring time of 100 days we can achieve for the most backward bin a statistical accuracy of 10% and for the most forward bin of 1.5% (for further details see table 2.2.4).

Meson Photoproduction

Different exclusive photoproduction reactions can be measured simultaneously with the RCS measurement, if a less stringent trigger is applied allowing in addition to the one charged cluster from the recoil proton more than one neutral cluster. All count rates and accuracies given below refer to a measuring time of 100 d.

π^0 and η photoproduction events are extracted from the simulated sample by looking for events with one charged and two neutral clusters in the calorimeter. Figure 2.2.3 shows the obtained invariant mass distribution for these two cluster events. There are two clean narrow peaks at the π^0 and η mass (σ width: 17MeV and 25MeV) almost without background. For π^0 the signal to background ratio is for all CM bins (-0.6< $cos\theta_{CM}$ <0.6) better than 100, for η better than 10. The η peak is about a factor of 10 smaller, because of the smaller cross section compared to π^0 (about factor 4) and the $\gamma\gamma$-decay branching (factor 2.5). The statistical precission we reach is for π^0 in $\Delta cos\theta_{CM}$ bins of 0.2 at 90° in the CM system (minimum of the cross section) about 3.5%, for the most forward and backward bins about 1%. For the η the respective numbers are 11% and 4%.

The proposed detector system allows besides π^0 and η also a measurement of photoproduction of the vector mesons ω and Φ at photon energies of 12

GeV. The ω is identified in the decay channel $\omega \rightarrow \pi^0 + \gamma$ (branching ratio of 8.5%), the Φ in the channel $\Phi \rightarrow \eta + \gamma$ (branching of 1.26%). The Monte Carlo sample is therefore scanned for events with one charged cluster (recoil proton) and three neutral clusters with an invariant mass of the ω and Φ respectively. A further background suppression is achieved, if we demand, that in the case of the ω two out of the three neutral clusters originate from a π^0 and for the Φ from an η.

The invariant mass distribution for events surviving the ω selection cuts are shown in figure 2.2.4. The ω peak is clearly separated from background events, mainly π^0 events (peak at the π^0 mass), where due to shower fluctuations the two decay photons were reconstructed as three neutral clusters. Expected count rates and accuracy for the different CM bins are given in table 2.2.6.

A measurement of Φ photoproduction is in contrast to the ω possible only at forward angles because of the smaller cross section compared to the ω and the smaller branching ratio for the detection channel $\Phi \rightarrow \eta + \gamma$. The obtained invariant mass distribution (figure 2.2.5) shows a clean peak at the Φ mass with no underlying background. The peak at 0.55GeV corresponds to η events ($\eta \rightarrow \gamma + \gamma$) which were reconstructed incorrectly as three cluster events. Up to now only data for the extreme forward angles $-t < 1GeV^2$ exist. With the proposed detector and photon flux we are able to extend this range up to $t = -3GeV^2$ as can be seen from figure 2.2.6. A coverage of this range is of special interest, because it permits a discrimination between a pomeron exchange and a two-gluon-exchange model [6]. In the later model a sharp drop in the cross section is expected at $-t > 1GeV^2$ with a minimum around $t = -2.5GeV^2$. For simplicity we have assumed in the simulation for the pomeron model a cross section

$$\frac{d\sigma}{dt} = 2\mu bGeV^{-2}e^{3GeV^2 t},$$

yielding the projected accuracy shown in figure 2.2.6 for CM bins Δt=0.1 GeV^2. For this cross section we expect a few hundred events in each Δt bin in the t range around -2.5GeV^2, whereas in the two gluon exchange model the event rate will be far below detection threshold.

Conclusions

The proposed 2π forward calorimeter in combination with a scintllating fibre vertex detector is well suited to measure RCS at energies as high as 12 GeV. In addition, simultaneously with the RCS process, many exclusive photoproduction reactions can be studied in the pQCD domain. We have explicitly shown the feasibility to measure the exclusive π^0, η, ω and Φ photoproduction on the proton. Concerning the Φ it will be possible to discriminate between a pomeron exchange and a two gluon exchange model.

In conclusion the proposed apparatus is a multi-purpose system which al-

lows to address many different physics issues improving our knowledge about the structure of the nucleon and mesons.

I would like to thank G. Anton, L. Van Hoorebeke, R. Van de Vyver and many others for fruitfull discussions and significant contributions to this work.

Bibliography

[1] M.Deutsch et al., Phys. Rev. D8 (1973) 3828

[2] J.Duda et al., Z. Phys. C17 (1983) 319

[3] M.A.Shupe et al., Phys. Rev. D19 (1979) 1921

[4] M.Quedzuweit, Diploma thesis (Universität Erlangen-Nürnberg, unpublished) 1998

[5] C.Küppersbusch, Diploma thesis (Universität Erlangen-Nürnberg, unpublished) 1998

[6] J.-M.Laget et al., Nucl. Phys. A581 (1995) 397

Table 2.2.2: *Comparison of kinematics of the RCS process, π^0 and η photoproduction at 12 GeV*

$\gamma p \to \gamma p$				
$cos(\theta_{cm})$	$\Theta_\gamma[deg]$	$\Theta_p[deg]$	$p_\gamma[GeV/c]$	$p_p[GeV/c]$
0.6	11.08	36.79	9.69	3.11
0.0	21.95	20.50	6.23	6.65
-0.6	42.41	10.59	2.76	10.13
$\gamma p \to \pi^0 p$				
$cos(\theta_{cm})$	$\Theta_\pi[deg]$	$\Theta_p[deg]$	$p_\pi[GeV/c]$	$p_p[GeV/c]$
0.6	11.07	36.78	9.69	3.11
0.0	21.92	20.50	6.23	6.64
-0.6	42.27	10.59	2.77	10.13
$\gamma p \to \eta p$				
$cos(\theta_{cm})$	$\Theta_\eta[deg]$	$\Theta_p[deg]$	$p_\eta[GeV/c]$	$p_p[GeV/c]$
0.6	10.90	36.65	9.71	3.07
0.0	21.41	20.46	6.28	6.56
-0.6	40.23	10.58	2.84	10.00

Table 2.2.3: *Comparison of minimum open angle between the two decay photons from π^0 photoproduction at 12 GeV and granularity (in degrees) of the proposed calorimeter for different laboratory angles Θ.*

Lab Angle [deg]	minimum openening angle for π^0 decay	granularity
11	1.6	0.8
20	2.3	1.1
30	3.5	1.7
40	5.1	2.5
50	7.2	3.8
70	12.2	4.7
90	17.8	5.1

Table 2.2.4: *Expected signal to background ratio for the measurement of RCS at 12 GeV for different center of mass angles and statistical error in 100 d measuring time (simulation results).*

$cos\Theta_{CM}$	signal/background	statistical error
-0.6 - -0.4	0.8	10%
-0.4 - -0.2	2.5	7.5%
-0.2 - 0.0	6.4	6.5%
0.0 - 0.2	15	4.8%
0.2 - 0.4	30	3.1%
0.4 - 0.6	39	1.5%

Table 2.2.5: *Expected countrate for the measurement of RCS at 12 GeV for different center of mass angle bins incorporating reconstruction efficiency factors*

$cos\Theta_{CM}$	$\frac{d\sigma}{dt}[\mu bGeV^{-2}]$	reconstruction efficiency	countrate [1/h]
-0.6 - -0.4	1.7×10^{-7}	0.54	0.09
-0.4 - -0.2	2.0×10^{-7}	0.54	0.10
-0.2 - 0.0	2.7×10^{-7}	0.45	0.11
0.0 - 0.2	4.8×10^{-7}	0.41	0.18
0.2 - 0.4	1.1×10^{-6}	0.43	0.43
0.4 - 0.6	4.5×10^{-6}	0.46	1.88

Table 2.2.6: *Expected countrates for the measurement of ω photoproduction at 12 GeV for different center of mass angle bins (simulation results)*

$cos\Theta_{CM}$	countrate per 100 days	expected error
-0.6 - -0.4	400	5%
-0.4 - -0.2	250	6%
-0.2 - -0.0	120	9%
0.0 - 0.2	85	11%
0.2 - 0.4	60	13%
0.4 - 0.6	820	4%
0.6 - 0.8	32600	0.6%
0.8 - 1.0	2.1×10^7	0.02%

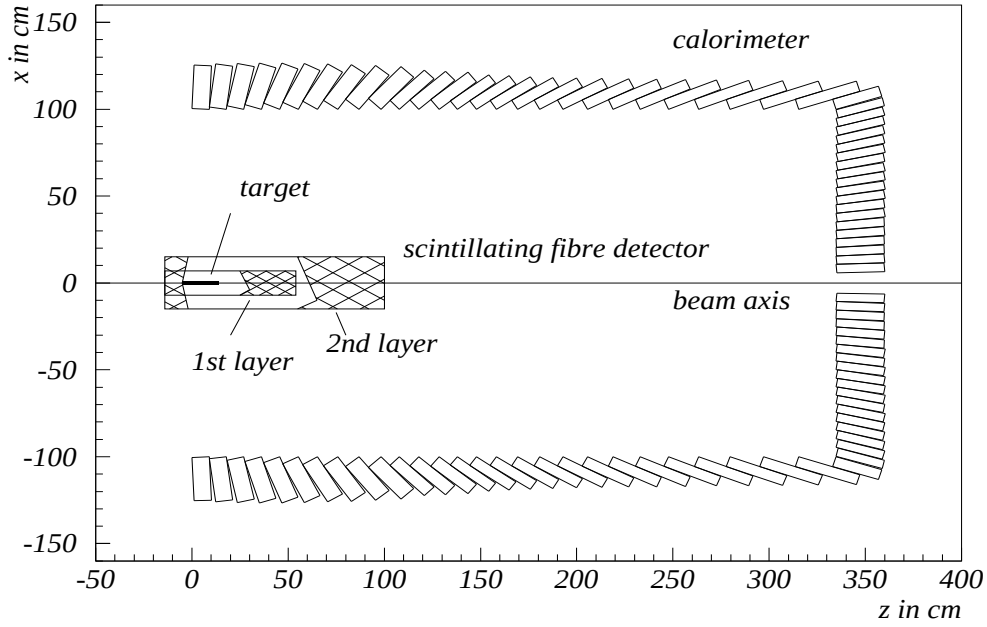

Figure 2.2.1: *Proposed detector system for the RCS experiment*

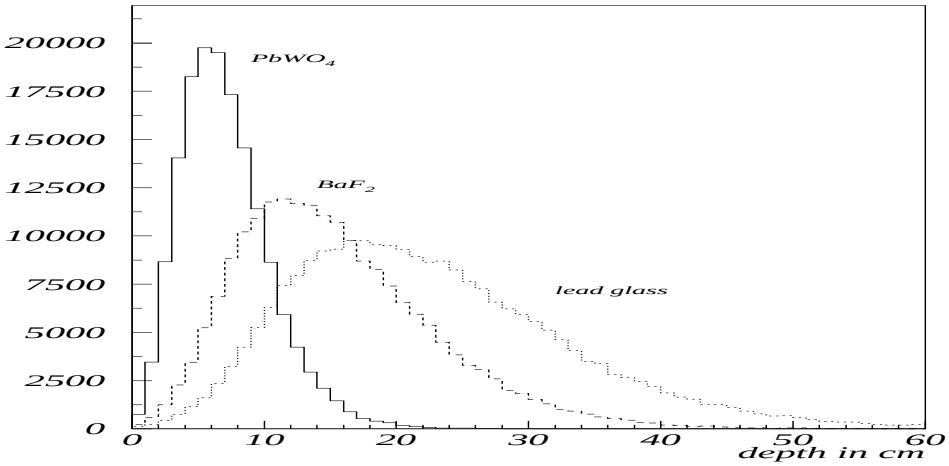

Figure 2.2.2: *Extension of an electomagnetic shower induced by a 10 GeV photon for different commonly used materials (simulation results)*

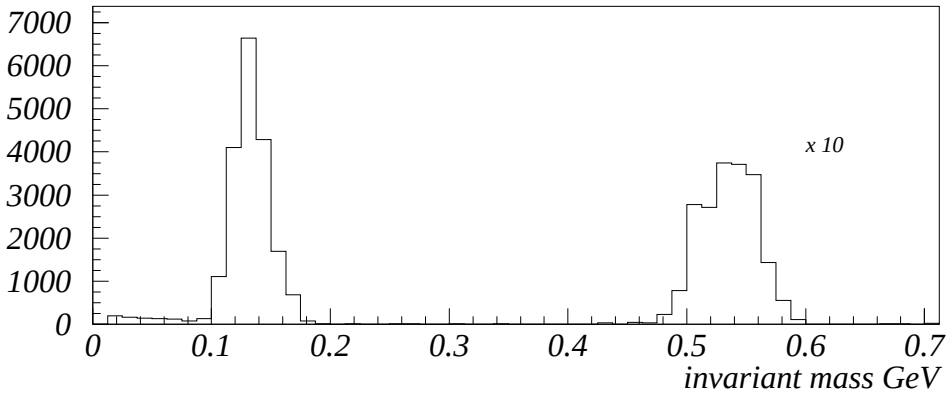

Figure 2.2.3: *Reconstructed invariant mass distributions for π^0 and η events, 2 neutral clusters (simulation results); η peak enlarged by a factor of ten*

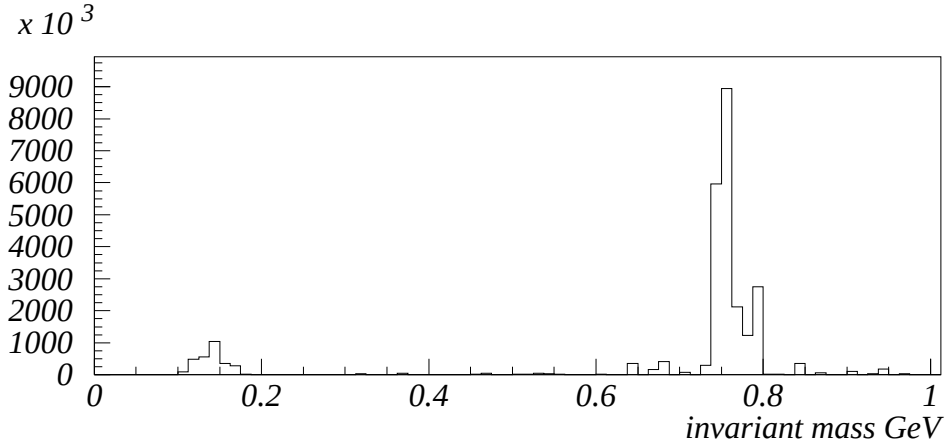

Figure 2.2.4: *Invariant mass distributions for ω selection cuts (3 neutral clusters, for details refer to text), simulation results*

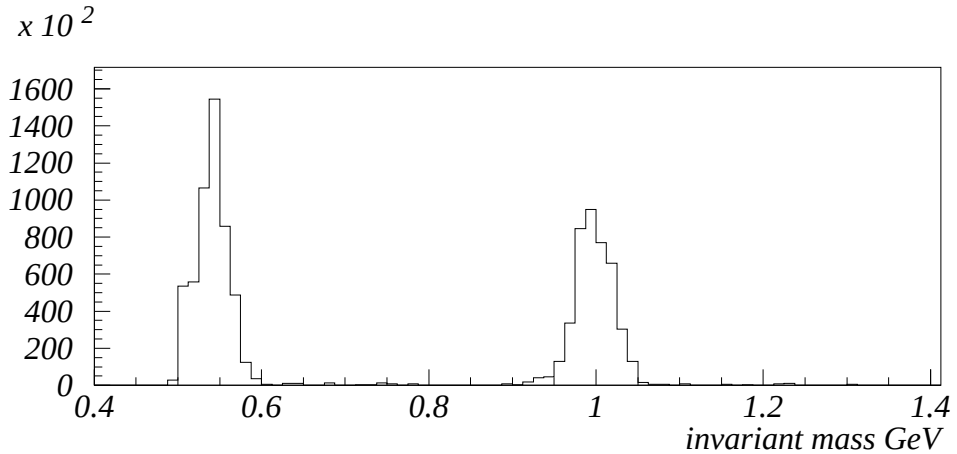

Figure 2.2.5: *Invariant mass distributions for Φ selection cuts (3 neutral clusters, for details refer to text), simulation results*

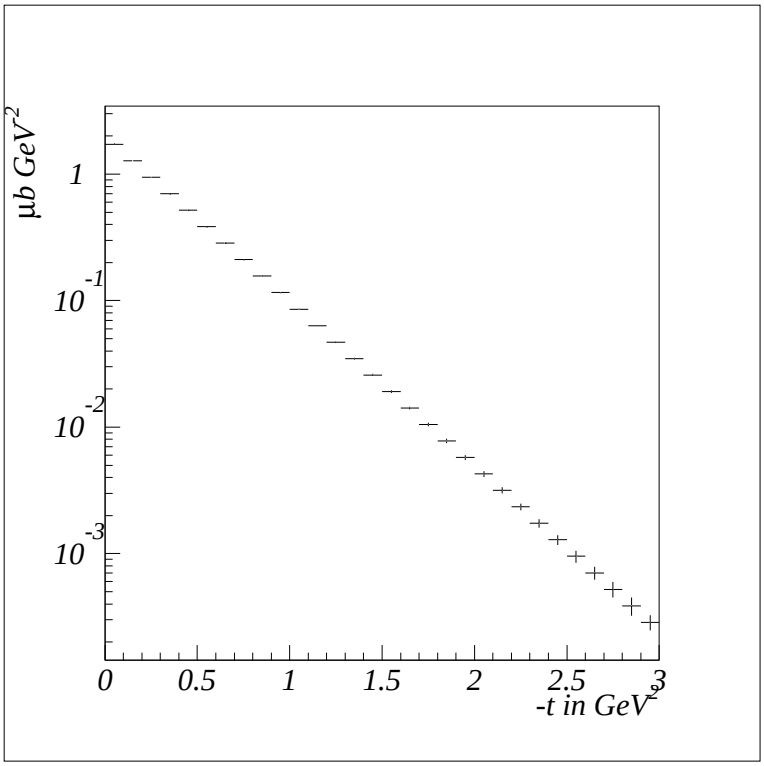

Figure 2.2.6: *Expected accuracy for* Φ *cross section measurement for 100 days measuring time (for details see text), simulation results*

2.3 Asymmetries in total real photo absorption

Björn Seitz and Klaus Helbing

Helicity dependent photo absorption measurements at $Q^2 = 0$ provide a unique tool to investigate the nucleon spin structure. They provide new constraints on Regge theory and to trajectories connected to polarization observables. Furthermore, the high energy behavior of the integrand of GDH sum rule which is strongly connected to the Ellis Jaffe and Bjorken sum rules will be investigated. In this contribution we review the physical relevance and discuss experimental options of such measurements in the energy region of about 3 to 30 GeV.

2.3.1 Introduction

See Chapter 1, Section 1.12.

2.3.2 Physical Motivation

See Chapter 1, Section 1.12.

2.3.3 Experimental Aspects

The experiment proposed in this paper deals with the helicity dependence of total photo absorption for a wide range of photon energies. This requires circularly polarized photons and longitudinally polarized nucleons to define the initial helicity state together with a total absorption detector. Total photo absorption cross sections can be measured in several ways:

- by an exclusive measurement identifying all reaction channels, deducing their individual cross sections and adding up to the total. This requires a rather complicated apparatus, as soon as multi particle final states become important. Furthermore, the individual uncertainties of each reaction channel increase the systematic error.
- by an inclusive measurement, where only the number of produced hadrons is detected, neglecting the identification of the reaction where it came from. This keeps the setup rather simple, but requires a good knowledge of detection efficiencies and a large solid angle, since corrections for these effects might prove difficult to estimate.
- by an absorption measurement, where the difference between the number of incoming and outgoing photons is counted. This requires a rather

simple setup, but gives quite large uncertainties in the final results, since the atomic cross section has to be known quite accurately and has to be subtracted from the result to obtain the true number of hadronic events.

This leads to a considerable uncertainty, since the atomic cross sections are by several magnitudes larger than the hadronic ones. Therefore, this method is not considered in the following.

General considerations at HERA

The experimental setup at DESY can be kept comparatively simple. Circularly polarized photons can be produced by Compton backscattering of circular Laser light on the HERA electron beam. Using this technique, photon energies of 13 GeV and a polarization degree of well above 0.8 can be achieved with a Pockels cell and a standard Argon laser. Using frequency doubled lasers, photon energies up to 18 GeV are possible with the existing electron ring.

Even higher photon energies can be achieved if coherent bremsstrahlung is exploited to produce circularly polarized photons. The upper limit for the photon energy is in this case the energy of the primary lepton beam [Seit 98]. The drawback of this technique is that the maximum degree of polarization is given by the polarization of the lepton beam. This is expected to be of the order of 0.7.

Longitudinally polarized Nucleons can be obtained by well established techniques like Butanol in frozen spin mode or new techniques like a frozen HD target, which e.g. is now under development for the low energy experiments at GRAAL and LEGS (see Section 3.8). For these targets, a polarization degree of 0.8 seems to be feasible.

In the proposed energy region, multiple particle states will dominate the reactions.The reconstruction of all these reaction channels would be very complicated. Therefore the inclusive method has been chosen. It requires a highly efficient detector for charged and neutral reaction products and a high coverage of solid angle. Similar techniques have be chosen for experiments in the upper resonance region at ELSA and SPring 8, since these experiments face the same situation. This also helps to keep the cost of such an experiment quite low.

Example setup at HERA for the "APOLLON area"

The following section describes some first ideas for an experimental setup at the proposed APOLLON facility[1] at HERA (See also Section 1.10 and the Appendix). For the photon flux the same limits are chosen as for APOLLON. If the real photon facility would run in parallel to the collider experiments, this is a realistic upper limit.

[1] i.e. an area close to the electron and proton beam with intersecting beam pipes

The APOLLON design goal is a photon flux of $4 \times 10^6 s^{-1}$ in the energy range 16.5 GeV $< E_\gamma <$ 18.5 GeV. This will be reached by using a frequency doubled cw Argon laser and an amplifying optical cavity. Since this need for a high power UV Laser is the most complicated case, lower photon energies should be much easier to produce with a given laser apparatus. Using the same setup without the frequency doubling would give an photon beam with 10 times the flux at $E_\gamma = 12.5$ GeV.

Since the energy of the incoming photon will be determined by the tagger in coincidence with an event in the detector, a fast trigger is desirable to get a good timing resolution. This is mandatory for an experiment using tagged photons to facilitate the separation of true coincidences ("good events") from random background. A second timing signal could be taken from the HERA bunch frequency, but nevertheless, a part of the setup should consist of fast detectors with excellent timing properties.

The geometry of the detector has to follow certain boundary conditions. The place where to put the setup is limited by the HERA electron and proton beam pipes and the space available in the HERA East Hall. Since the separation between photon beam line and electron beam is quite small, the electron beam pipe has to pass through the detector. Furthermore, since the aim is an inclusive measurement, no background should be produced by that beam line, which enters the detectors. One design goal is to keep the detector as simple as possible. Therefore it will be quite difficult to separate background events and every effort has to be taken to make this contribution as low as possible.

The need for a large solid angle coverage favors a barrel-like geometry. Kinematical considerations – most of the events will be peaked in the forward region – will permit to put the target in the upstream part of the detector and not in its centre. This facilitates also the design of the target, which can be kept rather compact and will remain easily accessible.

Figure 2.3.1 shows a possible design of such an detector. It consists of an octagonal barrel of Lead Glass detectors, which is left open where the electron beam pipe goes through. Lead Glass is sufficiently fast and has a good efficiency for photons and fast charged particles in this energy range. In addition a similar barrel of fast plastic scintillators is put in the middle. This should serve as a fast trigger detector and, additionally, allow to separate charged from neutral events.

The backward region can be kept open for kinematical reasons. The front part will be covered by a similar sequence of plastic scintillators and a lead glass array, with a hole for the electron beam pipe and the primary photon beam. A common problem of forward angle detectors is, that all the atomic background is peaked into the forward region. Whether an additional detector for suppressing this background will be necessary is subject to further studies.

In the far forward region, a photon flux monitor should be installed for normalization purposes. Here the same detector as for APOLLON could be

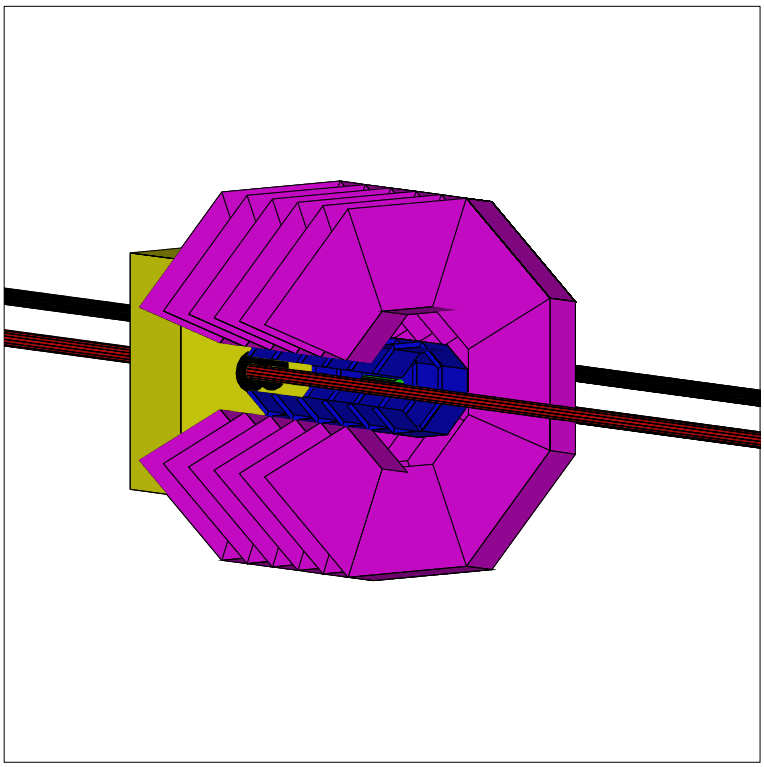

Figure 2.3.1: GEANT picture of a possible setup at HERA

used.

The detector system is quite compact and uses only known techniques. The total number of detector modules is about 60, so standard VME 64 channels modules can be used, which offer compact electronics and a fast and convenient read out.

Setup at a dedicated facility

Like in subsection 'Example setup at HERA for the Apollon area' the measurement of the total photo absorption cross section by the inclusive method is considered but, in contrast now, an experimental area is assumed to be available without disturbing beam pipes.

In this scenario a slightly modified version of the GDH-Detector could be used which is currently in operation at ELSA to measure the GDH sum rule.

The concept of the GDH-Detector is based upon the measurement of the cross section by the detection of all hadronic processes with maximum efficiency with regard to solid angle and to detection probability. The suppression of electromagnetic background is achieved by means of a threshold Čerenkov

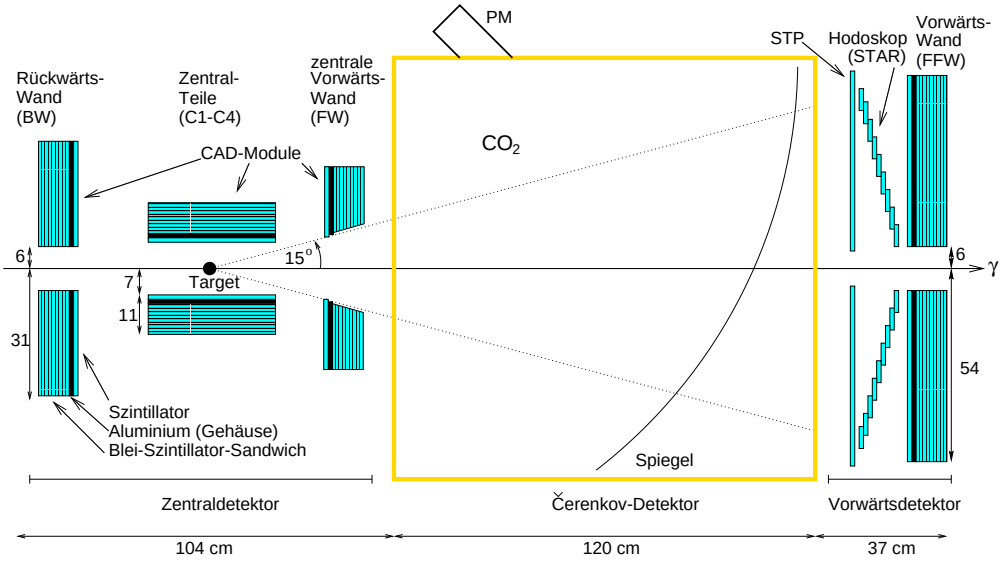

Figure 2.3.2: Schematic view of the GDH-detector

counter [Helb 93]. Hadrons are detected with CAD[2]-modules which have a scintillator-lead-sandwich structure. More than 99 % of the total solid angle around the target are covered by these modules. The complete setup consists of the 'Backward Wall' (to detect particles scattered in backward direction), the Central Parts (4 CAD-modules to cover the solid angle cylindrically around the target), the Forward Wall (to detect particles flying in forward direction), the Čerenkov detector (to veto electromagnetic events), the STAR-detector (to give an azimuthal resolution) and the Far Forward Wall (to cover the solid angle in the forward direction which is not covered by the Forward Wall) (see figure 2.3.2). This setup has been tested in Bonn using the PHOENICS beam in measurements on total cross sections of unpolarized targets of C, CH_2, CD_2 [Helb 97, Saue 98]. A method has been developed which enables one to subtract background without rejecting hadronic events. This gives the possibility to measure the total cross section without having to apply any corrections or extrapolations due to inefficiencies or unseen processes. Excellent agreement with previously measured data has been found. Higher precision data than previously available for carbon were obtained.

A schematic view of the GDH-Detector as it is in use at ELSA is shown in Fig. 2.3.2.

The only modifications needed for operation at higher energies up to 30 GeV concern the threshold Čerenkov veto counter. Since at these energies the produced pions become more and more relativistic, the Čerenkov threshold has to be lowered. The refractive index corresponding to a threshold low enough is

[2]Charged particles And Decay photons

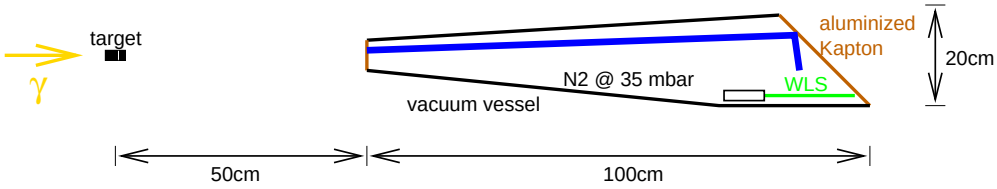

Figure 2.3.3: Underpressure threshold Čerenkov veto counter

given by

$$n = \sqrt{\frac{\gamma^2}{\gamma^2 - 1}},\ \gamma^{\pi^\pm}_{\max} \simeq 200 \Rightarrow (n-1)\cdot 10^6 \simeq 11 \qquad (3.1)$$

Such a low refractive index cannot be achieved with any gas at atmospheric pressure. This means that the Čerenkov counter has to be rebuilt as a vacuum vessel. Then a convenient choice could be N_2 at a pressure of 35 mbar. For the detection of the hadrons it is necessary that this vacuum vessel does not absorb the reaction products. A conic structure therefore is recommended to keep the "dead" solid angle at a minimum. In addition, the stronger Lorentz boost and the kinematical correlation of the produced electrons and photons of the background processes enables one to reduce the polar angle coverage to $\theta = 3°$ of the Čerenkov veto as compared to the setup currently in use with its 15° coverage.

A suggestion for such a new underpressure Čerenkov counter is given in Fig. 2.3.3. The Čerenkov light produced in the vessel is reflected by the aluminized kapton entrance and exit foils. The reflected light is absorbed by a wave length shifter which guides the reemitted light to a photo multiplier.

Thus, at an experimental area without intersecting beam pipes one could easily reuse the GDH-Detector in conjunction with a new Čerenkov counter.

Acknowledgments
We would like to thank G.Anton, M.Düren, M. Schumacher and R. Van de Vyver for many interesting and fruitful discussions.

Bibliography

[Helb 93] K. Helbing: Konzeption eines Detektors zur Überprüfung der Drell-Hearn-Gerasimov Summenregel, Diploma thesis, Bonn, 1993

[Helb 97] K. Helbing, Messung von totalen Photoabsorptionsquerschnitten mit dem GDH-Detektor, PhD thesis, Bonn, 1997

[Saue 98] M. Sauer, PhD thesis, Tübingen, 1998

[Seit 98] B. Seitz, F. A. Natter et. al.: Using Coherent Bremsstrahlung for high energy photons at HERA and ELFE, this proceedings

2.4 Apollon

M. Düren

The theoretical motivation for the Apollon project has already been briefly presented in Chapter 1, Section 1.10 and will not be repeated here.
For an extensive description of the proposed experiment, we refer the reader to the Appendix where the full proposal (about 40 p.) is reproduced. This experiment has been designed such that, with the use of a real photon beam produced by laser backscattering, it could be installed at the present HERA ring at DESY.
This proposal can also be downloaded from the web at :

http://dxhra1.desy.de/apollon/documentation.html

2.5 Inverse Deeply Virtual Compton Scattering Experiment

M. Diehl, M. Düren, G. Anton

As described in Section 1.13, the inverse deeply virtual Compton scattering ($\overline{\text{DVCS}}$) process offers a unique experimental option to measure skewed parton distributions of the nucleon. To perform a measurement, a real photon beam of sufficient energy and luminosity is required, and a detector is needed which measures the final state electron or muon pairs. The important kinematical variables are the energy of the incoming real photons E, the invariant mass of the final state lepton pair $Q'^2 = q'^2$, and the scaling variable $\tau = Q'^2/s$ with $s = 2EM + M^2$ being the center of mass energy of the event and M the nucleon mass. Because of the correlation of the variables τ and Q'^2, given by

$$Q'^2 \;=\; \tau\,(2EM + M^2), \tag{5.1}$$

it is necessary to have a wide spectrum of beam energies as one needs to measure the process as a function of both variables τ and Q'^2 in order to check the predicted scaling behavior in Q'^2 and to extract the SPDs.

A tagged Compton backscattered beam of real photons offers exactly this possibility as it gives a relative flat distribution of photons in a wide energy range. Taking a photon energy range of e.g. $E = 4 \ldots 12$ GeV, and applying the kinematical cuts $Q'^2 > 1$ GeV^2 and -0.5 GeV$^2 < t < 0$ GeV^2 to the data, the $\overline{\text{DVCS}}$ cross section can be measured as a function of the two relevant variables τ and Q'^2 for $\tau = 0.04 \ldots 0.48$, i.e., both in the sea and valence range of the SPDs, with a maximum value for Q'^2 of 11 GeV^2. The invariant momentum transfer t to the proton can be extracted from the measured lepton momenta. The exclusivity of the event has to be determined either by directly measuring the final state proton or by reconstructing its momentum from the beam and lepton momenta.

A first sketch of a possible detector for $\overline{\text{DVCS}}$ at ELFE is shown in fig. 2.5.1. Here the muon pair is measured in a dipole spectrometer. The final state proton is detected in a vertex detector.

Calculations of the cross section of $\overline{\text{DVCS}}$ and especially of the interference term of BH pair production and $\overline{\text{DVCS}}$ will have to show if the count rates are in an acceptable range to be measured with today's technology. As discussed in Section 1.13, the interference term can be accessed by lepton charge and spin asymmetries. The real photon beam can be highly polarized, the target can be polarized, and the charge asymmetry can be obtained from the decay angles of the lepton pair. A wealth of information can thus be obtained at ELFE about the dynamics of $\gamma + p \to \gamma^* + p$ at amplitude level.

As a side remark we mention that the $\overline{\text{DVCS}}$ experiment described here can at the same time be used to measure J/ψ production at threshold (see Section

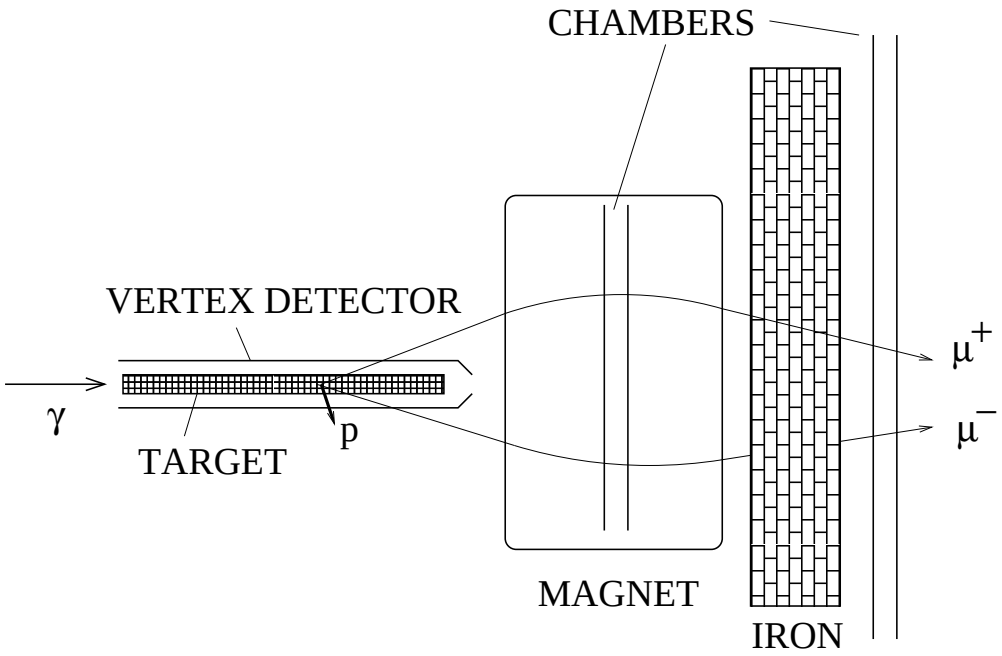

Figure 2.5.1: *A simplified sketch of a $\overline{DVCS}$ detector: the real photon hits a long, pencil-like target. The recoil proton is detected in the vertex chamber. A magnetic spectrometer measures the momenta of the outgoing muons. The muon-identification is done by an iron absorber, followed by muon chambers.*

1.4) and to determine the gluon polarization as described in the Apollon section 1.10 (and in the Appendix) of the present report.

2.6 Detector Considerations

G. Anton, N. d'Hose, K. Helbing and R. Van de Vyver

In the previous sections, 3 types of experiments are identified that could be performed at the planned photon facility and for which there exists an adequate scientific justification :

1. Compton scattering of real photons
2. asymmetries in total real photon absorption
3. photoproduction of J/ψ mesons (Apollon)

The general physics constraints imposed by the various experiments are listed in Table 2.6.1; these requirements will, to some extent, also determine the detector characteristics.

Experiment	Apollon	photoabsorpt.	RCS	Mes. spec.
E_γ [GeV]	> 18	3 - 20	8 - 12	3 - 20
tagging rate [MHz]	> 4	1 - 2	100/GeV	10
duty factor [%]	>1	>10 - 20	>50	>50
energy resol. ΔE [%]	<0.5	<3	<0.1	<0.1
linear polarization [%]	-	-	-	30 - 80
circular polariz. [%]	>50	>50	>50	>50
Target	p,n	p,d	p	p,(n)
Target polarization	>50	>50	>50	>50
Target density [g/cm^2]	5 - 10	3 - 5	5 - 10	5 - 10
Reaction	$J/\psi \to \mu^\pm, e^\pm$	$\gamma p \to X$	$\gamma p \to \gamma p$	$\gamma p \to \gamma M$
polar angle θ [deg]	2 - 40	0.5 - 170	2 - 90	2 - 90
PID	$\mu^\pm, e^\pm$ magnet	hadron absorp. elm. suppress.	p, γ calorim. no magnet	p, K, π magnet

Table 2.6.1: *General physics constraints determined by the various experiments*

From this table it is obvious that the requirements imposed on a detector are rather specific for the various proposed experiments and different from what earlier has been proposed for the ELFE physics programme (such as e.g. FAST, the Forward Angle Spectrometer [1]. Consequently, special detectors have been designed and optimized for the different experiments. In a later stage of the project it may be necessary to combine the different requirements and abilities in order to design and develop one single detector for all experiments. This can be done once the boundary conditions for the realization of the photon beam project are known.

A relatively simple detector will be needed for the measurement of asymmetries in total photo aborption (see also Sections 1.12 and 2.3). In Fig. 2.6.1 the detection set-up is shown which is presently being used in the GDH-experiment at ELSA/Bonn [2]. This consists of a central scintillator detector (CAD modules), a gas (or aerogel) threshold Cherenkov counter for the suppression of the electromagnetic background, and some forward components which cover the smaller angles. Such simple and relatively low-cost device could easily be adapted for the measurements in the 3 - 20 GeV energy range. As such, this experiment which does not put very stringent requirements on the beam characteristics could serve as a pilot project for the initial tests of the real photon facility.

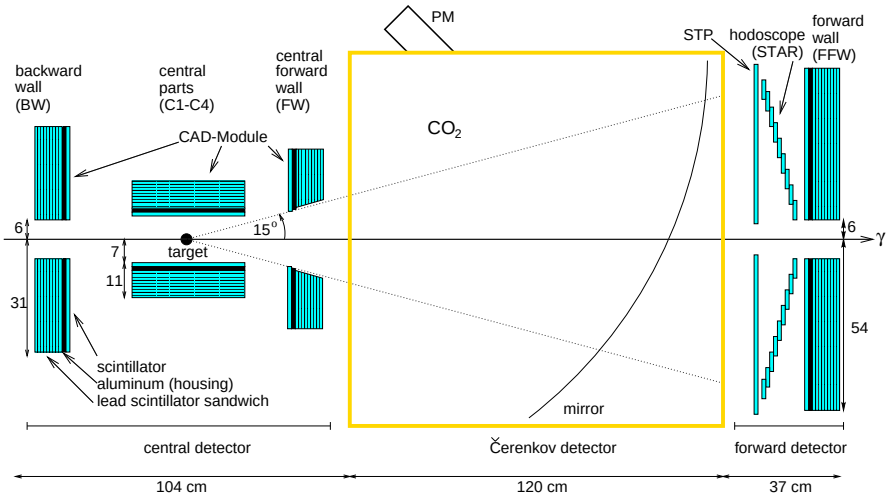

Figure 2.6.1: *The global detection system for the GDH experiment at ELSA/Bonn*

For the Apollon project (see Section 1.10 and the Appendix) there exists a detailed lay-out of the experimental set-up including the proposed detector; this latter is shown in Fig. 2.6.2. It was designed for installation at the HERA ring (DESY,Hamburg) where the real photon beam would be produced using the Laser Backscattering technique. The decay muons of the produced J/ψ's will be detected in the modular toroidal magnetic spectrometer, allowing also magnetic analysis and further hadron absorption. For a full description of the system, the reader is referred to the Appendix. Also in this case it seems obvious that the Apollon collaboration has a precise view of its experimental needs and it is not expected that the project would meet further major difficulties.

The proposed study of Real Compton Scattering (see section 2.2) seems to be the most demanding experiment, both from the point of view of beam requirements (photon flux !) as well as from detector specifications. Indeed,

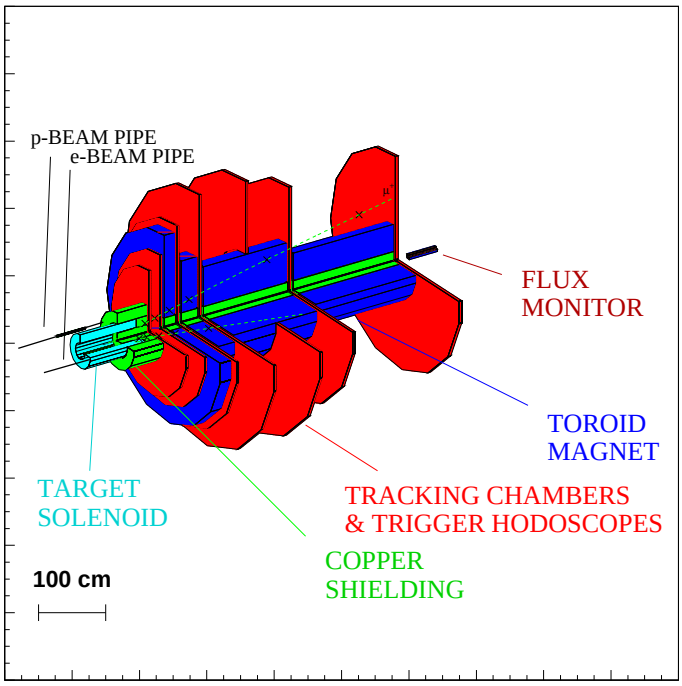

Figure 2.6.2: *The Apollon detector*

this measurement requires a large acceptance detector (see fig. 2.6.3) for both final state particles, the photon and the proton, in order to distinguish this real Compton process from competing reactions such as photoproduction of π^o's . The resolution in angle and momentum should be thus good that a clear separation between those final states is possible. A rather detailed study of these issues is given in Section 2.2 to which the reader is referred.
As far as the experimental study of the photoproduction of vector mesons is concerned, the present group has not looked in detail at the specific detector needs (within the framework of the ELFE project, some studies were performed for such 'large solid angle detector' called MEMUS [3]; this will not be further discussed here). However, in the case of vector mesons (i.e. $\omega, \Phi, ...$) which decay into photons, a full simulation has been carried out with the detector for real Compton scattering (see also Section 2.2).

From the previous discussion, it follows that it is very unlikely that just one detector system could satisfy all the requirements as imposed by the various experiments. On the other hand, not all proposed systems need to be extremely expensive. Nevertheless, once a clear view will be available concern-

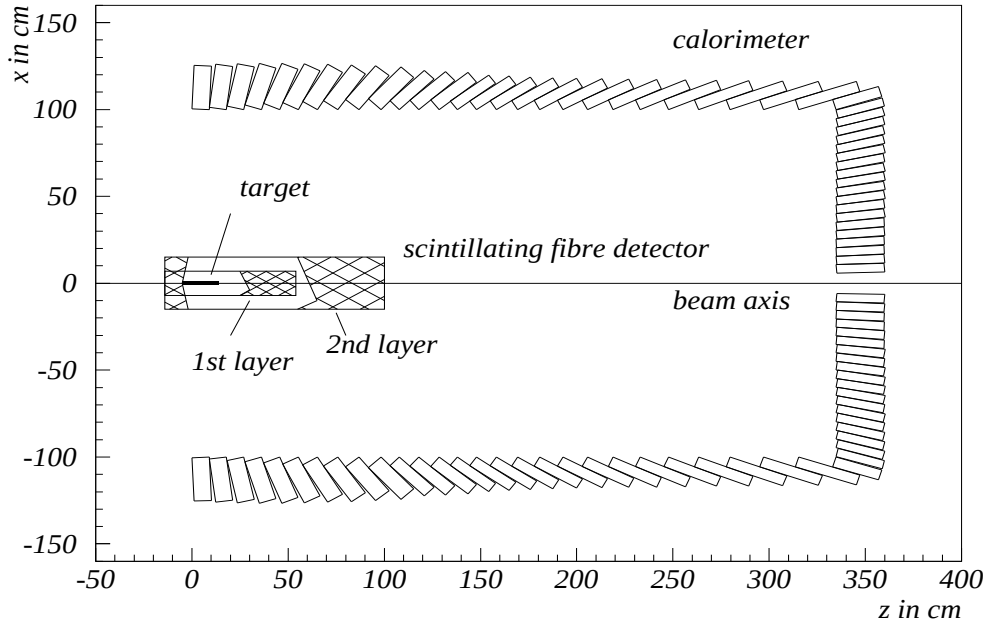

Figure 2.6.3: *Proposed detector system for the RCS experiment*

ing the ELFE facility, an attempt should be made to merge all views and one should try to come up with just one (or two, at most) detector design(s). Let's note that presently further efforts are being made inside Europe aiming at the development of appropriate detectors for ELFE [4].

Bibliography

[1] Conference Proceedings of 'The ELFE Project, an Electron Laboratory for Europe', Mainz, Germany (7-9 October 1992), Eds. J. Arvieux and E. De Sanctis, ISBN 88-7794-060-3 (1993) p. 32-38

[2] K. Helbing, *Messung von totalen Photoabsorptionsquerschnitten mit dem GDH-Detektor'*, PhD thesis, Universität Bonn (Juli 1997)

[3] Proceedings of the Second ELFE Workshop on Hadronic Physics : 'Prospects of Hadron and Quark Physics with Electromagnetic Probes', Saint Malo, France, (23-27 September 1996), Eds. N. d'Hose, B. Frois, P.A.M. Guichon, B. Pire and J. Van de Wiele, *Nucl. Phys.* **A622** (1997) 157c-165c, **and** Proceedings of the Parallel Sessions, report DAPNIA-SPhN-96-35 (1996)

[4] 'The informal working group on ELFE detectors' (Spokesperson : D. von Harrach, Mainz)

Chapter 3

Photon Beam Production Methods & Technical Requirements

3.1 Introduction

K. Helbing, R. Van de Vyver and L. Van Hoorebeke

The open question in all previous proposals and discussions is that, at this very moment, no dedicated high-energy, continuous beam electron accelerator facility is available for these purposes in Europe, notwithstanding the recommendations by NuPECC [1]. On the other hand, there do exist a couple of detailed proposals of which one might lead to realization in the near future.
Apart from the specific ELFE proposal [2], a project which seems to be very unlikely to be realized in its original form, the other options are listed in the table below, i.e. ELFE@DESY and ELFE@CERN.

	FTE@TESLA	ELFE@DESY	ELFE@CERN	HALL D
Maximum energy [GeV]	250 - 500	25	25	12 (24)
Energy spread [10^{-4}]	5	20	10	< 10
Maximum current [A]	10^{-8}	3.10^{-5}	10^{-4}	$3 \cdot 10^{-6}$
Duty cycle [%]	0.4	90	100	100
Polarization orientation	any	vertical	vert./other	vert./other
Degree of pol. [%]	80	70	80 / 40	80 / 40

As there exist specific plans (and the final decision is expected to be taken within a couple of years) for the construction of an e^+e^- 500 GeV collider at DESY, also the possibility has been foreseen to extract a 250-500 GeV electron beam and lead it to a so-called FTE *(Fixed Target Experiments)* area; however, such a beam should only have a duty cycle of about 0.4% while its current is limited to about 0.01 μA. The general lay-out of such facility is shown in Fig. 3.1.1. It seems clear that such option does not satisfy the actual ELFE characteristics.

For completeness, in the same table also the specifications of the Hall D project at TJNAF, USA are listed [3].
Our main interest goes to both ELFE@... options. The first one, ELFE@DESY has been described in ref. [4],[5]; in this project, proposed in 1995, it is suggested to combine TESLA and the HERA ring, using the latter as a stretcher for ELFE. The principle is the following (quoted from ref. [5]):

- short pulses are produced at low frequency (10 Hz) by TESLA and accumulated in the HERA ring until they fill the ring;
- the stored beam is then slowly extracted from the ring over the time period between the accelerator pulses by switching on nonlinear lenses in the ring that induce a controlled beam instability (resonant growing of particle oscillation amplitudes);

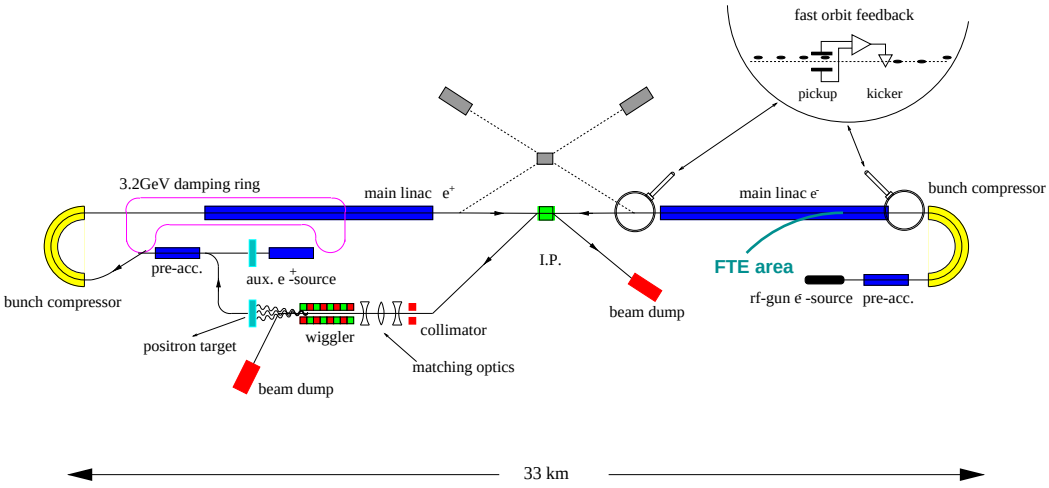

Figure 3.1.1: *General lay-out of the e^+e^- collider at DESY, together with the indication of the FTE area*

- when the ring is empty, new pulses from the accelerator are stored and the extraction process starts again.

Such 'pulse stretcher' scenario has been successfully applied at ELSA (Bonn), AmPS (Amsterdam), etc. with the aim to increase the duty cycle of the available pulsed electron linac. One important advantage of the present option is that the needed ring already exists (HERA), while the e^+e^- collider (TESLA project) requires the construction of a superconducting linac (25 GeV). A principal lay-out of the facility is shown in Fig. 3.1.2.

The maximum extracted current amounts to about 30 μA with a duty cycle of 88%. Drawbacks of this ELFE solution might be its rather poor emittance, its rather high energy spread and the background situation of the extracted beam. On the other hand, one should take into consideration that the existing HERA ring disposes over 4 relatively large, experimental halls although also here some space limitations might show up.
In this proposal, some attention was also paid to the possibility of providing a *Photon Beam for ELFE*, using the laser backscattering technique; its maximum energy could reach 16 GeV with the choice of an appropriate laser. As far as the photon flux is concerned, one should keep in mind that it is proportional to the electron beam intensity, to the laser power and to the electron-laser interaction length. If one would use the electrons *inside* the storage ring (current : about 150 mA), one would obtain a photon flux of roughly three orders of magnitude higher than with the extracted beam. However, also in this storage ring option, the need exists for employing a standard continuous laser coupled to an optical amplification cavity (amplification factors of around 1000 do not seem to be